NazendeNur BAYRAM

A Ph.D. Thesis

AGU 2023

DEVELOPMENT OF BREAST CANCER TARGETED, MULTIFUNCTIONAL CROSS-LINKED MICELLE NANOCARRIERS

A THESIS
SUBMITTED TO THE DEPARTMENT OF BIOENGINEERING
AND THE GRADUATE SCHOOL OF ENGINEERING AND SCIENCE
OF ABDULLAH GUL UNIVERSITY
IN PARTIAL FULFILLMENT OF THE REQUIREMENTS
FOR THE DEGREE OF
DOCTOR OF PHILOSOPHY

By
Nazende Nur BAYRAM
May 2023

DEVELOPMENT OF BREAST CANCER TARGETED, MULTIFUNCTIONAL CROSS-LINKED MICELLE NANOCARRIERS

A THESIS
SUBMITTED TO THE DEPARTMENT OF BIOENGINEERING
AND THE GRADUATE SCHOOL OF ENGINEERING AND SCIENCE
OF ABDULLAH GUL UNIVERSITY
IN PARTIAL FULFILLMENT OF THE REQUIREMENTS
FOR THE DEGREE OF
DOCTOR OF PHILOSOPHY

By
Nazende Nur BAYRAM
May 2023

SCIENTIFIC ETHICS COMPLIANCE

I hereby declare that all information in this document has been obtained in accordance with academic rules and ethical conduct. I also declare that, as required by these rules and conduct, I have fully cited and referenced all materials and results that are not original to this work.

Name-Surname: Nazende Nur BAYRAM
Signature :

REGULATORY COMPLIANCE

Ph.D. thesis titled "Development of Breast Cancer Targeted, Multifunctional Cross-Linked Micelle Nanocarriers" has been prepared in accordance with the Thesis Writing Guidelines of the Abdullah Gül University, Graduate School of Engineering & Science.

Prepared By	Advisor
Nazende Nur BAYRAM	Prof. Dr. Sevil DİNÇER İŞOĞLU
Signature	Signature

Head of the Bioengineering Program
Assist Prof. Dr. Altan ERCAN
Signature

ACCEPTANCE AND APPROVAL

Ph.D. thesis titled “Development of Breast Cancer Targeted, Multifunctional Cross-Linked Micelle Nanocarriers” and prepared by Nazende Nur Bayram has been accepted by the jury in the Bioengineering Graduate Program at Abdullah Gül University, Graduate School of Engineering & Science.

26 / 05 / 2023

(Thesis Defense Exam Date)

JURY:

Advisor : Prof. Dr. Sevil Dinçer İŞOĞLU

Member : Assoc. Prof. Dr. Murat TOPUZOĞULLARI

Member : Assoc. Prof. Dr. Aysun ADAN

Member : Assoc. Prof. Dr. Ömer AYDIN

Member : Assist. Prof. Dr. İsmail AKÇOK

APPROVAL:

The acceptance of this Ph.D. thesis has been approved by the decision of the Abdullah Gül University, Graduate School of Engineering & Science, Executive Board dated ….. /….. / …….. and numbered ……..……. .

…….. /…….. / ……..

Graduate School Dean

Prof. Dr. İrfan ALAN

ABSTRACT

DEVELOPMENT OF BREAST CANCER TARGETED, MULTIFUNCTIONAL CROSS-LINKED MICELLE NANOCARRIERS

Nazende Nur BAYRAM
Ph.D. in Bioengineering Department
Advisor: Prof. Dr. Sevil DİNÇER İŞOĞLU

May 2023

In this thesis, we developed two different micelle-based nanocarriers, which are pH-responsive and core cross-linked micelle (CCMs), and specifically target HER2 receptor on breast cancer cells. Intracellularly degradable and stabilized micelles were prepared by core cross-linking and RAFT polymerization in the presence of an acid-sensitive cross-linker. Poly(OEGMA) and poly(SBMA) were used as shell parts of these micelles in order to compare the effect of hydrophilic coatings on nanocarrier characteristics. In the first design, we applied drug conjugation (Doxorubicin) with a cleavable linker while in the second design, we used the encapsulation method for drug loading. Targeted micelles were obtained by coupling of HER2-specific peptides (VSSTQDFP and LTVSPWY) and antibody (Herceptin) to POEGMA and poly (SBMA) based CCMs, respectively. These nanocarriers are designed to be stable in blood circulation but cleavable intracellulary to achieve controlled drug release. Nanocarriers were characterized structurally by FTIR and ^{1}H-NMR spectroscopies for all synthesis and conjugation steps. Moreover, nanocarriers and drug-loaded formulations were investigated by Zetasizer, Nanosight, and TEM/SEM analysis. The results showed that designed nanocarriers have a very high potential for HER2-specific targeted drug release for the treatment of breast cancer. This thesis holds significant importance due to its successful demonstration of two distinct systems exhibiting high stability, pH sensitivity, and high selectivity for HER2-targeted therapy of breast cancer.

Keywords: HER2 targeting; pH-responsive; cross-linked micelle; micelle nanocarrier; RAFT; breast cancer

ÖZET

MEME KANSERİ HEDEFLİ, ÇOK FONKSİYONLU, ÇAPRAZ BAĞLI MİSEL NANOTAŞIYICILARIN GELİŞTİRİLMESİ

Nazende Nur BAYRAM
Biyomühendislik Anabilim Dalı Doktora
Tez Yöneticisi: Prof. Dr. Sevil DİNÇER İŞOĞLU

Mayıs 2023

Bu tez çalışmasında, meme kanseri hücrelerinde HER2 reseptörünü hedefleyen, pH'a duyarlı ve çekirdeği çapraz bağlı (ÇÇM), misel bazlı iki farklı nanotaşıyıcı geliştirilmiştir. Stabilitesi arttırılmış, aynı zamanda hücre içinde parçalanabilir özellikte olan miseller, asite duyarlı bir çapraz bağlayıcı varlığında RAFT polimerizasyonu ile çekirdeği çapraz bağlanarak hazırlanmıştır. Hidrofilik kabuk kısmının nanotaşıyıcı özellikleri üzerindeki etkisini karşılaştırmak için, misellerin kabuk parçalarında poli(OEGMA) ve poli(SBMA) kullanılmıştır. İlk tasarımda ilaç (DOX) parçalanabilir bir bağlayıcı ile konjuge edilirken, ikinci tasarımda inkübasyon yoluyla yüklenmiştir. Hedeflenen miseller, HER2'ye özgü peptitlerin (VSSTQDFP ve LTVSPWY) ve antikorun (Herceptin) sırasıyla poli(OEGMA) ve poli(SBMA) bazlı ÇÇM'lere bağlanmasıyla elde edilmiştir. Bu nanotaşıyıcılar, kan dolaşımında kararlı, ancak kontrollü ilaç salımını sağlamak için hücre içinde parçalanabilir olacak şekilde tasarlanmıştır. Nanotaşıyıcılar, tüm sentez ve konjugasyon adımlarında yapısal olarak FTIR ve ^{1}H-NMR ile karakterize edilmiştir. Ayrıca, nanotaşıyıcılar ve ilaç yüklü formülasyonlar, boy ve boy dağılımı ile morfolojik açıdan ışık saçılması ve TEM/SEM analizleri ile incelenmiştir. Sonuç olarak, tasarlanan nanotaşıyıcıların meme kanseri tedavisi için HER2'ye özgü ilaç salımı için oldukça yüksek potansiyele sahip olduğu görülmüştür. Bu tez çalışması, meme kanserinin HER2 hedefli tedavisi için yüksek stabilite, pH duyarlılığı ve yüksek seçicilik sergileyen iki farklı sistemin başarılı bir şekilde elde edilmiş olması nedeniyle büyük önem taşımaktadır.

Anahtar kelimeler: HER2 hedefleme; pH duyarlı; çapraz bağlı misel; misel nanotaşıyıcı; RAFT; meme kanseri

Acknowledgements

I would like to express my special thanks of gratitude to my advisor Professor Dr. Sevil Dinçer İşoğlu, for giving me this opportunity and supporting me in performing this thesis study. Secondly, I would also like to express my sincere thanks to Associate Prof. Dr. İsmail Alper İşoğlu for his help, patience, and guidance throughout my thesis study.
I also would like to thank Dr. Anil K Sood and Dr. Bülent Özpolat for supporting me throughout the TUBITAK (The Scientific and Technological Research Council of Turkey) 2214-A program.

During my thesis, I was supported by the TUBITAK 2211-A program and YÖK 100/2000 Ph.D. program, TUBITAK 1001 with Project number: 116R057 and TUBITAK 1003 with Project number: 216S639. I would like to express my sincere thanks to these programs. Also, the part of this thesis studies given in Chapter 2 was supported by TUBITAK with Application No: 1059B142100283 within the scope of 2214-A International Research Fellowship Program. I am very grateful to the authorities who provided financial support to complete the thesis work.

I would also like to thank Burhan Kabataş, who helped me with all the procedures from the very beginning of the doctoral process, made this education easier for me and added a lot to me.

I would also like to give my deep and sincere gratitude to my family with all my heart; my parents, Atıf and Fatma Akşit; my lovely aunt Şerife Akşit; my brother Abdüssamed and my sisters Seren, Beyza, Cemile, and Reyyan; my step-parents, Cemil and Meryem Bayram and my friends especially my laboratory colleagues, who have been a part of my life with their beautiful energies and motivations, for their unflagging support, endless love and patience throughout my life.

Last but not least, my deepest gratitude must be submitted to my earing, supportive, and loving husband, Ferdi Caner Bayram. Thanks a million times for motivating, supporting, and loving me through this thesis.

TABLE OF CONTENTS

LIST OF FIGURES

LIST OF TABLES

LIST OF ABBREVIATIONS

4-VP	4-vinyl pyridine
ABC	Accelerated Blood Clearance
AC	Antibody conjugated core cross-linked micelles
ACVA	4,4-Azobis(4-cyanovaleric acid)
AEMA	N-(2-Aminoethyl) methacrylamide
AIBN	Azobisisobutyronitrile
AIs	Aromatase inhibitor
ATRP	Atom transfer radical polymerization
BP	Benzoyl peroxide
CCMs	Core cross-linked micelles
CMC	Critical micelle concentration
CMs	Cross-linked micelles
CTA	Chain transfer agent
CTA	4-cyano-4-(thiobenzoylthio)pentanoic acid
CTEM	High Contrast Transmission Electron Microscopy
DCIS	Ductal carcinoma in situ
DEGMA	Diethylene glycol methyl ether methacrylate
DHB	Dihydroxybenzoic acid
DIPEA	N,N-diisopropylethylamine
DLS	Dynamic Light Scatterring
DMAEP	2,2-dimethoxy propane
DMF	Dimethyl formamide
DMSO	Dimethyl sulfoxide
DOX	Doxorubicin
DTDP	2,2-dithiodipyridine
DTT	Dithiothreitol
DVB	Divinylbenzene
EDC	N-(3-dimethyl aminopropyl)-N′-ethyl carbodiimide hydrochloride
EE	Encapsulation efficiency

EF2KC	Elongation Factor-2 Kinase
EGDA	Ethylene glycol diacrylate
EGFRs	Epidermal Growth Factor Receptors
EMCH	N-ε-maleimidocaproic acid hydrazide
EPR	Enhanced Permeability and Retention
ETA	Ethanolamine
FTIR	Fourier Transform Infrared Spectroscopy
GLOBOCAN	Global Cancer Observatory
HEMA	2-hydroxyethyl methacrylate
HER2	Human Epidermal Growth Factor Receptor 2
HOBT	1-hydroxy benzotriazole hydrate
IDC	Invasive ductal carcinoma
ILC	Invasive lobular carcinoma
LCIS	Lobular carcinoma in situ
LCST	Lower critical solution temperature
LE	Loading efficiency
MALDOX	Maleimide- modified Doxorubicin
MBA	N,N'-methylenebis(acrylamide)
MTT	(3-(4,5-Dimethylthiazol-2-yl)-2,5-Diphenyltetrazolium Bromide)
MWCO	Molecular weight cut off
NCs	Nanocarriers
NMP	Nitroxide-Mediated Polymerization
NMR	Nuclear Magnetic Resonance Spectroscopy
OEGMA	Oligoethyleneglycol methyl ether methacrylate
PAA	Poly(acrylic acid)
PASP	Poly(aspartic acid)
PBLA	Poly(β-benzyl-L-aspartate)
PBS	Phosphate Buffer
PC	Phosphatidylcholine
PC	Peptide conjugated core cross-linked micelles
PCL	Poly(ε-caprolactone)
PDI	Polydispersity Index
PDS	Pyridyl disulfide

PEG	Polyethylene glycol
PEGDA	Poly(ethylene glycol) diacrylate
PEI	Polyethyleneimine
PEO	Poly(ethylene oxide)
PHA	Poly(hydroxyalkanoates)
PLGA	Poly (lactic-co-glycolic acid)
PLLA	Poly(L-lactic acid)
PMMA	Poly(methyl methacrylate)
PNIPAM	Poly(N-isopropylacrylamide)
POEGMA	Poly(oligo(ethylene glycol) methyl ether methacrylate)
PPO	Poly(propylene oxide)
PST	Polystyrene
p-TSA.H2O	p-toluenesulfonic acid monohydrate
PVP	Poly(N-vinylpyrrolidone)
RAFT	Reversible addition-fragmentation chain transfer
SBMA	N-(3-Sulfopropyl)-N-methacroyloxyethyl-N,N-dimethylammonium betaine
SEM	Scanning Electron Microscopy
SERDs	Selective estrogen receptor degraders
SERMs	Selective estrogen receptor modulators
TAM	Tumor-Associated Macrophages
TCEP	tris(2-carboxyethyl)phosphine
TEA	Triethylamine
TEM	Transmission Electron Microscopy
TFA	Trifluoroacetic acid
TNC	Triple Negative Breast Cancer
UCST	Upper critical solution temperature

To my family

Chapter 1

Introduction

1.1 Breast Cancer

Breast cancer has been the most frequently diagnosed type of cancer globally, causing a significant public health burden. It is estimated that 2.3 million new cases emerged in 2020. The rate of the disease varies considerably between countries and regions, with most cases occurring in undeveloped countries. However, developing countries remain disproportionately exposed to breast cancer deaths. If current trends continue, breast cancer's burden is expected to rise to over 3 million new cases and 1 million deaths per year by 2040, primarily due to population growth and aging [1].

The most recent statistics from the Global Cancer Observatory (GLOBOCAN) indicate that 19.3 million new cancer cases were diagnosed globally in 2020, resulting in approximately 10 million cancer-related deaths. Among all cancer types, breast cancer has become the most prevalent, accounting for 11.7% of all cancer cases worldwide, with 2,261,419 new diagnoses (Figure 1.1). In Turkey, the latest GLOBOCAN data reveals that 233,834 new cancer cases were reported in 2020, with breast cancer ranking as the second most widespread cancer type after lung cancer, with 24,175 new cases [2].

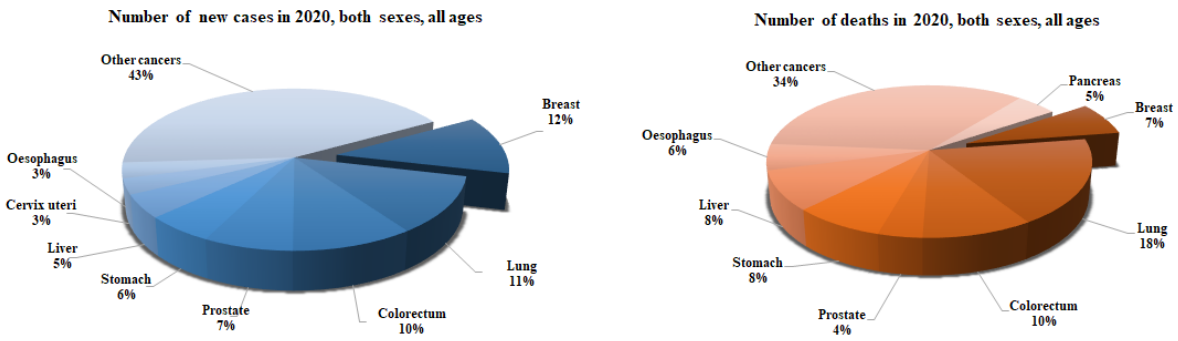

Figure 1.1 Incidence of breast cancer statistic from the Global Cancer Observatory [1]

Breast cancer is categorized based on various characteristics, such as the location of the tumor and the type of cells involved. The most common type of breast cancer classifies as;

- Ductal carcinoma in situ (DCIS) develops in the breast's milk ducts and is considered a non-invasive or early-stage cancer.
- Invasive ductal carcinoma (IDC) is the most widespread type of breast cancer, constituting approximately 80% of all cases. IDC begins in the milk ducts and then invades the surrounding breast tissue.
- Lobular Carcinoma In Situ (LCIS) is characterized by the presence of abnormal cells in the breast lobules. These atypical cells do not extend beyond the lobules into the nearby breast tissue.
- Invasive lobular carcinoma (ILC) begins in the breast's milk-producing glands and can spread to other breast parts.
- Inflammatory breast cancer is a rarer but particularly aggressive form of breast cancer and can cause symptoms such as redness, swelling, and warmth without a noticeable lump in the breast.

Breast cancer is classified into several molecular subtypes, including luminal A, luminal B, HER2-positive, and triple-negative breast cancer. These subtypes are determined based on the presence or absence of specific molecular markers on the surface of cancer cells, which help guide treatment decisions and predict patient outcomes.

- Luminal A breast cancer: This subtype is characterized by the presence of estrogen receptors (ER) and/or progesterone receptors (PR) on the cancer cells. It tends to have a lower proliferation rate and is associated with a better prognosis compared to other subtypes. Luminal A breast cancers are typically hormone receptor-positive and HER2-negative.
- Luminal B breast cancer: Luminal B subtype also expresses estrogen receptors and/or progesterone receptors but may have a higher proliferation rate and be more aggressive than Luminal A tumors. Some Luminal B tumors may also overexpress the HER2 receptor. Treatment strategies for Luminal B breast cancer often involve hormone therapy and, in some cases, HER2-targeted therapies.
- HER2-positive breast cancer: This subtype is characterized by overexpression or amplification of the HER2 receptor (Human epidermal growth factor receptor 2).

HER2-positive breast cancer tends to be more aggressive and has a higher risk of recurrence.

- Triple-negative breast cancer (TNBC): TNBC does not express estrogen receptors, progesterone receptors, or HER2 receptors. It represents a subtype of breast cancer that lacks targeted therapy options currently available for the other subtypes. TNBC tends to be more aggressive, but in some cases, it can respond well to chemotherapy. Research is ongoing to identify new treatment approaches for TNBC.

Other less common types of breast cancer include phyllodes tumors, angiosarcomas, and Paget's breast disease [3–5].

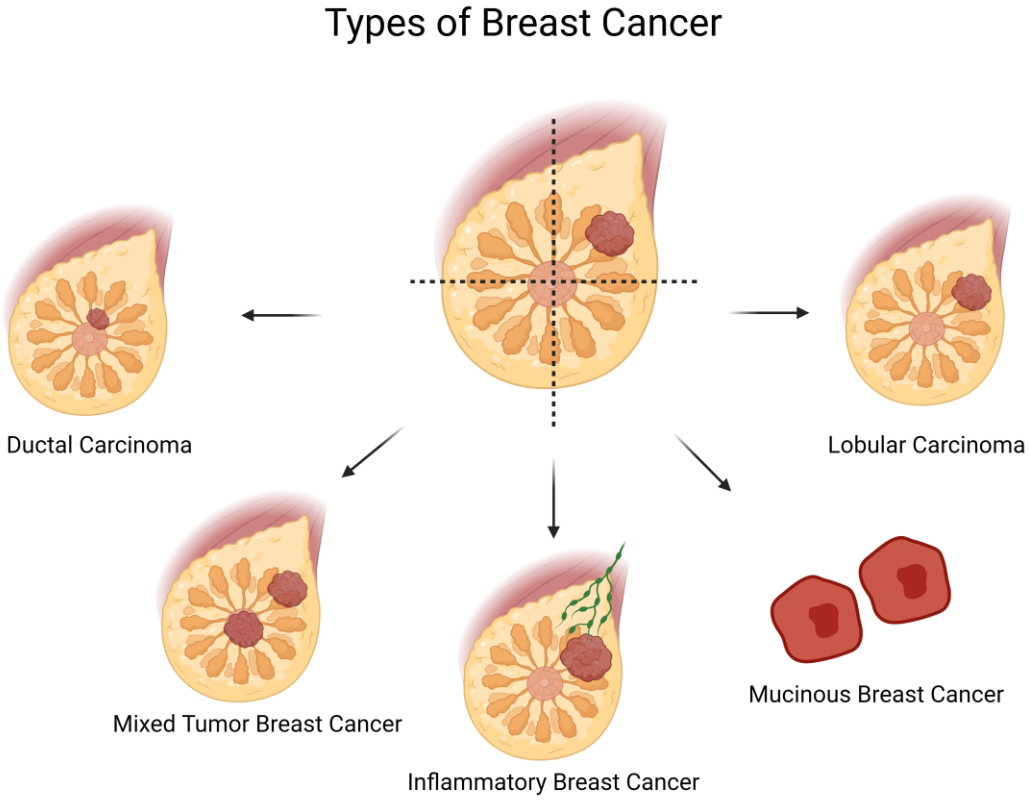

Figure 1.2 Schematic illustration of types of breast cancer

1.1.1 HER2-Positive Breast Cancer

HER2-positive breast cancer is originated from the overexpression of the HER2 receptor protein. The HER2 receptor, also known as ErbB2, is a member of transmembrane protein classified under the epidermal growth factor receptors (EGFRs).

It is encoded by the ERBB2 gene and is overexpressed in about 20-25% of breast cancers. These features make it an essential target for breast cancer therapy. The HER2 receptor comprises the extracellular domain, transmembrane domain, and intracellular domain. The extracellular domain is made up of four subdomains (I-IV) that are responsible for ligand binding and receptor dimerization. The transmembrane domain is a single helical structure anchoring the cell membrane receptor. The intracellular domain composes tyrosine kinase activity responsible for downstream signaling events. The HER2 receptor does not have a known ligand, but it can heterodimerize with HER1, HER3, and HER4, to form functional signaling complexes. When a ligand binds to another EGFR family member, it induces conformational changes that activate the tyrosine kinase activity of both receptors, leading to the phosphorylation of specific tyrosine residues on the intracellular domains resulting in activation of downstream signaling pathways which regulate cell proliferation and differentiation. Overexpression of HER2 results in high dimerization and signaling activity of the receptor, resulting in enhanced cell growth and survival, even in the absence of a ligand [6,7].

The molecular mechanisms underlying HER2-positive breast cancer have been extensively studied, and various therapies have been discovered to target the HER2 protein and its downstream signaling pathways.

1.1.2 Treatment of Breast Cancer

Breast cancer treatment regimens vary based on factors such as the type and stage of cancer, age and health status of the patient, and the presence of specific genetic mutations. These treatment regimens contain surgery, radiation therapy, chemotherapy, hormone therapy, immunotherapy, and targeted therapy approaches. The surgical approach includes breast-conserving surgery (lumpectomy) or mastectomy, removing the entire breast tissue. Lymph node removal may also be performed. In the radiation therapy approach, high-energy radiation kills cancer cells. The chemotherapy approach, known as the most widely used approach, uses drugs that kill the cancer cell or prevent it from dividing and growing. Chemotherapy may be utilized before or after surgery. There are several chemotherapy agents that are commonly used alone or in combination with other therapies to treat breast cancer. Some of these include; anthracyclines (Doxorubicin, Epirubicin), taxanes (Paclitaxel), platinum agents (Cisplatin, Carboplatin), and Capecitabine. In the hormone therapy approach, the hormone-blocking agent promotes cancer growth in hormone receptor-positive breast cancers.

Tamoxifen which is known as a selective estrogen receptor modulator (SERMs), is among the most frequently used drugs that block estrogen's effects on breast cancer cells. Also, Anastrozole and Letrozole, which are known as aromatase inhibitors (AIs), block the production of estrogen in postmenopausal women. Other types of hormone therapy may include ovarian suppression or ablation, which involves stopping the ovaries from producing estrogen. Fulvestrant, which is known as selective estrogen receptor degrader (SERD), blocks and degrades the estrogen receptor. Hormone therapy is typically used for hormone receptor-positive breast cancers. Immunotherapy which has been receiving attention recently, is a newer type of therapy that uses the body's immune system to recognize and attack cancer cells. [8,9]. These treatment approaches can be classified under targeted therapy and untargeted therapy. Untargeted therapy, or conventional therapy, includes chemotherapy, radiation therapy, and surgery. These treatments are targeted only to cancer cells and can affect both cancerous and healthy cells. Targeted therapy involves using drugs targeting specific proteins or genes that contribute to cancer growth, such as HER2-positive breast cancers. Targeted therapies such as Trastuzumab, Pertuzumab, and Lapatinib effectively treat HER2-positive breast cancer by blocking the HER2 protein and/or inhibiting downstream signaling pathways [10–12]. Other therapies, such as chemotherapy and hormone therapy, may also be combined with targeted therapies to improve treatment outcomes [13]. In this type of treatment regimen, small molecules are widely used, but they have several disadvantages, such as difficulties in targeting specific tumor sites, leading to reduced efficacy and possible side effects in healthy tissue. Furthermore, they can be quickly eliminated from the bloodstream with hepatic and renal clearance, which makes them unsuitable for sustained drug delivery. Additionally, small molecules can be toxic and require extensive optimization to reduce toxicity. At this point, the potential of polymer-based drug delivery systems for enhancing the efficacy and safety of cancer treatments comes to the fore. Encapsulation of the drug by the use of the polymer ensures the prevention of drug degradation and targeted delivery of the drug to the tumor site. With this approach it can reduced the required dosage of the drug, mitigating the risk of adverse effects in healthy tissues, and facilitating sustained drug release, resulting in a prolonged therapeutic effect [14–16].

1.2 Polymer Therapeutics

Polymer therapeutics refer to therapeutic agents composed of polymers or molecules made up of many repeating subunits. These polymers can be formulated into various drug delivery systems, such as polymer-drug conjugates, polymer protein conjugates, and polymeric nanoparticles. Polymeric drugs are gaining popularity because of their capacity to enhance drug absorption, targeted delivery, and decreased side effects. Besides conferring a prolonged release of the active therapeutic agent, polymeric drugs can be engineered to exhibit site-specific delivery to specific body areas, thus offering enhanced therapeutic efficacy.

Polymer therapeutics classify as mainly into three groups;

1. Polymer- protein conjugates
2. Polymer- small molecule inhibitor conjugates
3. Polymeric nanoparticles

[17,18].

1.2.1 Polymer Protein Conjugates

Despite the clinical value of proteins, the low stability, rapid clearance, and immunogenicity of protein drugs are important issues to be addressed. Polymer-protein conjugates are a class of drug delivery system that involves binding a protein to a polymer. This system helps to enhance the protein's stability, solubility, and bioavailability. In addition, this system can be developed to target specific cells and/or tissues and can be used for controlling the release of the drug molecule over time [19]. Due to its water solubility, lack of charge, and biocompatibility features, polyethylene glycol (PEG) is a frequently utilized polymer to produce conjugates. The conjugation of PEG to a protein therapeutic confers several beneficial effects, such as steric repulsion of antigenic epitopes and reduced immunogenicity. These changes also protect the therapeutic from proteolytic degradation and its clearance from the mononuclear phagocyte system. Furthermore, PEG increases the molecular mass and hydrodynamic radius of the therapeutics, reducing its renal filtration and improving its stability and longevity in the

plasma. Altogether, these factors minimize the dosing interval while increasing the safety of the drugs [20,21]. Below is a list of drugs approved by the FDA that have been modified with PEGylation.

Table 1.1 List of drugs approved by the FDA that have been modified by PEGylating [22]

Trade Name	PEGylated entity	Indications	Approved Year
Adagen (Enzon Pharmaceuticals)	ADA	ADA-SCID	1990
Oncaspar (Enzon Pharmaceuticals)	L-asparaginase	Acute lymphoblastic leukemia	1994
PegIntron (Merck & Co.)	Interferon α2b	Hepatitis C	2001
Pegasys (Genentech)	Interferon α2a	Hepatitis B and hepatitis C	2002
Neulasta (Amgen)	G-CSF	Chemotherapy-induced neutropenia	2002
Somavert (Pfizer)	HGH receptor antagonist	Acromegaly	2003
Macugen (Bausch & Lomb)	Anti-VEGF aptamer	Neovascular age-related macular degeneration	2004
Mircera (Roche)	Epoetin beta	Anaemia associated with chronic kidney disease	2007
Cimzia (UCB Pharma)	Anti-TNF Fab′	Crohn's disease, rheumatoid arthritis, psoriatic arthritis, and ankylosing spondylitis	2008
Krystexxa (Horizon Pharma)	Uricase	Chronic gout	2010
Plegridy (Biogen)	Interferon β1a	Relapsing multiple sclerosis	2014
Movantik (AstraZeneca)	Naloxone	Opioid-induced constipation	2014
Adynovate (Baxalta)	Factor VIII	Haemophilia A	2015
Palynziq (BioMarin)	Phenylalanine ammonia-lyase	Phenylketonuria	2018
Jivi (Bayer)	Factor VIII	Haemophilia A	2018

Asparlas (Servier Pharma)	L-asparaginase	Leukemia	2018
Fulphila (Mylan GmbH)	G-CSF	Infection during chemotherapy	2018
Revcovi (Leadiant Bioscience)	Recombinant adenosine deaminase	ADA-SCID	2018
Palynziq (BioMarin Pharmaceutical)	Recombinant phenylalanine ammonia-lyase	Phenylketonuria	2018
Udenyca (Coherus Biosciences)	G-CSF	Infection during chemotherapy	2018
Ziextenzo (Sandoz)	G-CSF	Infection during chemotherapy	2019
Esperoct (Novo Nordisk)	Recombinant antihemophilic factor	Hemophilia A	2019
Nyvepria (Pfizer Inc.)	G-CSF	Neutropenia associated with Chemotherapy	2020
Empaveli (Apellis)	Pentadecapeptide	Paroxysmal nocturnal hemoglobinuria (PNH	2021
Skytrofa (Ascendis)	Human growth hormone	Growth hormone deficiency	2021
BESREMi (PharmaEssentia Corp)	Interferon	Polycythemia vera	2021
Fylnetra (Amneal Pharmaceuticals)	G-CSF	Neutropenia	2022
Stimufend (Fresenius Kabi)	G-CSF	Neutropenia	2022
Rolvedon (Spectrum Pharmaceuticals)	G-CSF	Febrile neutropenia	2022

Although PEGylating is a commonly used method to improve the therapeutic efficiency of drugs, a significant limitation of PEGylating is the non-biodegradability of PEG molecules. PEGs are synthetic polymers that are not naturally found in the body and can accumulate in various tissues and organs. This accumulation can cause toxicity and immunogenicity issues, limiting the long-term use of PEGylated therapeutics.

Additionally, PEGs can interfere with the normal functioning of proteins by masking their epitopes or altering their conformation [23,24]. Researchers have been developing alternative biodegradable polymers to address these limitations that can replace PEGs. Some of the polymers as an alternative to PEG include polysaccharides such as hyaluronic acid, chitosan, dextran, and polyamine acids. These polymers can be modified to include functional groups that can be used for conjugation to drugs or proteins. Another approach to address the non-biodegradability of PEGs is to use shorter PEG chains. PEGylated protein therapeutics currently approved use PEGs with a molecular mass of 40 kDa or less near the glomerular filtration threshold, which is around 50 kDa. This allows the PEGylated protein to be eliminated from the body through renal clearance. However, shorter PEG chains may reduce the efficacy of PEGylation in some cases [25]. Several alternative polymers to PEG can be used for drug conjugation, each with advantages and disadvantages. POEGMA (poly(oligo(ethylene glycol) methyl ether methacrylate) is a polymer composed of hyperbranched structures of oligo ethylene glycol methacrylate (OEGMA) moieties; it has turned out to be a promising biodegradable alternative to PEG for use in various biomedical applications. Unlike PEG, which contains ether bond that is not susceptible to enzymatic cleavage or hydrolysis, POEGMA contains ester bonds that are susceptible to enzymatic and hydrolytic cleavage, which facilitates its degradation into smaller molecules that might be eliminated from the body. This property makes POEGMA a promising option for drug delivery and biomedical applications, as it may reduce the potential long-term health risks associated with PEG [24]. Poly(N-vinylpyrrolidone) (PVP) is also a water-soluble polymer and has superior properties, such as good biocompatibility and low immunogenicity, which makes it an attractive alternative to PEG [26]. In addition, polysaccharides, which are natural polymers, for instance, hyaluronic acid, chitosan, and dextran, which are considered biocompatible and biodegradable, can also be an alternative to PEGs. [27]. Polyamino acids, including polylysine, polyglutamic acid, and polyaspartic acid, and polyesters such as poly (lactic-co-glycolic acid) (PLGA), poly(ε-caprolactone) (PCL), and poly(hydroxy alkanoates) (PHA) also are considered as alternative polymers within this group [28]. Finally, zwitterionic polymers, including positively (cationic) and negatively (anionic) charged functional groups in the same structure, cause them to interact strongly with water molecules to form a superior hydrophilic property, making them a solid choice for PEG. [29]. Determining an appropriate polymer for the conjugation of a drug or protein necessitates considering multiple parameters, including the conjugate's size, charge, and

hydrophobicity, as well as the preferred pharmacokinetics and pharmacodynamics characteristics of the conjugate. Also, parameters such as biocompatibility, biodegradability, and immunogenicity of the polymer, as well as its chemical stability and ease of conjugation, should be considered before selecting an alternative to PEG for drug conjugation.

1.2.2 Polymer Drug Conjugates (PDCs)

This drug delivery system involves conjugating a drug to a polymer. The drug is typically conjugated to the polymer via a covalent bond, and the resulting conjugate has the ability to release the drug slowly and gradually over a prolonged period. These conjugates also have advantages compared to the traditional drug delivery methods, such as improved stability, targeted delivery, and extended release of active compounds. Additionally, PDCs are able to be tailored to target specific tissue types, allowing for more targeted and effective treatments [30,31].

1.2.3 Polymeric Nanoparticles

These are small colloidal particles with diameters ranging from 1 and 100 nm that are commonly used as drug delivery vehicles due to their potential to protect potential drugs and target specific cells or tissues [32]. Compared to hydrophilic linear polymers and dendrimers, colloidal polymeric nano assemblies provide more intricate and adaptable structures due to the ability to design both their core and surface components, leading to greater control over their properties and functions [33–35]. Polymeric nanoparticles typically exhibit a core-shell structure, wherein a hydrophobic core is combined and stabilized by a hydrophilic corona. These polymeric nanoparticles are able to be formed by precipitation or emulsification methods in the presence of surfactants. As an alternative, amphiphilic block copolymers comprising both hydrophilic and hydrophobic blocks within the same structure can spontaneously arrange themselves in aqueous media, leading to the formation of polymeric micelles. These structures offer advantages such as high drug loading capacity due to their solid structure, controlled drug release via diffusion or degradation of the polymer matrix, and sequestration of drugs in the hydrophobic core [36,37].

Polymeric nanoparticles are able to be categorized based on their source and physiochemical properties. Based on their sources, they might be broadly categorized into

synthetic polymeric nanoparticles, which are prepared by synthesizing polymers via chemical reactions or modifying existing polymers and then using them to form nanoparticles including poly (lactic-co-glycolic acid) (PLGA), polyethylene glycol (PEG), and polyethyleneimine (PEI) nanoparticles and, natural polymeric nanoparticles which are prepared from naturally occurring polymers including proteins, polysaccharides, and lipids such as albumin nanoparticles, chitosan nanoparticles, and liposomes [38,39]. Synthetic polymeric nanoparticles have certain advantages compared to natural polymeric nanoparticles. Firstly, synthetic polymeric nanoparticles are able to be synthesized with a high degree of control and reproducibility, resulting in the consistent quality of nanoparticles. Natural polymeric nanoparticles, conversely, can have batch-to-batch variations that can affect the features of the resulting nanoparticles. Also, they are often more stable than natural polymeric nanoparticles, which are able to prone to degradation in the body. This increased stability can lead to a longer circulation time and more sustained drug release.

Furthermore, synthetic polymeric nanoparticles can be modified and optimized to improve specific properties, including the capacity of drug loading, particle size, and release kinetics. This flexibility enables the design of nanoparticles tailored to the specific necessity of a particular drug delivery application. Natural polymeric nanoparticles can elicit immune responses in the body, leading to adverse effects such as inflammation and allergic reactions. On the other hand, synthetic polymers are often less immunogenic and can be designed to minimize immune responses [40,41].

Based on their physiochemical properties, shape, and size composition, polymeric nanoparticles can be broadly categorized into nanocapsules, nanospheres, dendrimers, polymeric nanogels, and polymeric micelles [42,43]. To elaborate on these polymeric nanoparticles, nanocapsules have a core-shell structure, where the core includes the drug or other payload, and the shell is made of a polymer. The shell can be solid or porous and can be designed to control drug release [44]. Nanospheres are spherical nanoparticles made of a single polymer. They can be either solid or porous and range in diameter from 10 to 200 nanometers [45]. Dendrimers are nanoparticles made of polymers that are highly structured and have a branching shape. They can be synthesized with high precision during the synthesis process. They have a defined size and shape and can be modified with functional groups for targeted drug delivery [46]. Polymeric nanogels are three-dimensional cross-linked networks of polymers and can swell in water to form nanoscale particles. It can be utilized to encapsulate hydrophobic drugs and could be

designed to respond to changes in pH, temperature, or other stimuli [47]. Polymeric micelles are nanoparticles formed by the self-assembly of amphiphilic block copolymers as a result of the interaction of hydrophilic or hydrophobic groups in an aqueous medium. These structures have a hydrophobic core surrounding the drug and a hydrophilic shell that provides stability [48].

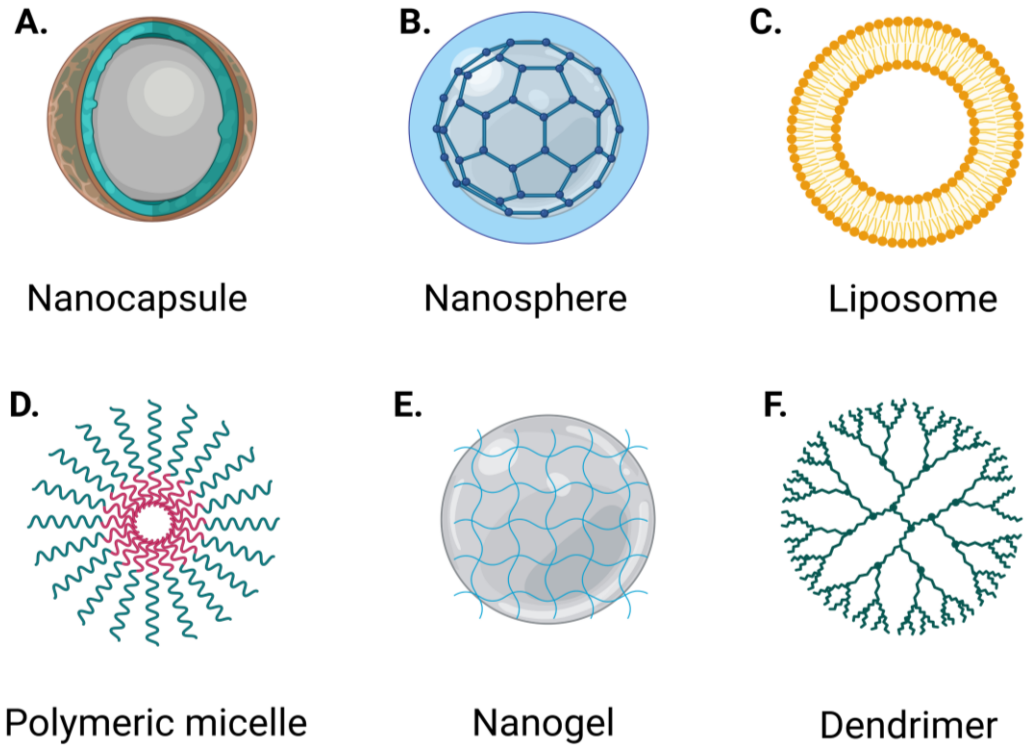

Figure 1.3 Different types of polymeric nanoparticles for drug delivery. (a) nanocapsule, (b) nanosphere, (c) liposome, (d) polymeric micelle, (e) nanogel, and (f) dendrimer

1.2.3.1 Polymeric Micelles

Polymeric micelles are structures that consist of two or more polymer blocks with different hydrophobicity in the aqueous medium, and these blocks come together spontaneously due to these interactions. The resulting structure, which is called as amphiphilic block copolymer, has two parts, the core and the shell, and the shell part, which provides stability and solubility, shows hydrophilic properties, while the core part, which provides the loading of the drug, shows hydrophobic properties. Polymeric micelles' size typically ranges from 1 to 100 nanometers [49]. The hydrophilic block is usually a water-soluble polymer such as PEG, also known as poly(ethylene oxide) (PEO), poly(N-vinyl-2-pyrrolidone) (PVP), poly(vinyl alcohol), poly(vinyl alcohol-co-vinyl

oleate), poly(N-isopropyl acrylamide) (PNIPAM) or poly(acrylic acid) (PAA). In contrast, the hydrophobic block is a water-insoluble polymer such as poly (lactic-co-glycolic acid) (PLGA) or poly(caprolactone) (PCL), poly(propylene oxide) (PPO), poly(β-benzyl-L-aspartate) (PBLA), poly(L-lactic acid), (PLLA), poly(aspartic acid) (PASP), polystyrene (PST), poly(methyl methacrylate) (PMMA), poly(4-vinyl pyridine), and various polyacrylates [50,51]. Micelle formation has also been achieved using tri-block copolymers and graft copolymers, which offer unique benefits for drug delivery and gene transfer applications, such as modulating drug release, extending circulation time, and incorporating targeting groups. For instance, ABC-type triblock copolymers made up of monomethoxy-PEG, poly(2-(dimethylamino) ethyl methacrylate), poly(2-(diethylamino)ethyl methacrylate), as well as amphiphilic derivatives of PEO with poly(propylene oxide) (PPO) like Pluronics®, and poly (amino acid) block copolymers have been utilized for micelle formation. Furthermore, recent studies have reported using tetra- or penta-block copolymers for micelle formation [52].

Formation of the polymeric micelles has occurred through the self-assembly of amphiphilic block copolymers in a selective solvent. The hydrophobic block will aggregate to form the micelle core, while the hydrophilic block will form the micelle corona. When the block copolymer is dissolved in a selective solvent, the hydrophobic blocks come together to minimize their contact with the solvent, forming the micelle core. The hydrophilic blocks extend outwards to form the micelle corona, which provides stability by preventing the hydrophobic core from aggregating with other micelles or with the solvent. The formation of polymeric micelles can be further facilitated by applying energy to the system, such as sonication or gentle stirring, which can accelerate the self-assembly process. The size and shape of the resulting micelles depend on various factors, including the size and composition of the block copolymer, the solvent quality, and the concentration of the block copolymer [53–55]. Critical micelle concentration (CMC) is a term used to describe the concentration of amphiphilic molecules in a solution at which micelle formation begins to occur. In aqueous solutions, amphiphilic molecules can self-assemble into aggregates called micelles, in which the hydrophobic tails cluster together to form the micelle core while the hydrophilic heads are exposed to the surrounding solution. At concentrations below the CMC, amphiphilic molecules exist as monomers, but as the concentration of surfactant is increased, the hydrophobic tails begin to interact with one another to form micelles. The CMC is the point at which the free energy of micelle formation is minimized, and above this concentration, further increases in

amphiphilic molecules concentration will result in the growth of existing micelles rather than the formation of new ones. (Figure 1.4).

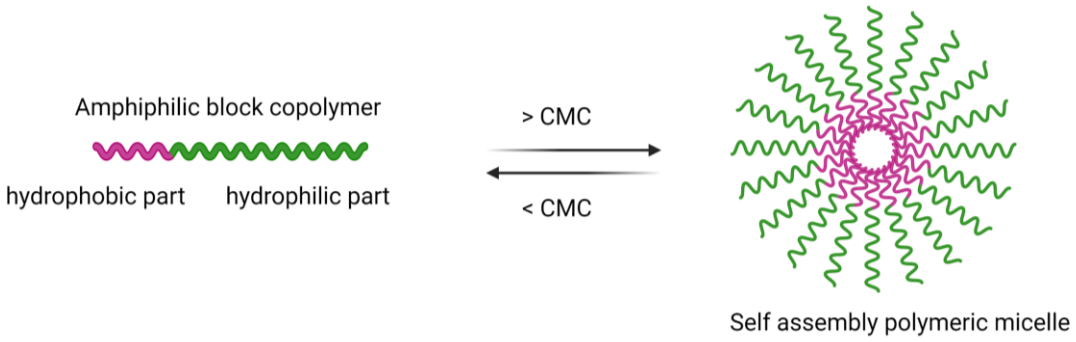

Figure 1.4 Schematic representation of polymeric micelle formation

Polymeric micelles can be designed based on their ability to react to environmental stimuli, including temperature, pH, or ionic strength. Stimulus-sensitive polymeric micelles can be engineered to release drugs in a controlled and targeted manner, and the stimulus-sensitive nature of these polymeric micelles makes them useful for different applications such as drug delivery, imaging, and biosensors [56].

Several types of stimuli-responsive polymeric micelles could be broadly classified as pH-responsive, temperature-responsive, redox-responsive, light-responsive, and enzyme-responsive, which are demonstrated in Figure 1.5. pH-responsive micelles are designed to respond to alterations in pH, such as the acidic environment of tumors. They typically contain acidic or basic groups that can undergo ionization in response to alteration in pH, leading to changes in the micelle structure and drug release [57]. Temperature-responsive micelles are formed responding to changes in temperature, such as the elevated temperatures found in tumors. They typically contain polymers that have lower critical solution temperature (LCST), or upper critical solution temperature (UCST) features that can undergo a phase transition at a specific temperature, leading to changes in the micelle structure and drug release [58]. Redox-responsive micelles are formed responding to alteration in the redox environment, including the high glutathione levels in tumor cells. They typically contain disulfide bonds that can be cleaved by reducing agents, leading to changes in the micelle structure and drug release [59]. Light-responsive micelles are designed to respond to light, including near-infrared light, which can penetrate deep into tissues. They typically contain photoresponsive groups, such as

azobenzene or spiropyran, that can undergo reversible isomerization in response to light, leading to changes in the micelle structure and drug release [60]. Lastly, enzyme-responsive micelles are designed to respond to certain enzymes. For example, micelles can be functionalized with specific enzymes that cleave the polymer backbone, causing the micelles to release their cargo in response to enzymatic activity [61].

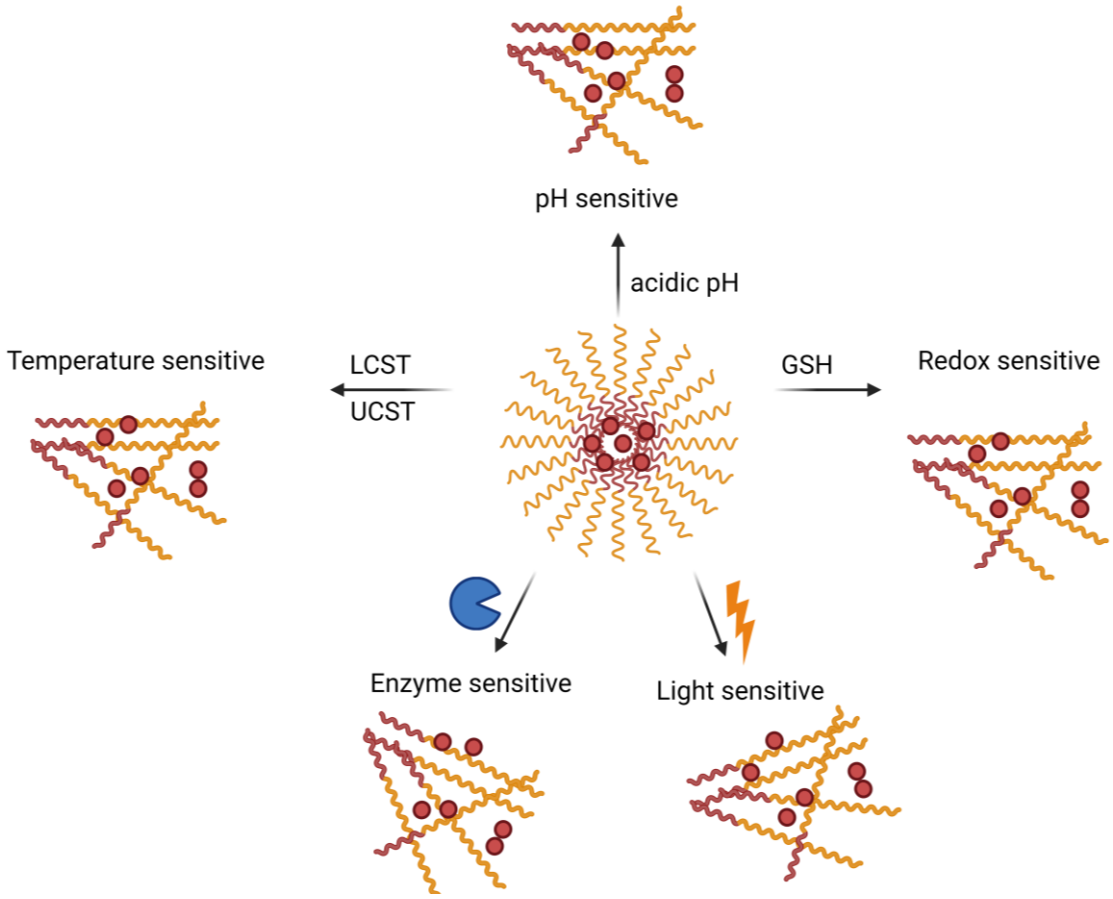

Figure 1.5 Schematic representation of stimuli-responsive micelles

While self-assembled micelles have advantages like ease of preparation and versatility in drug loading, they also have some limitations. Firstly, self-assembled micelles have limited stability, especially in biological environments where they can be susceptible to degradation and dissociation, resulting in premature drug release. Also, they have limited loading capacity for hydrophobic drugs because of the small size of the micelle core, and this limits their use for drug delivery applications that require high drug loading. Moreover, they typically exhibit fast drug release kinetics, which may not be suitable for sustained drug delivery applications [62].

1.2.3.1.1 Cross-linked Micelles (CMs)

New approaches are being developed to improve the stability and efficacy of polymeric micelles in order to improve their potential as effective drug delivery vehicles. The development of CMs could be attributed to the limitations of self-assembled micelles with respect to stability. CMs are a type of polymeric micelles in which the hydrophobic core or hydrophilic shell, or intermediate layer of the micelle, is cross-linked, providing improved stability and control over drug release. Crosslinking can be achieved by incorporating a crosslinking agent, which creates covalent bonds between the polymer chains in the core or shell of the micelle. This provides a more robust structure, with the cross-linked core providing improved mechanical strength and disassembly resistance under physiological conditions. CMs have given promise as drug-delivery vehicles because of their improved stability, longer circulation time, and better targeting capabilities [63].

Various methods have been provided to create stable micellar structures, including cross-linking techniques. One such method involves using bifunctional agents to cross-link pre-formed micelles and produces CMs. In addition to post-assembly cross-linking methods, CMs can be prepared by utilizing bifunctional agents in their monomeric form during polymerization. This entails the incorporation of the bifunctional agent into the micelle structure, facilitating the formation of CMs.

Based on various chemical approaches, several methods have been reported to prepare CMs. To give details about them, firstly, alkyne-azide click chemistry is very commonly used, and it involves the reaction between an alkyne and an azide group in the presence of a copper catalyst, resulting in the formation of a triazole linkage. Michael addition is another chemical approach involving the reaction between a nucleophile and a Michael acceptor, which leads to forming a carbon-carbon bond. Also, the amidation or esterification approach, which involves the reaction between a carboxylic acid or its derivative and an amine or alcohol also utilized for preparing CMs [64]. Lastly, with radical polymerization, which is one of the standard approaches, CMs can be formed as a result of the interaction of the polymerizable groups in the core or shell part of the amphiphilic block copolymer with the crosslinker. In this method, the amphiphilic block copolymer is first self-assembled into micelles in an aqueous solution. Once the micelles are formed, a crosslinking agent containing polymerizable groups is added to the reaction mixture, then a free radical initiator or a photo-initiator is added to this solution. The polymerizable groups in the crosslinking agent then react with each other in a radical

polymerization reaction, forming a covalent bond and crosslinking the core of the micelle. The resulting CMs have improved stability and mechanical strength compared to non-CMs. Different chemical approaches have been employed for radical polymerization in CMs, including photopolymerization using UV light or visible light, as well as free radical polymerization using a variety of initiators such as azobisisobutyronitrile (AIBN) or benzoyl peroxide (BPO) [65,66].

CMs could also be designed as stimuli-responsive, which makes their properties or behavior triggered by certain external stimuli such as changes in temperature, pH, or light-like self-assembly micelles. This is achieved by incorporating stimuli-sensitive components into either core or corona part of micelles, which can undergo conformational changes or disassembly/reassembly upon exposure to the stimuli. Cleavable systems for drug delivery, such as those used in CMs, provide numerous advantages compared to fixed drug delivery systems. Firstly, cleavable systems could be designed to release the loaded drug in a controlled manner in respond to various stimuli, such as pH, redox, or enzymatic milieu, which can improve their safety and efficacy. This allows for a more targeted drug release and can reduce the potential for off-target effects or toxicity. Also, they are biodegradable and can be broken down into non-toxic components, reducing the accumulation of drug delivery vehicles in the body and potentially minimizing side effects. Furthermore, they can be designed to release their payload more rapidly than fixed systems, providing faster therapeutic effects. Lastly, they can be engineered to respond to different stimuli depending on the target tissue or disease state. This allows a more personalized approach to drug delivery and can improve the specificity and effectiveness of treatment [67–69].

CMs can be classified as core and shell CMs (Figure 1.6). Different studies have proposed different locations for cross-linking, with some advocating core cross-linking and others favoring shell cross-linking. The options rely on numerous factors, including the drug encapsulation method and chemistry and the type of block copolymers used. While shell cross-linking can prevent premature drug release, it may also cause rigidity, which could limit the particle's "stealth" feature during blood circulation. On the other hand, core cross-linking may be preferable since it does not affect surface properties but may not be as effective in retaining the drug. For this reason, in this thesis, we preferred to cross-link the core part of our micelles [70,71].

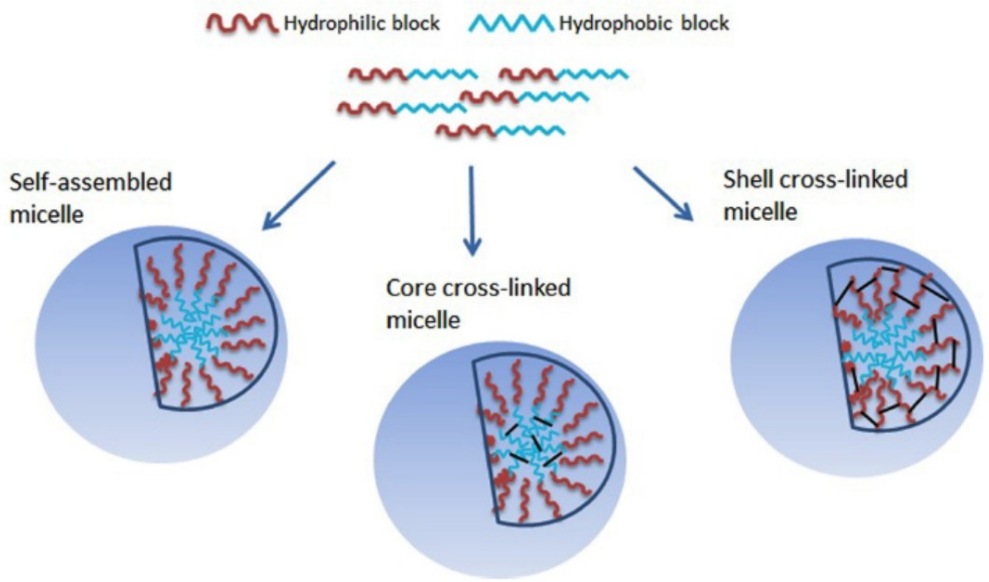

Figure 1.6 Formation of self-assembled, core cross-linked, and shell cross-linked micelles

1.2.3.1.1.1 Core Cross-linked Micelles (CCMs)

CCMs are a type of micelle structure that is stabilized by covalent bonds among the polymer chains in the core of the micelle. These covalent bonds, or cross-links, help to prevent the micelle from breaking down or disassembling over time. This makes CCMs more stable and useful than traditional micelles in several applications, including drug delivery, imaging, and sensing. Di- or triblock copolymers are commonly used to prepare CCMs. The copolymer's hydrophobic block(s) form the micelle's core, while the hydrophilic block(s) form the corona, which surrounds the core and stabilizes the micelle in water. Cross-linking of the core might be achieved using several methods, including photochemical cross-linking, chemical cross-linking, and enzymatic cross-linking using a bifunctional agent, radical polymerization, and disulfide bonds. The cross-linked region can be the core or a specific interface layer between the core and the shell [72,73].

Core Cross-linking by Bifunctional Agents

CMs can be obtained by using molecules with two reactive functional groups where the core forming block of the micelle has reactive functional groups. It is important that the reactive groups of the polymers remain stable throughout the polymerization process and have enough hydrophobicity to ensure the stability of the micelles. Common bifunctional agents used in CCM synthesis include divinyl benzene (DVB), which can react with the vinyl groups of the core-forming monomers; N, N'-methylene bis (acrylamide) (MBA), which can react with the shell-forming monomers; epoxy-carrying

acrylates which can react with diamines [74,75]. Other bifunctional agents that have been used in CCM synthesis include diacrylate monomers, such as ethylene glycol diacrylate (EGDA) and poly(ethylene glycol) diacrylate (PEGDA), ethylenediamine, hexamethylene diamine which can crosslink the core and shell of the micelle through the formation of covalent bonds [76,77].

Core Cross-linking by Reducible Disulfide Bonds

The usage of reducible disulfide bonds to obtain CCMs is a method for creating CMs that involve disulfide-containing cross-linkers. In this method, a core-forming monomer is polymerized to form the core of the micelle. Then, a disulfide group crosslinker is added to the reaction mixture, and it reacts with the core-forming polymer chains to form cross-linked structures through disulfide bond formation. The disulfide bonds are able to be reduced using a reducing agent, such as dithiothreitol (DTT), which cleaves the disulfide bond and releases the cross-linked micelle. The advantage of using disulfide bonds for cross-linking is that they can be cleaved in the presence of reducing agents, which can be useful for triggered drug release or other applications. Disulfide-containing cross-linkers can be synthesized using simple and inexpensive reactions, making them attractive for large-scale production. However, disulfide bonds can also be susceptible to cleavage in the presence of reactive oxygen species, leading to premature micelle structure degradation [78,79].

Core Cross-linking by Controlled Polymerization

In this method, a core-forming monomer is polymerized using a controlled polymerization technique to form the core of the micelle. Then, a cross-linker with reactive functional groups is added to the reaction mixture, which can react with the core-forming polymer chains to form cross-linked structures. The micelle shell can then be formed by polymerizing shell-forming monomers around the cross-linked core.

The advantage of using controlled polymerization techniques is that they allow for precise control over the molecular weight and dispersity of the polymer chains and the ability to incorporate functional groups or other additives into the polymer structure. This can result in CCMs with well-defined structures and properties. Atom transfer radical polymerization (ATRP) and Reversible addition-fragmentation chain transfer **(**RAFT) polymerizations are more well-accepted polymerization techniques to synthesize CMs. ATRP consists of the use of a transition metal catalyst to control the polymerization of monomers and provide to synthesize block copolymers with precise molecular weights and compositions [80].

RAFT polymerization is a technique of controlled radical polymerization that enables synthesizing of block copolymers with well-defined molecular weights and narrow molecular weight distributions. In this technique, a chain transfer agent (CTA) is used to control the polymerization of monomers. The RAFT process begins with forming a reversible complex between the CTA and a free radical initiator, allowing the controlled initiation of polymerization. The monomers are then added to the reaction mixture, and the polymerization proceeds in a controlled manner, with the CTA controlling the chain length of the growing polymer chain. During the polymerization, the CTA is transferred between the growing polymer chains, which allows forming of block copolymers with well-defined block lengths and compositions. The CTA can also be used to control the polymer chains' molecular weight and the resulting polymer's dispersity [81,82]. (Figure 1.7).

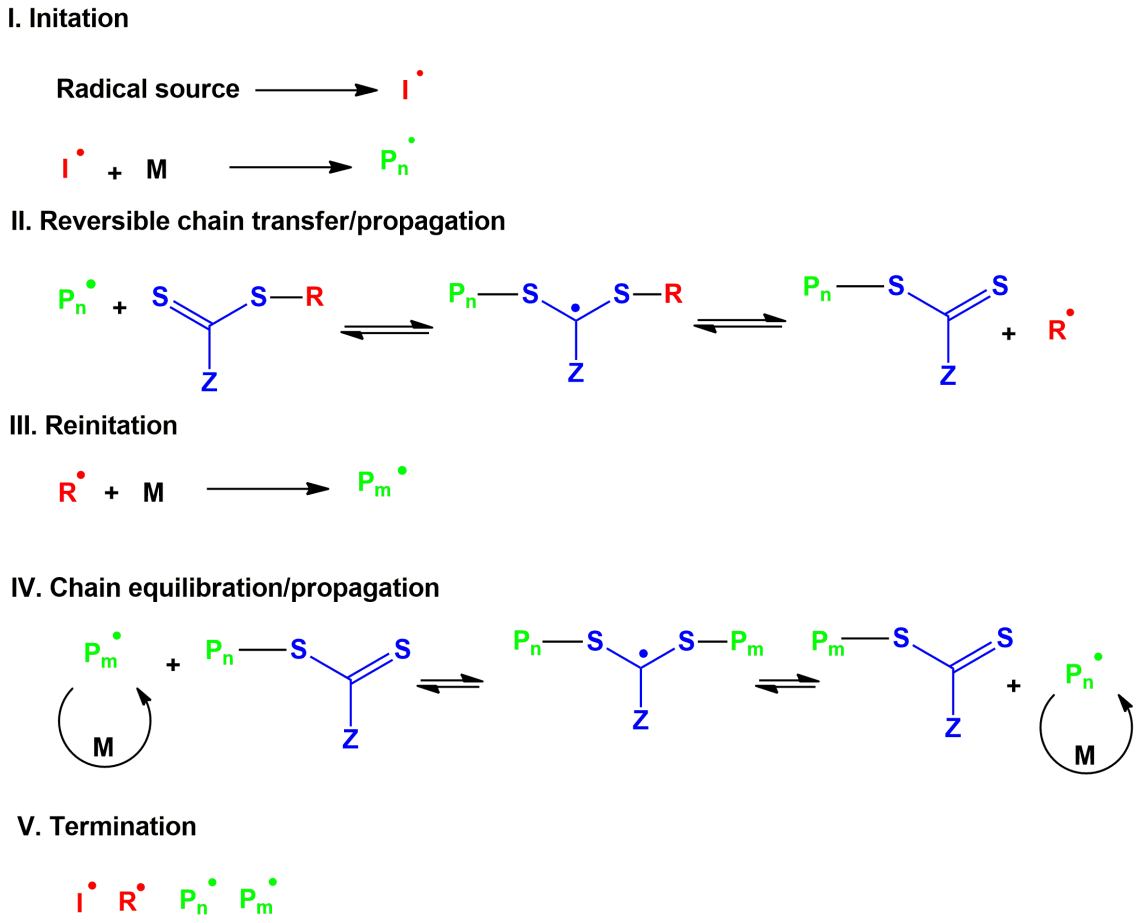

Figure 1.7 Proposed mechanism of reversible addition-fragmentation chain transfer polymerization [83]

RAFT polymerization offers numerous advantages compared to other polymerization techniques. Firstly, it provides for the synthesis of polymers with well-defined molecular weights, narrow molecular weight distributions, and controlled polymer chain architectures, enabling the synthesis of polymers with precise properties and functionalities, which is important for many applications. A wide range of monomers can be used to polymerize, including hydrophobic and hydrophilic monomers, which makes it a versatile technique that can be used to tailor the properties of the resulting polymer for specific applications, especially in drug delivery. Also, it can be carried out under mild reaction conditions and with various solvents, making it a convenient technique for many applications. Furthermore, it is tolerant to a wide range of functional groups such as vinyl, dienes, acrylamide, and methacrylamide, providing for the synthesis of polymers with diverse functionalities, and it can be easily scaled up for industrial production, making it a useful technique for large-scale polymer synthesis [83].

RAFT polymerization has the advantage of being able to tolerate a wide range of functional groups as substituents on 'R' or 'Z' groups. Retaining thiocarbonylthio groups in the polymeric product is a crucial feature of RAFT polymerization that allows for synthesizing block copolymers and end-functional polymers. However, the presence of these groups can be disadvantageous for some applications, and their removal or transformation is important for many polymer synthesis. Various methods, including reactions with nucleophiles and ionic reducing agents, oxidation, UV irradiation, thermolysis, and radical-induced reactions, can transform or remove the thiocarbonylthio group. Certain thiocarbonylthio groups can also be switched to enable control over the polymerization of a broader range of monomers in the RAFT process or used directly in other forms of radical polymerization like ATRP or Nitroxide-Mediated Polymerization (NMP) (Figure 1.8) [84].

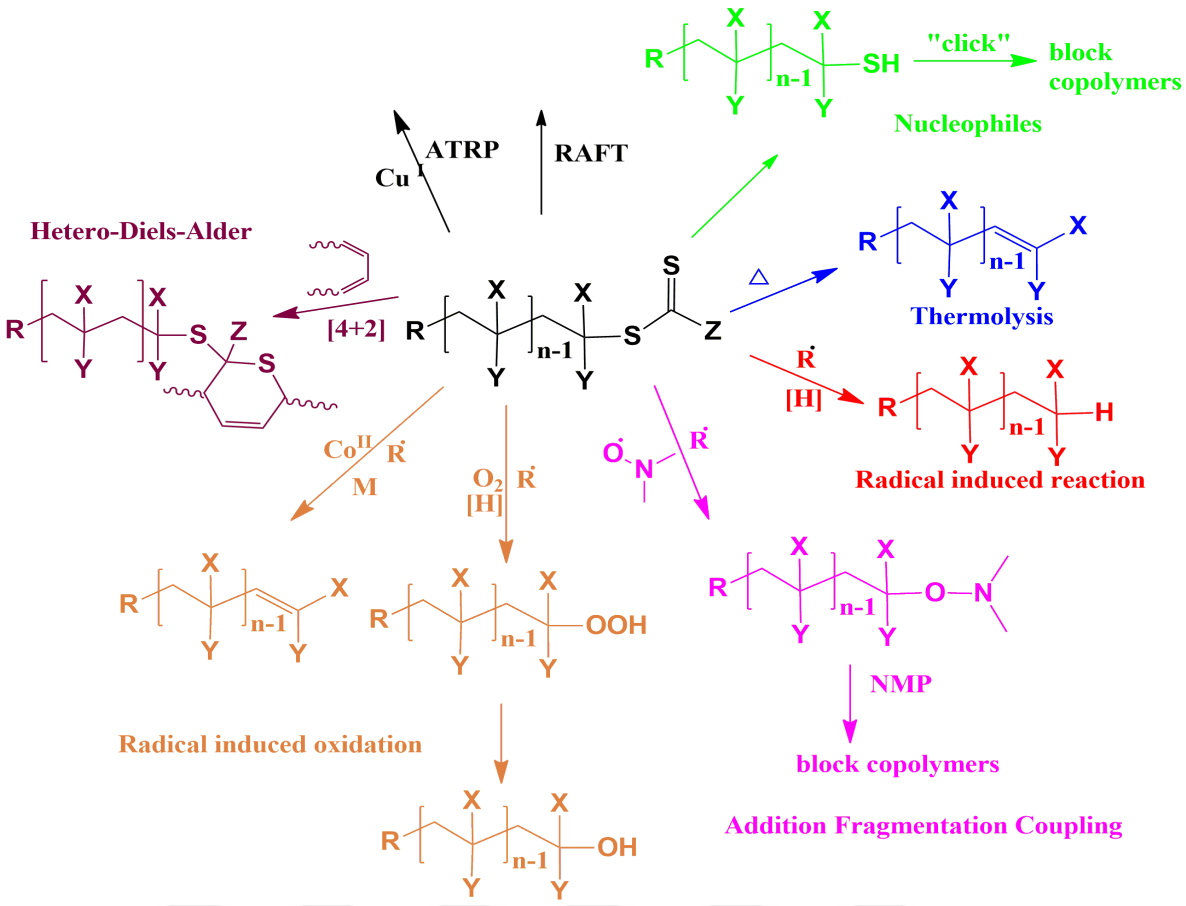

Figure 1.8 RAFT end-group transformation methods [84]

CCMs can be synthesized through (RAFT) polymerization. This technique uses a bifunctional RAFT agent with a hydrophobic and hydrophilic moiety to initiate the polymerization of hydrophobic monomers. The hydrophobic core-forming block is cross-linked through a difunctional crosslinker, which leads to the formation of a stable core. The hydrophilic shell-forming block is then added to the system to form the outer layer of the micelle. The cross-linking in the core of the micelle enhances the stability of the resulting structure and prevents the dissociation of the micelles under physiological conditions [85,86].

The synthesis of CCMs using degradable crosslinkers represents an important strategy in the design of drug delivery systems. By incorporating crosslinkers that can be degraded under physiological conditions, such as acetal- or ketal-based linkages, these micelles can disassemble and release their encapsulated cargo in response to specific triggers, such as changes in pH and redox potential. Several well-known pH-sensitive bonds exist, such as imine, hydrazone, oxime imine, and ortho ester bonds. These bonds have been extensively utilized in the development of drug delivery systems due to their

ability to allow targeted drug release based on variations in pH, which frequently occur in various physiological and pathological settings such as tumor microenvironments and inflammation (Table 1.2.) [87,88].

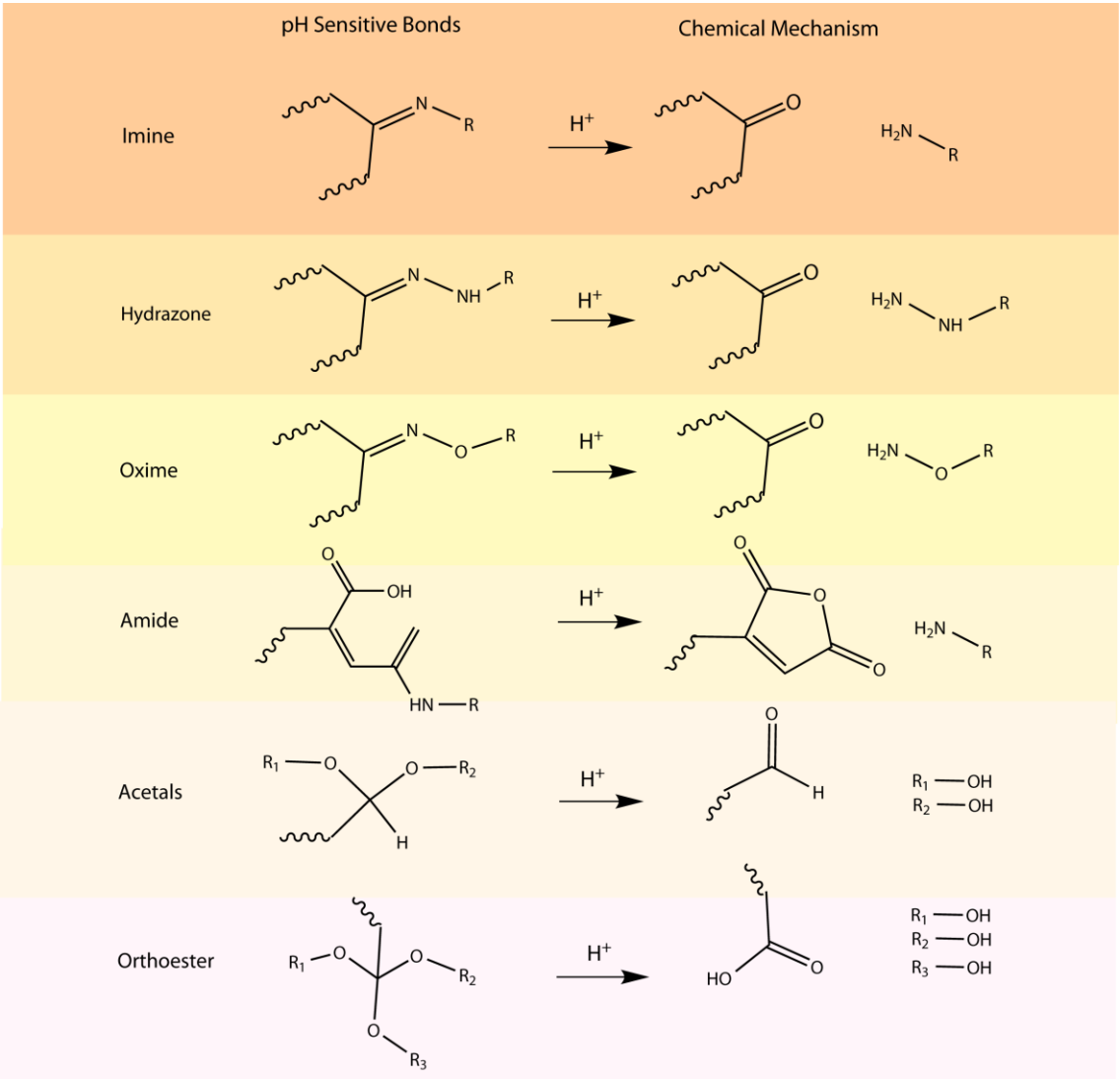

Table 1.2 pH-sensitive chemical bonds and release mechanisms in acidic conditions

Given more details, *imine bonds* are formed between a primary amine and a carbonyl group. Imine CMs can be synthesized by crosslinking polymers such as PEG or poly(L-lysine) with an imine-containing crosslinker, such as glutaraldehyde. *Hydrazone bonds* are formed between a hydrazide and a carbonyl group. Hydrazone CMs can be synthesized by crosslinking polymers such as PEG or poly(L-lysine) with a hydrazone-containing crosslinker, such as adipic acid dihydrazide. *Oxime bonds* are formed between a hydroxylamine and a carbonyl group. Oxime CMs can be synthesized by crosslinking

polymers such as PEG or poly(L-lysine) with an oxime-containing crosslinker 2,5-dioxopyrrolidin-1-yl-4-aminobenzaldehyde. *Amide bonds* are formed between a carboxylic acid and an amine. The stability of the amide bond is pH-dependent, and amide-CMs can be cleaved under acidic conditions. Amide CMs can be synthesized by crosslinking polymers such as PEG or poly(L-lysine) with an amide-containing crosslinker, such as N, N'-carbonyldiimidazole (CDI). *Acetal bonds* are formed between an alcohol and an aldehyde or ketone. Acetal CMs can be synthesized by crosslinking polymers such as PEG or PLA with an acetal-containing crosslinker, such as glyoxal-bis(2-hydroxyanil). *Orthoester bonds* are formed between an alcohol and an orthoester. Orthoester CMs can be synthesized by crosslinking polymers such as PEG or PLA with an orthoester-containing crosslinker, such as dimethyl orthoester bonds. All of the bonds mentioned above can be pH-sensitive, as the stability of the acetal bond is pH-dependent. Besides the pH-sensitive bond, several well-known redox-sensitive bonds exist, such as disulfide, selenoether, thioether, and boronic ester, aryl sulfonate ester bonds. These bonds also have been extensively utilized in developing drug delivery systems due to their ability to allow targeted drug release based on variations in redox. Given more details about them, *disulfide bonds* are formed between two cysteine residues, which are amino acids that contain a thiol (-SH) group. Disulfide bonds are cleaved by reducing agents, such as glutathione or cysteine, which react with the sulfur atoms in the disulfide bond to break it apart and form two thiol groups. Disulfide bonds can be incorporated into the crosslinker or the polymer backbone to create a redox-responsive system in CCMs *Selenoether bonds* are similar to disulfide bonds but are formed between a selenium atom and a carbon atom. Selenoether bonds are more stable than disulfide bonds in the presence of reducing agents due to the Se-C bond's higher dissociation energy than the S-C bond. Selenoether bonds can be cleaved by reducing agents, such as thiols or dithiothreitol (DTT), which react with the selenium atom to break the bond. *Thioether bonds* are formed between a sulfur atom and a carbon atom. Thioether bonds can be cleaved by reducing agents, such as DTT, which react with the sulfur atom to break the bond. Thioether bonds are more stable than disulfide bonds but can still be cleaved under reducing conditions. *Boronic ester* bonds are formed between a boron atom and an oxygen atom. Boronic ester bonds can be cleaved by hydrogen peroxide or other oxidizing agents, which react with the boron atom to break the bond. Boronic ester bonds are stable under reducing conditions but sensitive to oxidizing agents. *Aryl sulfonate* ester bonds are formed between an aryl sulfonate group and an alcohol group. Aryl sulfonate ester bonds can be

cleaved by electron-rich thiols or other reducing agents, which react with the aryl sulfonate group to break the bond. Aryl sulfonate ester bonds are stable under oxidizing conditions but sensitive to reducing agents.

1.3 Targeting Approaches in Nanoparticle-based Carriers

In order to develop effective cancer treatments, it is crucial to find ways to specifically target cancer cells while minimizing damage to healthy cells. Nanoparticles can be targeted to specific cells, tissues, or organs in several ways. This targeting can be achieved with passive or active targeting. Passive targeting approaches rely on the Enhanced Permeability and Retention (EPR) effect that allows nanoparticles to accumulate in the tumor tissue due to the leaky vasculature and poor lymphatic drainage in tumors. However, the extent to which nanoparticles can accumulate in tumors passively can vary depending on several factors, such as the size, shape, and surface charge of the nanoparticles and the specific characteristics of the tumor microenvironment. Some nanoparticles may not be able to penetrate the tumor tissue effectively or may be cleared from the body too quickly, leading to suboptimal drug delivery outcomes. Therefore, while passive targeting can be an effective strategy for drug delivery, it may not always be sufficient to achieve optimal results, and active targeting approaches may be needed to improve drug delivery specificity and efficacy [89–91].

At this point, active targeting approaches have been developed to improve drug delivery specificity and efficacy. These approaches refer to modifying the surface of the nanoparticles with ligands, which are molecules that specifically recognize and bind to receptors or other biomolecules on the target cells. These ligands can be antibodies, peptides, or other small molecules based on the molecular markers that are overexpressed or selectively expressed on the surface of the target cells and have high affinity and specificity for the target [92,93].

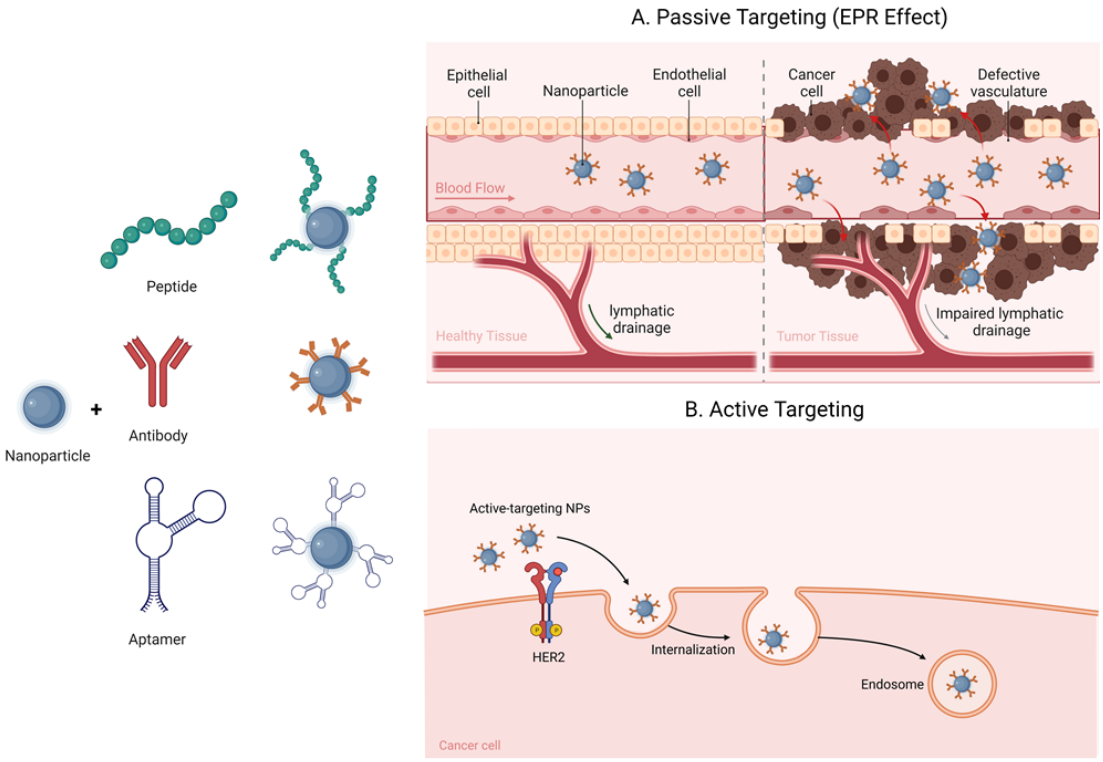

Figure 1.9 Passive drug targeting by enhanced permeation and retention (EPR) effect (active drug targeting) (B)

Active targeting can enable the delivery of therapeutic agents specifically to target cells, tissues, or organs while avoiding healthy tissues, thereby reducing the risk of side effects. Also, it can enhance the uptake of nanoparticles by the target cells, tissues, or organs, resulting in improved treatment outcomes. Moreover, active targeting can deliver multiple therapeutic agents, including drugs, genes, and imaging agents, in a single nanoparticle system, allowing more comprehensive treatment. While active targeting of nanoparticles has many advantages, it also has disadvantages. One of the main disadvantages is that the heterogeneity of the tumor microenvironment can affect the specificity and selectivity of targeting. Tumor cells can undergo genetic mutations, leading to changes in the expression of surface receptors or other biomolecules targeted by the ligands on the nanoparticle surface. This can result in decreased binding affinity and specificity, reducing the efficacy of the treatment. Another disadvantage is the potential immune response to the nanoparticle surface ligands. The body's immune system can recognize the foreign ligands on the surface of nanoparticles, leading to an immune response that can neutralize or clear the nanoparticles from the body before they

reach their intended target. Finally, active targeting can also increase the complexity and cost of nanoparticle development and production, as specific ligands must be identified and conjugated to the nanoparticle surface. This can also increase the time and regulatory requirements for clinical translation and approval. While active targeting may have some limitations and challenges, its potential advantages in improving treatment outcomes and reducing side effects make it a promising approach for developing targeted nanoparticle-based cancer therapies [94–96].

Several studies have investigated the potential of actively targeted nanoparticles for cancer therapy. One of the well-known approaches for breast cancer treatment is the development of nanoparticles functionalized with antibodies, peptides, and aptamers that target the HER2 receptors overexpressed on certain types of breast cancer cells. These nanoparticles have been promising to selectively deliver chemotherapy drugs or other therapeutic agents to HER2-positive cancer cells while minimizing exposure to healthy cells that do not overexpress HER2 receptors [6]. Also, another strategy is developing folate ligands functionalized nanoparticles for treating ovarian cancer. Folate receptors are overexpressed on the surface of ovarian cancer cells, and by using folate ligands as targeting moieties, these nanoparticles can enhance the uptake of therapeutic agents into the cancer cells, leading to improved treatment outcomes [97,98].

Chapter 2

PEG-based, HER2-targeted, Degradable CCMs for Specific and Dual pH-sensitive DOX Release

2.1 Introduction

Today, using nanocarriers (NCs) in cancer treatment is advantageous due to their passive and active targeting [99,100]. Polymeric micelles, which are formed by the physical association of amphiphilic block copolymers, are prone to disassemble with dilution when introduced into the blood, causing premature drug release. In order to solve this problem and increase the micelle's stability, cross-linking the core or shell parts of the micelle has emerged as an effective strategy [63,101–103]. Also, premature drug release from the micelles is still a problem in case the drug is loaded by the incubation method, which is occurred due to the weak physical interactions between the drug and the micelles. Therefore, many studies show that the chemical conjugation between the drug and the CCMs can increase both stability and drug retention in the nanocarriers [104,105]. pH variation through the body and cell compartments is a prominent environmental factor to be used for targeting specific regions with micelles having stimuli-sensitive groups. CMs can be designed as "smart" so that they can be disrupted in the acidic pH of the cell while they are stable in the physiological environment, which can provide pH-sensitive drug release [85]. This can be achieved using degradable bonds or stimuli-responsive polymeric blocks in the structure of micelle NCs [106]. In cancer cell targeting, acid sensitive bonds, which are acetal or hydrazone bonds, degradeding at acidic pH values can be very convenient since these bonds can allow the dissociation of nanocarrier and releasing the drug molecules in lysosomes or endosomes of cancer cells [106–108]. It was shown that micelles cross-linked with acid

degradable agents' exhibit much faster mode of action against cancer cells compared to the micelles cross-linked with non-degradable agents.

In order to reach multifunctionality with a nanocarrier, it can be conjugated with a targeting molecule so that it can selectively bind to target cells [109]. To do this, specific ligands that recognize cancer cells can be chemically incorporated into the nanocarrier, resulting in more selective drug release than conventional chemotherapy [110,111]. Whereby; a higher amount of cytotoxic agent reaches the tumor site, and peripheral toxicity is minimized.

Herein, in this chapter, we aimed to design a system comprising all required characteristics, such as selectivity, stability, facilitated drug release behavior, and safety, with one nanocarrier. To achieve this, we prepared breast cancer-targeted CCMs with double-moiety pH-sensitivity (degradability) in which the drug is conjugated to the polymer with pH-sensitive hydrazone bonds, and the micelle is core cross-linked with pH-sensitive acetal bonds. For the preparation of the micelles, we firstly synthesized the initial oligo ethylene glycol methyl ether methacrylate (OEGMA) block by RAFT polymerization as the outer shell of micellar nanocarrier, and then, it was copolymerized with diethylene glycol methyl ether methacrylate (DEGMA) and 4-vinyl pyridine (4-VP) that will form the core of the micelle. To obtain CCMs, we used an acid-sensitive cross-linker, which allows micelle formation during copolymerization in one pot. HER2-specific peptide (VSSTQDFP) [112,113] was conjugated to the shell of the micelle as the targeting moiety, while doxorubicin (DOX) was bound with acid-degradable acetal bonds to the micelle as the model drug against breast cancer cells.

2.2 Material Methods

2.2.1 Materials

Oligoethyleneglycol methyl ether methacrylate (OEGMA, Mn= 500 g/mol), diethylene glycol methyl ether methacrylate (DEGMA), 4-vinyl pyridine (4-VP), 2,2-dimethoxy propane (DMAEP), 2-hydroxyethyl methacrylate (HEMA), p-toluenesulfonic acid monohydrate (p-TSA.H2O), tris(2-carboxyethyl)phosphine (TCEP) hydrochloride, doxorubicin hydrochloride, 2,2-dithiodipyridine (DTDP), ethanolamine (ETA), 4-cyano-4-(thiobenzoylthio)pentanoic acid (CTA), azobisisobutyronitrile (AIBN), 4,4-Azobis(4-cyano valeric acid) (ACVA), triethylamine (TEA), Nε-maleimidocaproic acid hydrazide

(EMCH), trifluoroacetic acid (TFA) salt, N-(3-dimethylaminopropyl)-N′-ethylcarbodiimide hydrochloride (EDC), N,N-diisopropyethylamine (DIPEA) and 1-hydroxybenzotriazole hydrate (HOBT) were purchased from Aldrich and used as received. A synthetic peptide (VSSTQDF) was purchased from CASLO Laboratory ApS. Pierce Quantitative Fluorometric Peptide Assay was purchased from Thermo Scientific.

2.2.2 Methods

2.2.2.1 Synthesis of CCMs

As an initial step, OEGMA (Mn: 500) was polymerized in reactors capped with septa cap for 30 min at 70 °C under nitrogen gas in dimethyl formamide (DMF) using ACVA as an initiator in the presence of RAFT agent. The resulting polymer was purified by precipitation from diethyl ether three times. In order to demonstrate that the reaction followed the RAFT polymerization, a certain amount of samples was taken from the reaction medium with a syringe during polymerization, and these samples were used for gravimetric and molecular weight analyzes [114]. For molecular weight and conversion determination, NMR spectroscopy was not preferred because of difficulties due to the presence of solvent in samples taken during the reaction without purification. For the molecular weight test, samples were taken from the reaction medium for a certain period of time. The amount of polymer obtained and molecular weights of each sample were determined by Gel Permeation Chromatography (GPC). According to GPC analysis results, the molecular weight-conversion relationship and reaction kinetics were determined by plotting ln $[M]_0$ / ln $[M]_t$ – time and molecular weight-conversion plots. The ratio of initial concentrations of monomer / CTA / initiator ratio in which the reaction was performed according to the RAFT mechanism was determined, and the copolymer synthesis was continued with this ratio. Furthermore, since the RAFT functionality is important in the copolymerization, the conversion in macroCTA synthesis was kept low (example of the 2nd hour), ring protons appearing at 7.84, 7.48, and 7.32 ppm in the ^{1}H-NMR spectra where the functionality is approximately 60-70% and the agent appearing at around 2.2 ppm carboxyl group adjacent to $–CH_2$ protons were determined by the integration of peaks.

Secondly, the acid-sensitive crosslinker (2,2-dimethacryloxy-1-ethoxypropane) was used in the copolymerization, and the CCMs were synthesized as given in the literature [115]. For this purpose, a mixture of HEMA (0.1 mmol), 2,2, -dimethoxy propane (0.05 mmol), and p-TSA (5.10-4 mmol) was stirred at room temperature for 15 hours. The product

obtained was purified by silica gel chromatography using hexane-ethyl acetate, triethylamine as a mobile phase, and silica gel as the stationary phase. The solvent was removed by a rotary evaporator from the fractions determined by Thin Layer Chromatography (TLC) containing the crosslinker, and the product was obtained. The pure material was characterized by ^{1}H-NMR and ^{1}C-NMR spectra (NMR, Bruker 400, EU-TAUM). The following step was the preparation of CCMs by RAFT polymerization. To synthesize the micelle, macroCTA was dissolved in 5 ml water, and then varying amounts of 4-VP (1.0-0.25 mmol) and DEGMA (1.0-0.3 mmol) together with CL (1-10% mmol) were added. The reaction was performed overnight at 60°C using ACVA as the initiator (Figure 2.1). The formation of the CCMs was also confirmed by the turbidity formed in the solution. After the overnight reaction, the solution was dialyzed against water to remove the unreacted substances. The chemical structures of purified copolymer micelles were characterized by FTIR and ^{1}H-NMR spectroscopies, while the size and size distribution of the samples were determined by dynamic light scattering spectroscopy. Selected samples, which are CCM2 and CCM5, were analyzed by TEM to examine sizes and morphologies.

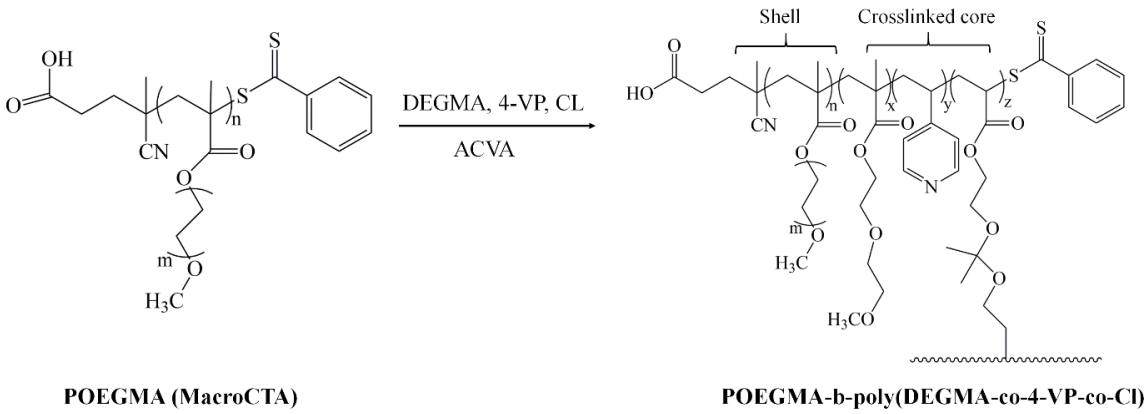

Figure 2.1 Synthesis of CCMs by RAFT polymerization using MacroCTA

2.2.2.2 Preparation of Drug Conjugated and Targeted CCMs

2.2.2.2.1 Pyridyl Disulfide (PDS) Modification of CCMs

PDS modification of the CCM through its core region for conjugation of the drug molecule was carried out according to the procedure in the literature [116]. Briefly, 500

mg of CCM2 and dithiodipyridine (70 mg, $3.2x10^{-4}$ mol) were dissolved in DMF (2 ml). The vial was sealed by rubber septum and purged with N_2 for 10 min. Ethanolamine (36.37 mg, $6.0x10^{-4}$ mol) was dissolved in DMF (1 ml), and 150 µl of this solution was added to the vial under N_2. The mixture was stirred at room temperature for 4 hours. The yellow-colored mixture was precipitated from cold diethyl ether and dried under a vacuum. The product was dissolved in water and then dialyzed against water/methanol (50:50) and only water, respectively. The product given in Figure 2.2 was lyophilized and examined by the ^{1}H-NMR spectrum.

2.2.2.2.2 Maleimide-Modified DOX (MALDOX) Synthesis

To synthesize maleimide-functionalized DOX, first, DOX.HCl (30.2 mg, 0.052mol) was neutralized with triethylamine (15.8 mg, 0.156mol). The mixture was dialyzed against water to remove redundant unreacted triethylamine, and then, the DOX solution was lyophilized. Following this, DOX (12 mg, 2.07×10^{-5}) mol and EMCH (14 mg, $4.1x10^{-5}$ mol) were dissolved in dry methanol (6 ml), and a few drops of trifluoroacetic acid (TFA) was added. The mixture was stirred overnight in the dark, and then methanol was removed using a rotary evaporator. The remaining mixture was precipitated using dry ethyl acetate. The final product (MALDOX) was stored under a vacuum. The pure sample was analyzed by ^{1}H-NMR and high-resolution MALDI-TOF mass spectrometers [105].

2.2.2.2.3 HER-2 Specific Peptide Conjugation

For peptide incorporation to the shell part of the CCM2, first, 100 mg of CCM2 was dissolved in 3 ml of DMSO/DMF (3:1) mixture, stirred at 60°C overnight, and the sample was taken from the oil bath and cooled to 25°C. EDC (3.07 mg), HOBT (2.23 mg), DIPEA (4.18 µl), and peptide (14.08 mg, VSSTQDFP) were added to this mixture and stirred at 60°C for two days. The mixture was dialyzed against the water with a 3500 MWCO cut-off membrane [110]. The product was lyophilized and analyzed by ^{1}H-NMR spectroscopy (Figure 2.2B).

2.2.2.2.4 Conjugation of MALDOX to CCMs

In this step, CCMs carrying the PDS group were conjugated to MALDOX (depicted in Figure 2.2) by using TCEP, as seen in Figure 2.2C Briefly, 100 mg micelle, MALDOX (3,75 mg, $5x10^{-6}$ mol) was dissolved in 4 ml dry methanol and then, TCEP (1.44 mg, $5x10^{-6}$ mol) was dissolved in dry methanol (2 ml) and added dropwise to the reaction medium. Subsequently, the mixture was stirred overnight in the dark and then dialyzed against dry methanol for two days, and the resulting product was precipitated from diethyl

ether three times. The final product was stored under a vacuum for analysis with ^{1}H-NMR spectroscopy [105].

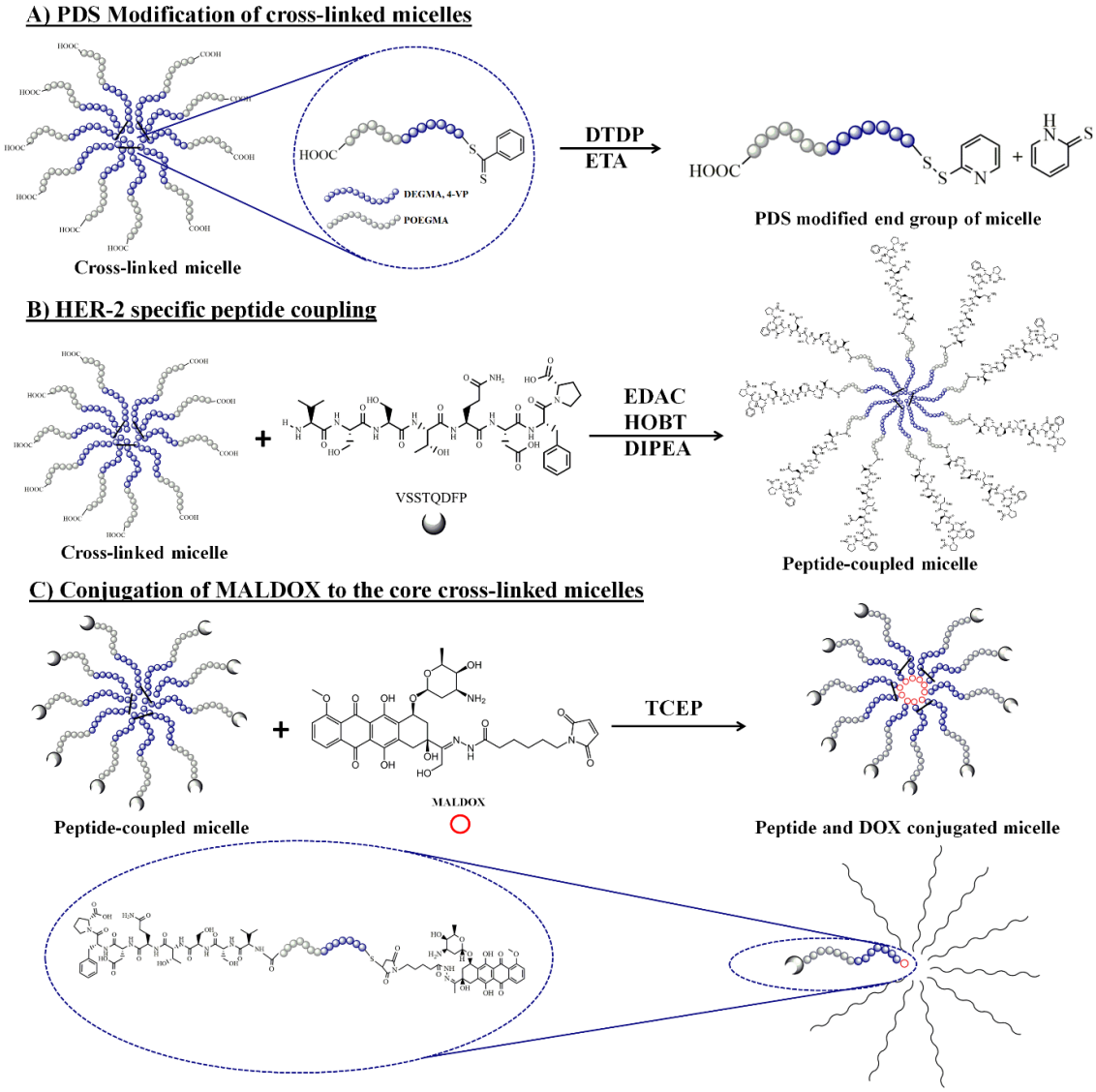

Figure 2.2 Drug and peptide conjugation to the CCMs

2.2.2.3 Characterization

NMR spectra of the samples were acquired by Bruker 400 (EU-TAUM) or Bruker Ultrashield 300 MHz liquid NMR spectrometers using related deuterated solvents. Size, size distributions, and zeta potential of the samples were obtained using Malvern Zetasizer NanoZS dynamic (DLS) and electrophoretic (ELS) light scattering spectrometry at 25°C using a refractive index value of 1.5. Samples were dissolved in

water for size measurement and water and PBS for charge measurement. High contrast transmission electron microscope (CTEM, 120 kV, METU Central Laboratory) was used to examine the size and morphology of the samples. The concentration of the samples dissolved in water was prepared between 0.1% and 1% (w/v) and then examined after drying by dropping 3-5 µl on a carbon-coated grid. Molecular weight and molecular weight distributions of the polymers were determined by the Viscotek TDA302 GPC system with Shim-Pack GPC804 column using THF as the mobile phase. The flow rate was 0.8 ml/min, and PS (Mw= 99,000 g/mol, PDI= 1.05, dn/dc= 0.165) was used as the single standard to calibrate the detectors. Mass spectra of the samples were acquired from an Ultraflextreme MALDI-TOF mass spectrometer (Bruker Daltonics, USA) equipped with a nitrogen UV-Laser operating at 355 nm. Spectra have been recorded in reflection-positive mode with an average of 5000 shots. Dihydroxybenzoic acid (DHB) was used as the MALDI matrix. Matrix and sample solutions were mixed to obtain a Wsample/Wmatrix ratio of 1:5. 1 µl of matrix/sample mixture was deposited on the sample plate, dried at room temperature, and analyzed.

2.2.2.4 Drug Release

1 ml of doxorubicin-conjugated micelle solution was placed in dialysis membrane tubes (FisherbrandTM Regenerated Cellulose Dialysis Tubing, 3500 MWCO). The whole tube was placed into citrate buffer (pH 4.5) or phosphate buffer (PBS) (pH 7.4) and shaken (70 rpm) at 37°C. At certain time intervals, 1 ml of buffer solution was withdrawn, and the fresh buffer was added. The release of the active substance was determined by measuring the absorption (at 496 nm) of the DOX molecule in withdrawn buffers, and the following formula was used to acquire the cumulative release plots [117].

$$CR\ (\%) = [(100 \times ((Vm \times C_{DOX(n)}) + (1\ ml \times \Sigma\ C_{DOX(n-1)}))] / W_0 \quad (2.1)$$

According to this, Vm: Emission media volume; W_0 (mg): the amount of drug loaded; $C_{DOX\ (n)}$: the amount of DOX (mg/ml) in the sample taken from the release medium; $C_{DOX\ (n-1)}$: (n-1). The amount of DOX in the sample taken from the media [118].

2.2.2.5 Degradation Study of CCMs

To evaluate the acid-triggered degradation of the micelles, the micelle solutions were incubated at pH 4.5 for up to 24 hours, and samples were taken from the mixture at different time intervals and analyzed by FTIR and DLS. GPC was also used in order to follow degradation in different acid exposure times.

2.3 Result and Discussion

2.3.1 Synthesis of CCMs

The CCMs were synthesized by copolymerization of 4-VP and DEGMA through the chain end of POEGMA macroCTA in different ratios in the presence of a cross-linker (yield 77 %). Here, micelle formation and copolymerization occurred simultaneously due to the cross-linking reaction and RAFT polymerization. CCMs via RAFT polymerization in the presence of a cross-linker have already been reported in the literature [101,102,105,115,119]. The obtained copolymer micelles were examined structurally by FTIR and ^{1}H-NMR spectroscopies. In the FTIR spectrum (Figure 2.3), the band at 1720 cm^{-1}, 2870 cm^{-1}, and 1100 to 1245 cm^{-1} were assigned to the groups of C=O, -CH_2- (-CH_3), and C-O-C, respectively. The peak intensity obtained at 1720 cm^{-1} increased due to the addition of cross-linker and DEGMA, while the peaks around 2900 and 3000 cm^{-1} were obtained due to the -CH_2- and -CH_3 groups in other units. In addition, an increase in the C-O-C peak at 1245 cm^{-1} was caused by the cross-linker. The addition of 4-VP to the structure was determined from the C=N stretch peak obtained around 1600 cm^{-1}.

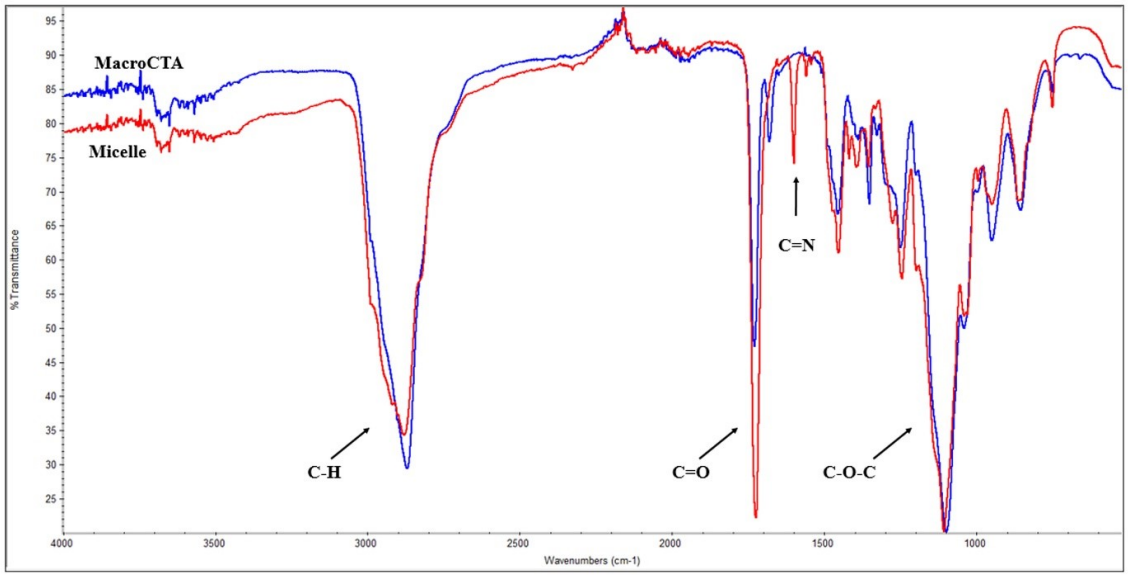

Figure 2.3 FTIR spectrum of MacroCTA and CCMs.

^{1}H-NMR spectrum, given in Figure 2.5A, reveals the successful synthesis of CCMs in which 4-VP protons are clearly observed at 7.0 and 8.5 ppm. Similar to the macroCTA's

NMR spectrum (Figure 2.4), the peaks related to ring protons of RAFT agent were obtained between 7.5-8 ppm as tiny peaks.

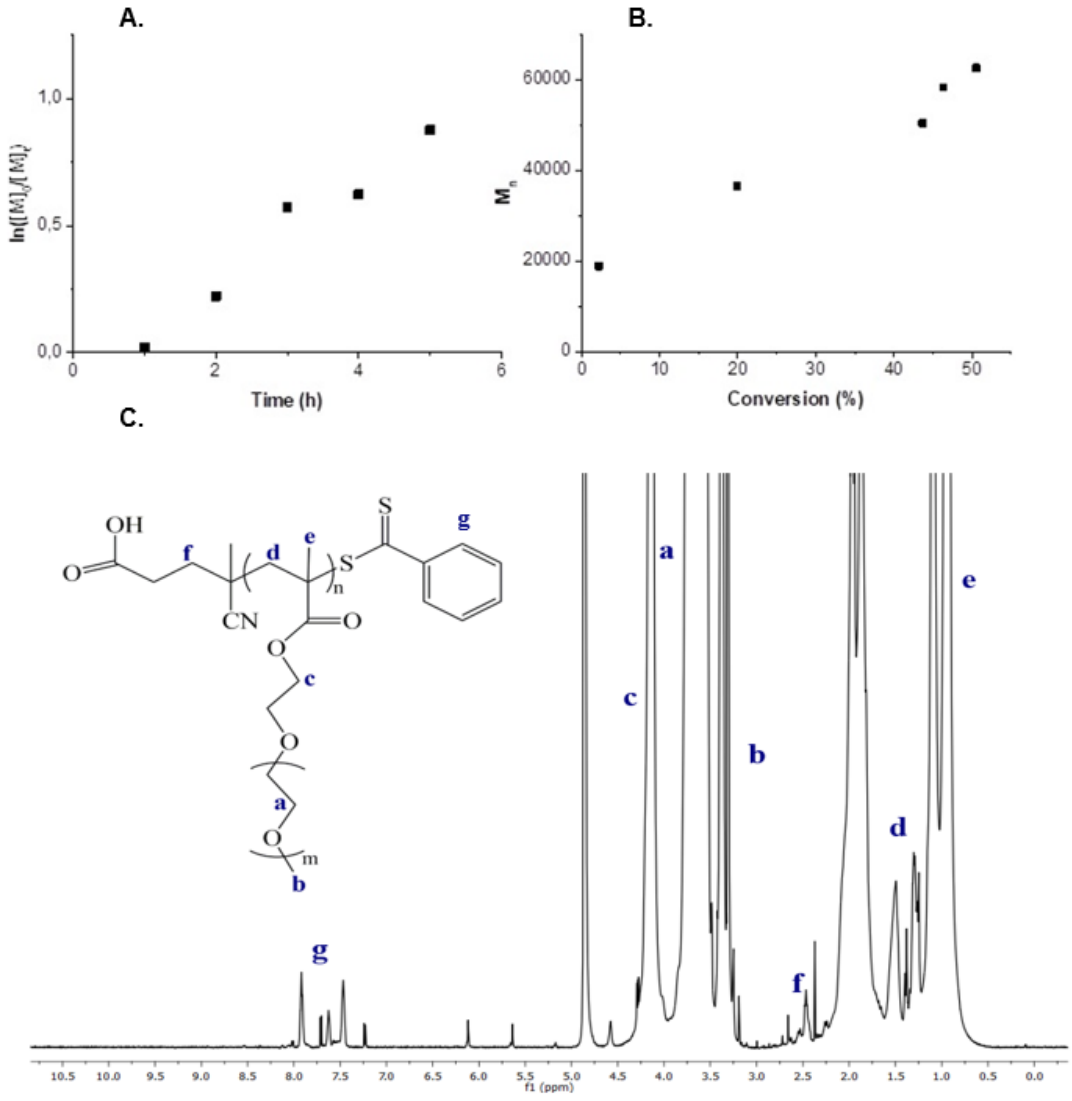

Figure 2.4 Conversion kinetics (A), conversion-molecular weight relationship of MacroCTA synthesis reaction (B), ^{1}H-NMR spectrum of POEGMA (C)

Then, the size and size distribution of micelles dissolved in water were analyzed by DLS spectrometry at 25 °C. The results given in Table 3 clearly show that micelles having diameters between 10-144 nm were obtained successfully with low polydispersity index (PDI) values. The increase in the internal structure of micelles with 4-VP and DEGMA ratios (0.25-1 mmol and 0.25-0.75 mmol, respectively) resulted in a noticeable increase in micelle size. Once we increase the amount of cross-linker, the chance of cross-linking reaction between the components and polymerization reaction increases. It also increases

the number of polymer chains in the core, which are connected to another polymer chain, and, finally, a cross-linked core. Depending on the amount of cross-linker, we obtain a denser core structure, and it eventually forms bigger micelles. The size difference of micelles is also noticeable from the appearance of the aqueous solutions. In Figure 2.5B, the size distributions of the micelles with hydrodynamic diameters of 70, 115, and 144 nm are given. In addition, TEM images of CCM2 and CCM5 are shown in Figure 2.5C-D. The diameter of the micelle determined by TEM was compatible with those measured by DLS spectrometry. In the next steps of the study, CCM2 was used for drug binding and peptide conjugation owing to the low PDI value and hydrodynamic diameter (between 10-100 nm) or the optimum EPR effect.

Table 2.1 Hydrodynamic diameters and PDI values of CCMs synthesized by using different amounts of DEGMA, 4-VP, and cross-linker (CL)

Sample	DEGMA (mmol)	4-VP (mmol)	CL (%)	Hydrodynamic Diameter (nm)	PDI
CCM1	0.25	0.25	5	10	0.161
CCM2	0.5	0.25	5	70	0.126
CCM3	0.75	0.25	5	83	0.161
CCM4	0.75	0.25	1	78	0.212
CCM5	0.75	0.25	10	116	0.175
CCM6	0.75	0.5	5	115	0.078
CCM7	0.75	1	5	144	0.123

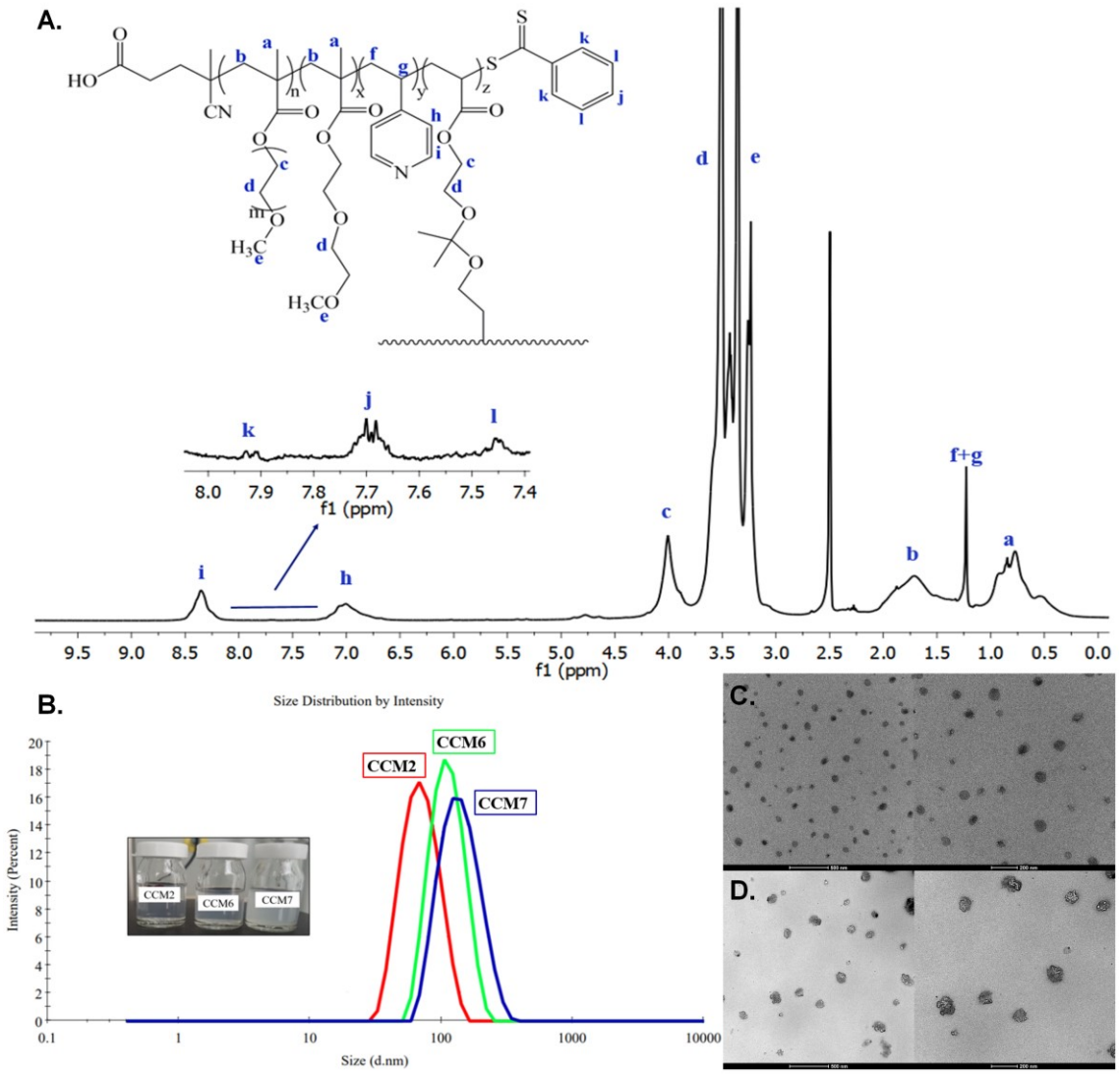

Figure 2.5 ^{1}H-NMR spectrum of CCM2 in DMSO-d6 (A), size measurements of selected micelles (CCM2, CCM6, CCM7) (B), TEM images of CCM2 (C), CCM5 (D) at different magnifications

2.3.2 Preparation of Targeted and Drug Conjugated CCMs

2.3.2.1 PDS Modification of CCMs and MALDOX Synthesis

In order to chemically bind the drug, first, the ω-end of the polymer chain was converted to the PDS group (Figure 2.2A) (yield 75 %). In the study of Boyer et al., the chemical shift of the ring protons attributed to the RAFT agent (at 7.4-7.5-7.8 ppm) shifted to 7.1-7.6-8.4 ppm, following the conversion to PDS [116]. In our study, Figure 2.6 shows that these peaks were around 7.3-7.6-8.4, which confirms PDS modification. Also, the color of the micelles solution turned yellow, which also confirms PDS modification.

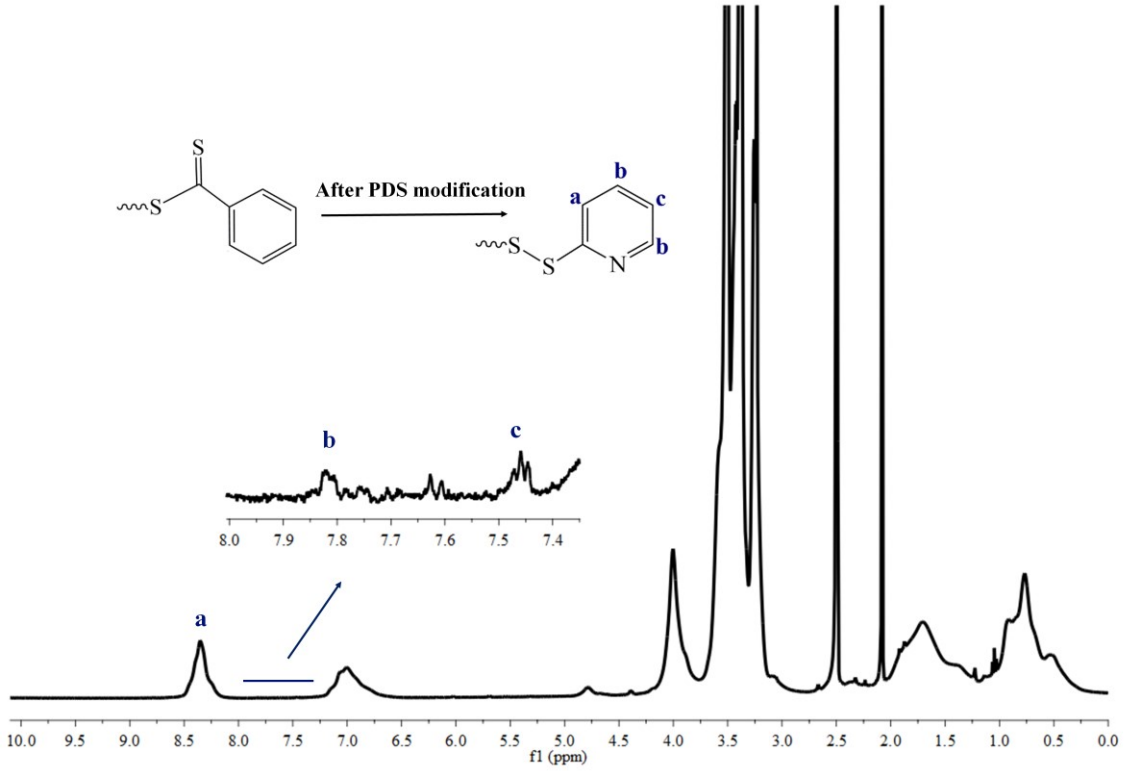

Figure 2.6 The ^{1}H-NMR spectrum of the CCMs obtained by conversion of ω-end to PDS in DMSO-d6

In order to conjugate the drug to the micelles via the PDS group, DOX.HCl was converted to DOX-maleimide (MALDOX), in which maleimide and DOX are linked with an acid-degradable hydrazone bond. In the studies that used hydrazone bonds between DOX and MAL, the released DOX after degradation of the hydrazone bond in an acidic environment maintains its activity [120,121]. The maleimide modification in DOX was confirmed by structural analysis with ^{1}H-NMR spectroscopy. According to Figure 2.7, the expected peaks of maleimide and hydrazone were shown at 7.0 and 9.4 ppm, respectively.

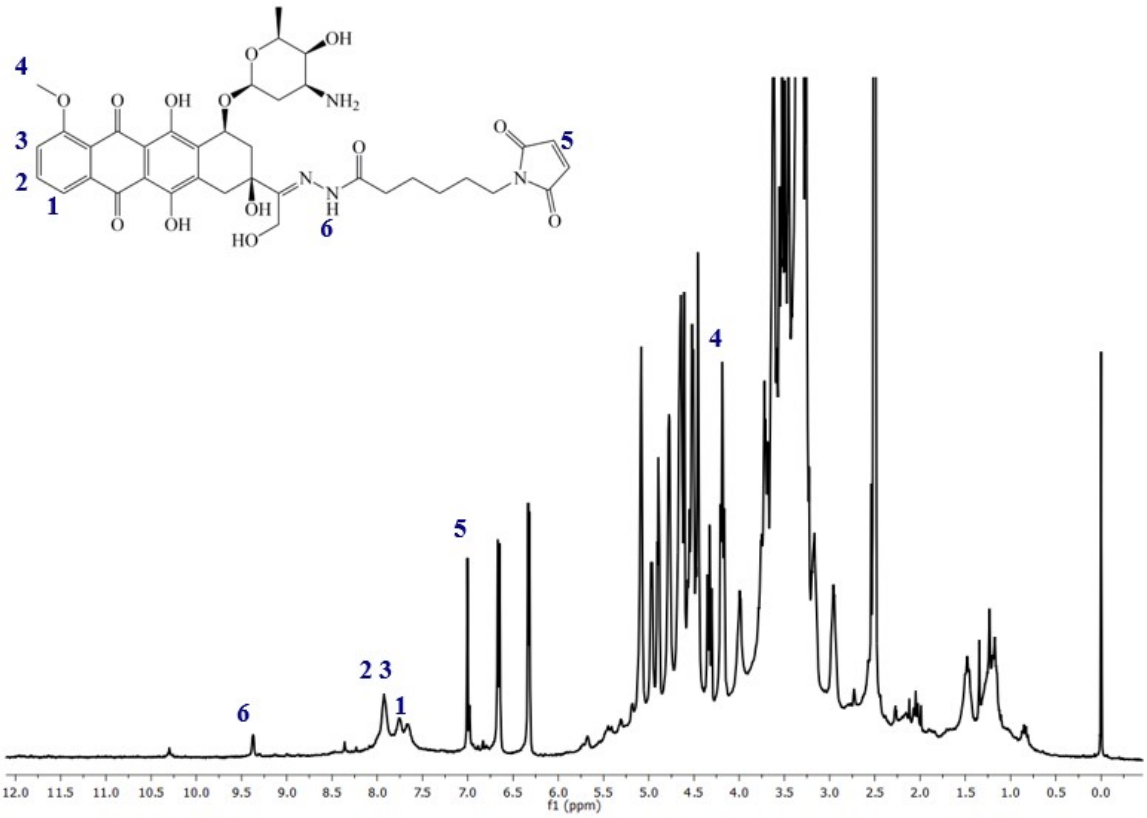

Figure 2.7 The ^{1}H-NMR spectrum of MALDOX in DMSO-d6

Furthermore, MALDOX ($C_{37}H_{42}N_4O_{13}$) was analyzed by a high-resolution MALDI-TOF mass spectrometer, and the molecular ion signal was observed as 809.24 (m/z) (Figure 2.8).

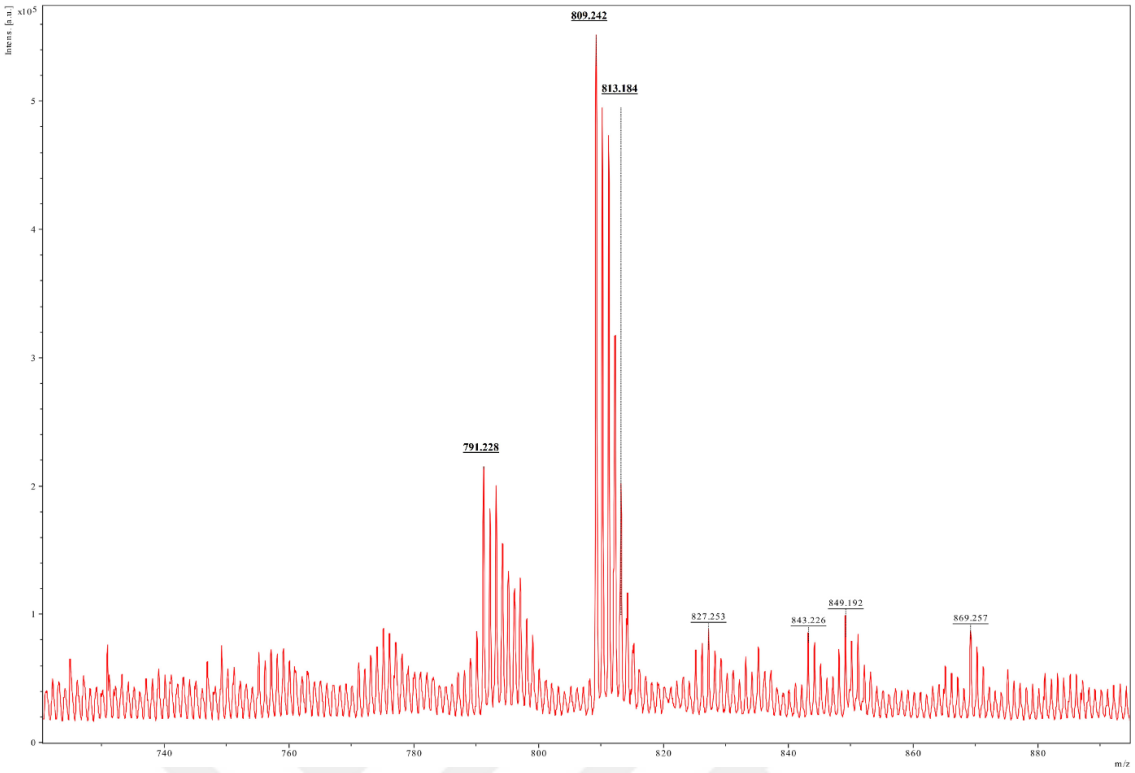

Figure 2.8 Mass spectrum of MALDOX acquired from MALDI-TOF mass spectrometer

This molecular ion is the result of the addition of Na^+ and K^+ ions by the separation of acidic hydrogen atoms in the molecular structure. The mass values below 700 m/z are the disintegration signals formed by the cleavage of some groups from the MAL-DOX molecule, and they coincide with the theoretical cleavage values [105].

2.3.2.2 Binding of Targeting Ligand (HER2-Specific Peptide) and DOX Conjugation to CCMs

The HER-2 targeting peptide (VSSTQDFP) was activated by NHS via the amino group and then covalently bound to the carboxyl end group from the RAFT agent on the micelle of CCM2 in the presence of carbodiimide (EDC) (yield 79 %) [110]. Figure 2.13A-D shows ^{1}H-NMR spectra of micelles with PDS modification (A), DOX conjugated micelles (B), peptide conjugated micelles (C), peptide and DOX conjugated micelles (D), respectively. In Figures 2.13.A-C, the peaks of the peptide and micelles were compared, and the amide bond of the peptide could not be differentiated due to existing amide bonds in the CMs, but the peaks associated with the peptide were observed to increase the intensity, unlike Fig. 2.13.A. Furthermore, peaks of the benzene ring in phenylalanine were observed at 7-7.5 ppm, and the methyl peak of threonine and the

proton of the aspartic acid-proline hydroxyl groups were shown at 1.2 ppm and 10.2 ppm, respectively. Size measurement was also performed, and the size of the peptide-bound micelles increased from 70 nm to 90 nm (CCM2, Figure 2.9).

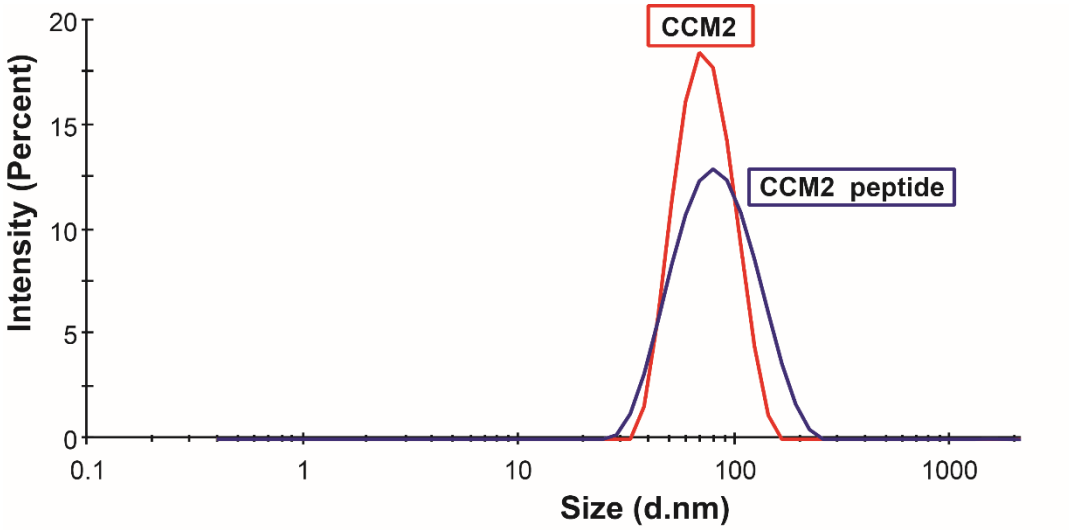

Figure 2.9 Hydrodynamic size distributions of CCM2 and peptide-bound CCM2

According to ^{1}H-NMR spectra and size measurements, the peptide was successfully conjugated into micelles. In addition to this, peptide conjugation was also confirmed by Pierce Quantitative Fluorometric Peptide Assay (Thermo Scientific, USA). The peptide-conjugated CCM2 sample was dissolved in water at a concentration of 1 mg/ml, and fluorescence was measured using Ex/Em at 390 nm/475 nm. According to the calibration graph given in Figure 2.10, the measured fluorescence corresponding peptide amount was determined as 7.30±1.56 µg/ml.

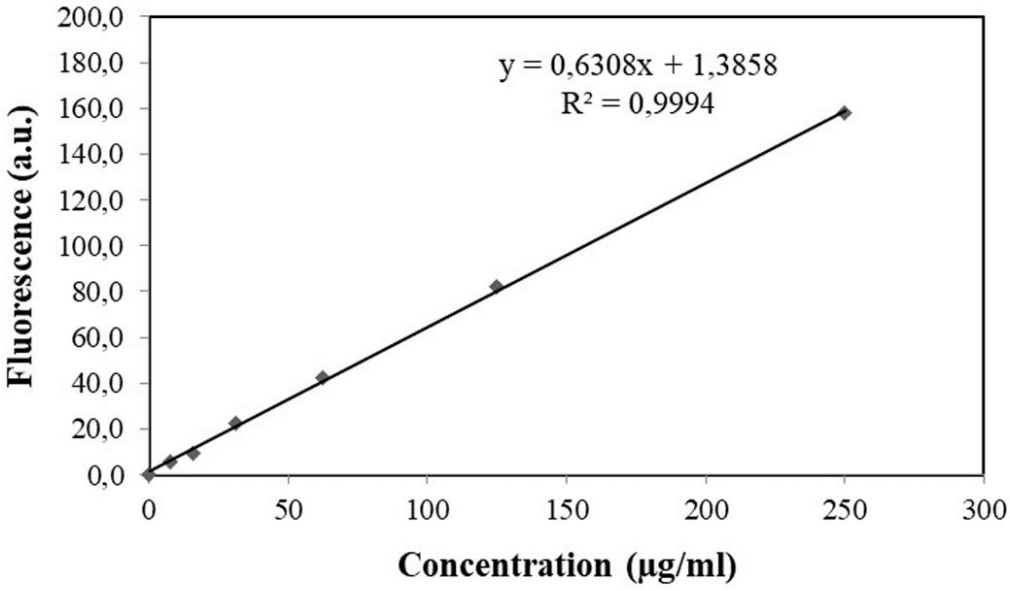

Figure 2.10 Calibration curve for fluorometric peptide assay

Following the peptide coupling to micelles, the prepared MALDOX was conjugated to micelles, and MALDOX-bound peptide-coupled micelles were characterized by ^{1}H-NMR spectroscopy. Figure 2.13B-D shows the ^{1}H-NMR spectra of MALDOX conjugated CCMs and MALDOX-peptide conjugated CCMs, respectively. In Fig.4B-D, the hydrazone group of MALDOX was clearly observed at around 9.5 ppm, which confirmed the conjugation of MALDOX to the micelle and peptide-coupled micelles. Also, the methyl peak of DOX was shown at 4-5 ppm. In the study of Jia et al., the peak of maleimide proton (observed with EMCH modified DOX, Figure 2.6) at 6.97 ppm was not present in the spectrum of DOX−micelle conjugate, revealing the reaction between the free thiol groups of the micelle and the maleimide group of DOX [105]. However, in our study, the absence of these peaks was not determined because a signal for the micelles at 7 ppm was present. As another confirmation for drug binding to micelle, the absorbance spectra of the DOX-conjugated samples were examined by UV-spectrophotometer (Figure 2.11) [122–125]. Accordingly, when the spectra of the micelle and drug-bound micelle were compared, the absorbance values at 502 nm of the drug were observed as 0.316 while it was 0.027 for the micelle, which indicates that the drug was bound to the micelle.

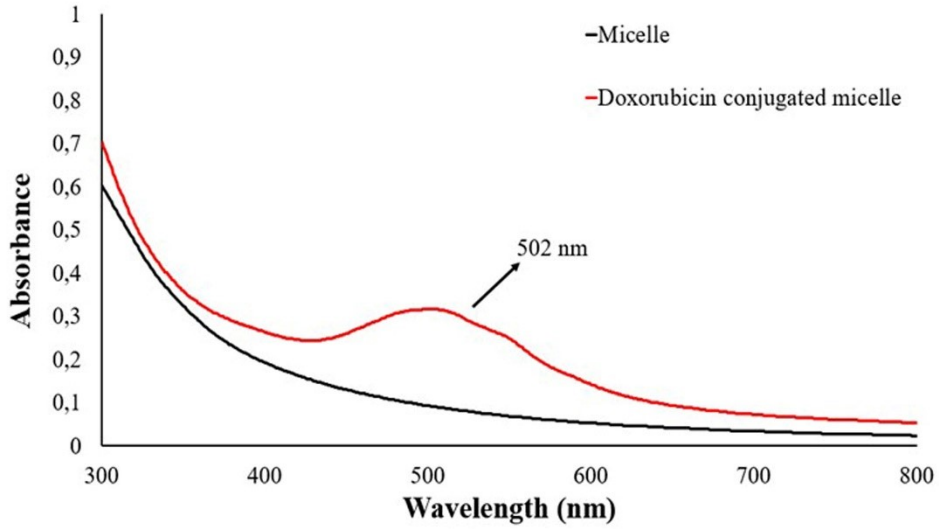

Figure 2.11 UV-Vis spectra of micelle and doxorubicin conjugated CCMs

Here, DOX quantity of CCM2 and peptide conjugated CCM2 were obtained as 2,4 ± 0,07 % (w/w) and 1,6 ± 0,08 % (w/w) with 63 ± 1,8 % and 42 ± 2,1 % conjugation efficiency, respectively. The relatively low rate of doxorubicin conjugation in the peptide-linked micelle compared to the peptide-unconjugated micelles may be caused by the inability of MALDOX to reach the core part due to the steric hindrance created by the peptide conjugated in the shell. Also, the size of DOX-conjugated CCM2 and DOX and peptide-conjugated CCM2 were 99 nm and 116 nm, respectively (Figure 2.12).

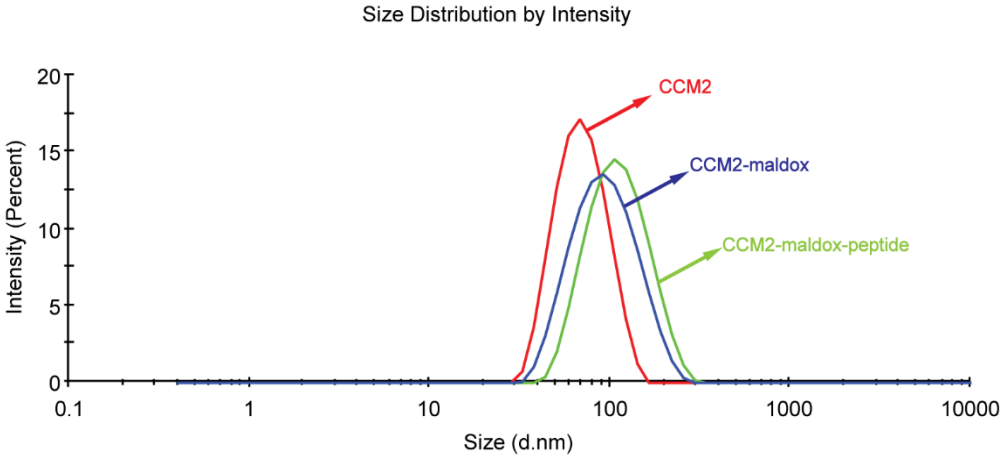

Figure 2.12 Hydrodynamic size distributions of CCM2, MALDOX conjugated CCM2, and peptide and MALDOX conjugated CCM2

In addition, the zeta potential of the micelles is an important feature as it affects the blood residence time and cellular uptake of the micelles. The zeta potentials of the DOX-conjugated CCM2 and DOX and peptide-conjugated CCM2 (in water) are -18.23±0.51 and -16.90±0.36, respectively. Also, these values in PBS are -6,24±0.47 and -6,45±0.34 for the DOX conjugated CCM2 and DOX and peptide conjugated CCM2, respectively.

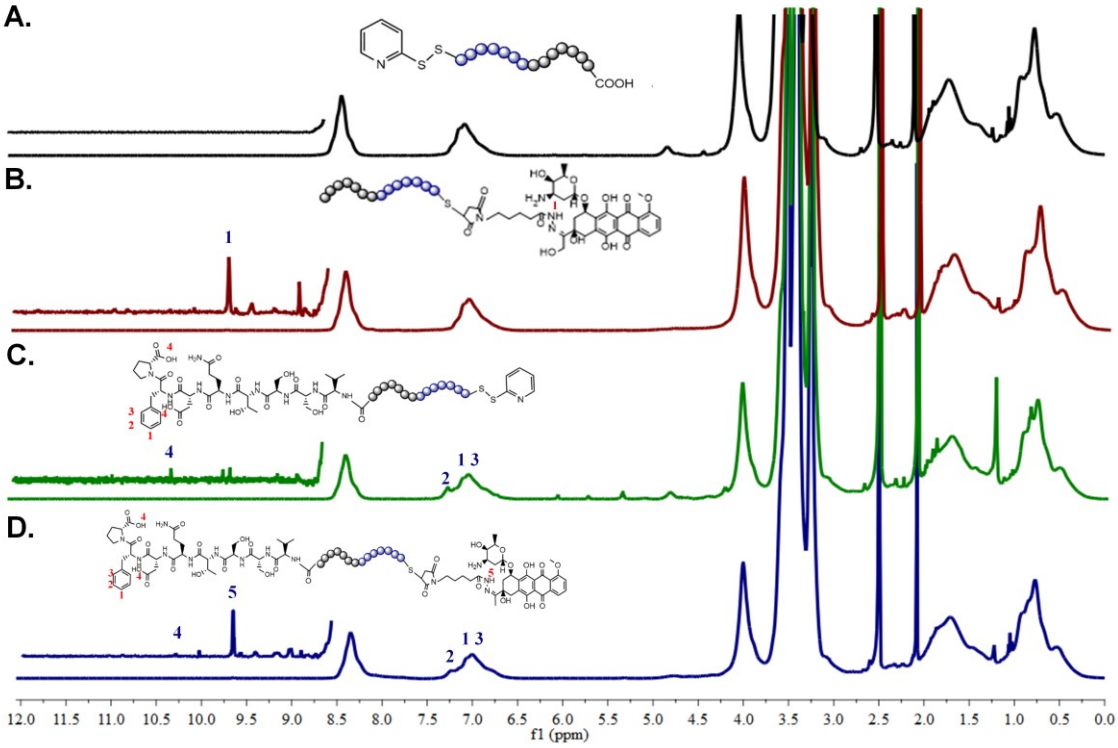

Figure 2.13 ^{1}H-NMR spectra of micelles with PDS modification (A), DOX-conjugated CCMs (B), peptide-conjugated CCMs (C), peptide and DOX-conjugated CCMs (D) in DMSO-d6

2.3.3 Drug Release

Due to the acidic character of intracellular endocytic vesicles and tumor environment, we conjugated DOX to the CCMs by acid-cleavable hydrazone linkage to obtain a polymeric smart system that can be stimulated by acidic pH through these sites for the drug release. In addition to the hydrazone linkage, acid-degradable acetal-based cross-links in the micellar core will also contribute to micelle disintegration and drug release. In this work, the release study was performed at pH 7.4, which is a characteristic of blood circulation, and at pH 4.5 for mimicking subcellular acidic organelles whose pH value is 4.5-5.5 [126,127].

Figure 2.14 shows the cumulative release of DOX at pH 4.5 and 7.4 from the DOX-conjugated CCMs as a function of time. As seen, 78% of DOX was released from the micelle at pH 4.5 by pH-based cleavage of acetal and hydrazone bonds, while only 31% of DOX was released at pH 7.4 in 24h, which reveals that CCMs exhibit a pH-dependent drug release profile.

In the release profile at pH 4.5, a burst release was observed in the first 5 hours, and more than 55% of the drug was released. Within the first 5 hours, there was about 15% DOX release at pH 7.4, which might be attributed to unconjugated DOX physically entrapped inside the particles, as also reported in a similar study by Wong et al. Note that we applied dialysis against ethanol at least 2 days after the conjugation process, which was supposed to be sufficient to remove the physically bound MALDOX, according to the literature [105]. However, the presence of other components in the micelle structure might cause additional physical interaction with DOX by possible π-π stacking between DOX and pyridine aromatic rings. It is important to note that micelles do not release a fraction of DOX molecules (22%) at pH 4.5, which can be explained by the dynamic nature of hydrazone bonds and interactions of doxorubicin with the degraded hydrophobic segments of the copolymer, as also explained in similar studies [128]. According to Qie et al.'s study, they synthesized PEG-di Dhyd-PLA-18K micelles containing pH-sensitive hydrazone bonds, and the release rate of these micelles in physiological (pH 7.4) and acidic environment (pH 4.5) was 38% and 75% in 24h, respectively [129]. Lee et al. synthesized doxorubicin conjugated PEO-PPO-PEO copolymer via hydrazone bond, and the DOX released out of micelles was 40% and 84% in pH 5 and pH 7.4 after 26h, respectively [130]. Furthermore, depending on release studies of nanoparticles consisting of acetal bonds in the previous studies, Chen et al. synthesized acetal base linkage containing pH-responsive biodegradable micelles, and according to their result, 98, 89, and 44% DOX was released at pH 4.0, 5.0, and pH 7.4 within 48 h, respectively [131]. Also, DOX release from a pH-insensitive carrier usually exhibits low pH sensitivity (release rate at 5.0 is about 1.8 times or less than neutral pH), as stated in Jia et al. 's study. In our study, we reached a 2.5-fold faster release at acidic pH compared to release at pH 7.4, which can be accepted as pH-dependent drug release [105].

It is obvious that the findings related to the DOX release from the micelle based on acetal-based cross-links and hydrazone bonds are consistent with similar studies in literature and allow better drug release control [105,122,123]. It should also be noted that using a cross-linking strategy in micelle structure allowed a more stable system in blood

circulation. As a result, we obtained a nanocarrier system that is stable in blood circulation with less disintegration in micelle assembly and dual-responsive pH sensitivity inside the cell, facilitating intracellular drug release.

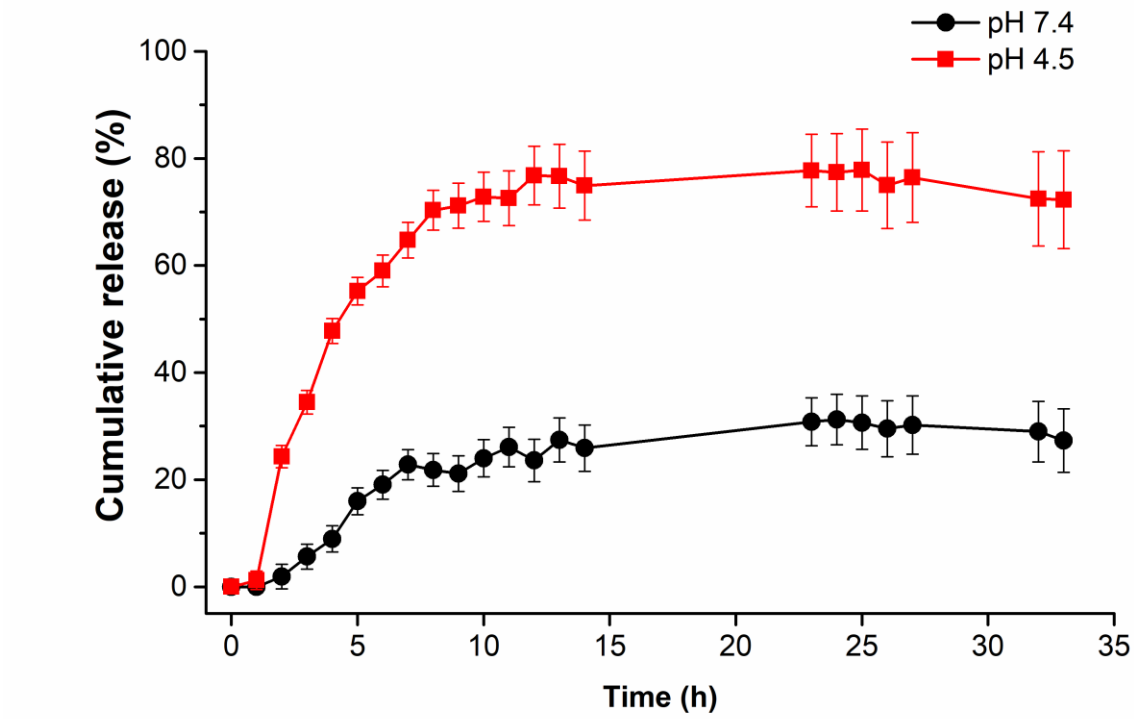

Figure 2.14 Cumulative release of DOX from CCMs at pH 4.5 and 7.4.

2.3.4 Degradation of CCMs

Due to acid-degradable bonds in the core cross-links of the micelles, they are expected to degrade at acidic conditions. In order to prove this, micelles (CCM2) were incubated at pH 4.5, 37°C for 24 hours. Samples were withdrawn from the medium (between 0-24 hours) and analyzed by DLS, FTIR, and GPC. First, micelle degradation was chemically shown by FTIR (Figure 2.15A1 and 2.15A2). It is evident that the intensity of the acetal group's peak around 1100 cm^{-1} decreased after acidic degradation (Figure 2.15A2). According to the size analysis (Figure 2.15B), the diameters of the particles were decreased while PDIs were increased with degradation time beginning within 2 hours. It demonstrated the formation of smaller chains causing higher PDIs by degradation. This was also proved by GPC, in which the retention volume of the particles

shifted to larger values meaning that the size of particles was smaller and eluting from the column later (Figure 2.16).

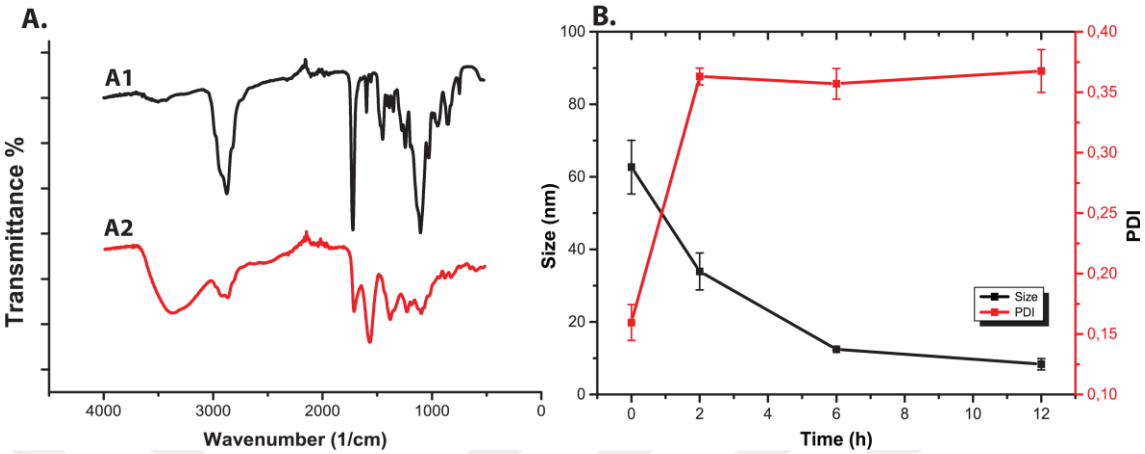

Figure 2.15 FTIR spectra for before (A1), after micelle degradation (A2), hydrodynamic diameter and size distribution of micelles (B) in PBS depending on the acid exposure time

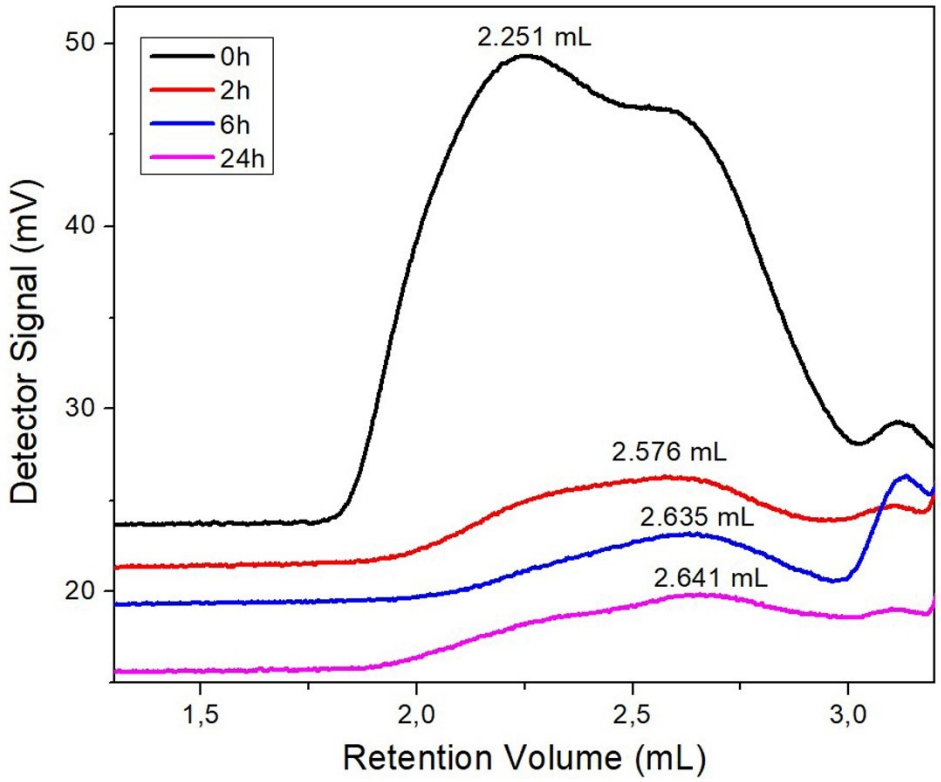

Figure 2.16 GPC chromatograms CCM2s exposed to the acidic solution for up to 24 hours

In the literature, Bhuchar et al. and Wang et al. prepared nanogels using 2,2-dimethacroyloxy-1-ethoxypropane (DMAEP), which is the same as our cross-linker, and they observed that their nanogels were unstable in the acidic environment (pH 4.5 and pH 5.2) which resulted in degradation within 2 h by measuring the hydrodynamic diameter [115,132]. To sum up, CCMs produced in this study can be degraded into tiny particles that can facilitate drug release by the effect of pH, which was supported by the literature.

To check the stability of the micelles for 6 months, we performed size analysis in PBS and observed that micelles maintained their sizes under these conditions. The size and size distribution of CCMs in PBS are given in Figure 2.17.

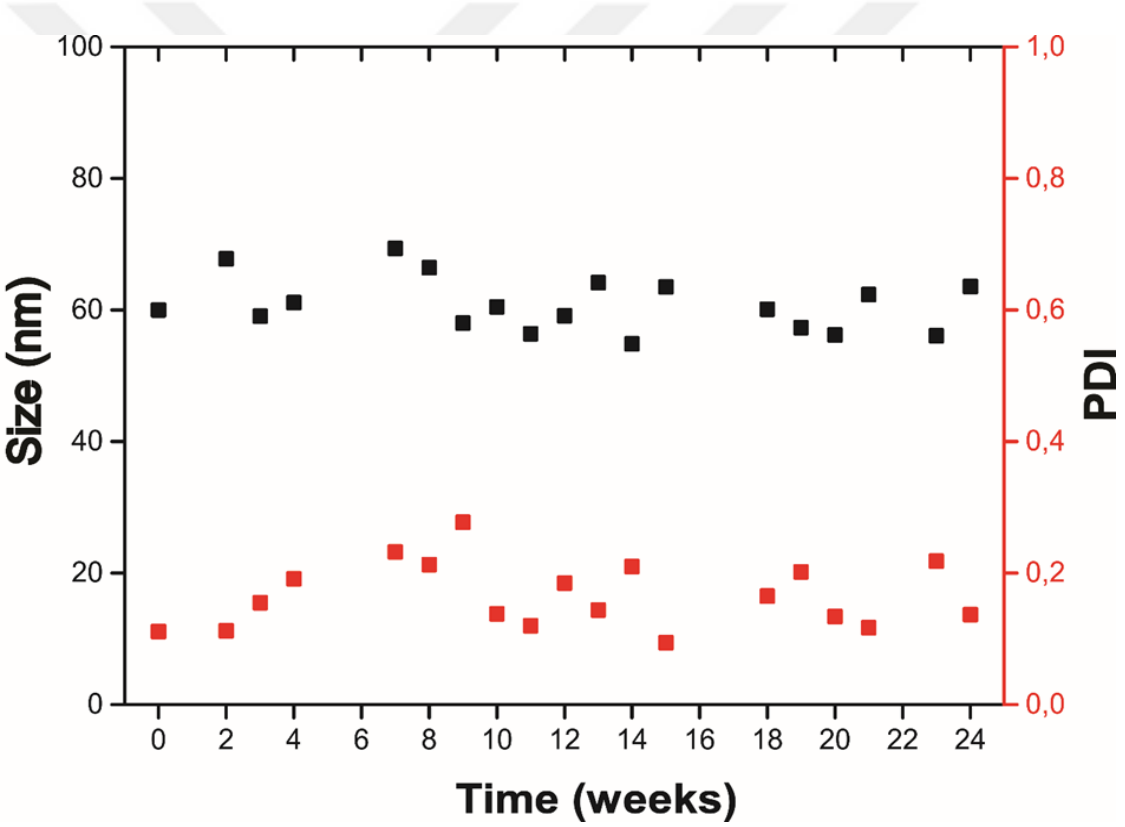

Figure 2.17 Size and size distribution of CCMs in PBS up to 24 weeks

Also, we performed an experiment in blood-simulated solution to check stability in the blood, and no change in the micelle size was observed at 37°C, even after one week (Figure 2.18).

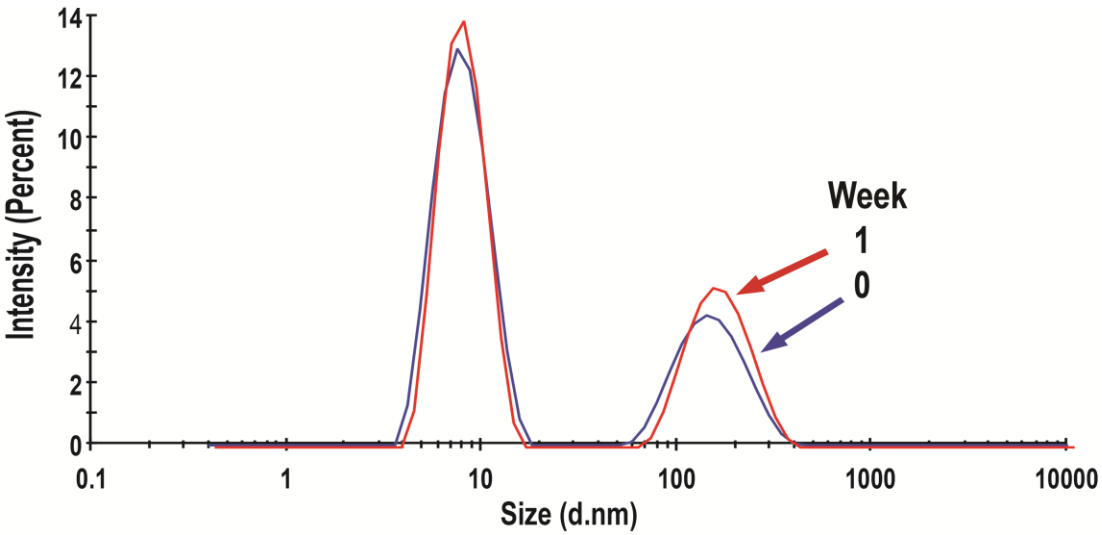

Figure 2.18 Size analysis of CCMs in blood simulated solution

As a result, these NCs are stable in PBS for up to 6 months, which means we can keep them for weeks in these conditions. Besides, in the case of intravenous (i.v.) administration, these NCs may keep their stability in terms of size for up to 1 week following the injection.

Chapter 3

PEG Based, Degradable and EF2 Kinase Inhibitor-Loaded CCMs

3.1 Introduction

Breast cancer subtypes are divided into 3 groups which are tumors sensitive to estrogen hormone constituting 60-70% of the disease, tumors sensitive to the estrogen hormone and HER-2 (human epidermal growth factor) receptors carrying constituting 15-20% of the disease, and tumors nonsensitive to estrogen hormone and HER-2 receptors as (Triple negative) constituting 15-20%. While hormone therapy and chemotherapy drugs are used in tumors sensitive to estrogen hormone, monoclonal drug therapy (trastuzumab) and standard chemotherapy agents that recognize the HER2 receptor are used in tumors carrying HER2 receptors, and cytotoxic chemotherapy approach is used in triple-negative tumors. The success rate of treatment increases with the use of HER2-specific antibodies, which is one of the targeted treatment options in HER2-positive cancer types [133]. Eukaryotic Elongation Factor-2 Kinase (EF2K), which is a non-receptor kinase unlike classical receptor kinases, is a potential biomarker as a molecular target and causes poor prognosis in triple-negative breast cancer (TNC) [134–138]. Studies showed that EF2K is highly expressed in the majority of TNC and HER2 + BC patients, and this is associated with disease progression and shorter patient survival. Also, these studies confirmed that EF2K could be used as a potential therapeutic target in various BC and HER2+ tumor models, and EF2K promotes UNMK tumorigenesis and progression by inducing clinically important oncogenic signaling pathways that lead to the accumulation of tumor-associated macrophages (TAMs), promoting tumors and contributing to the tumor microenvironment. However, Ozpolat et al. achieved eEF2K

inhibition by using RNA interference, which is one of the genetic methods. In addition, their group developed the new EF2 small molecule inhibitor, which caused, not only suppressed tumor growth significantly but also the use of this inhibitor with doxorubicin, which is a standard chemotherapy agent, increased the effectiveness of doxorubicin [134]. Overall, they showed that EF2K is a critical trigger of progression in TNBC and HER2+ tumorigenesis progression by promoting tumor growth and invasion. EF2K inhibition has become critical in the treatment of TNBC. Because EF2K gene expression-reduced mice have a normal phenotype and inhibition of its expression in vivo models does not cause side effects, suggesting that EF2K may serve as a safe and excellent therapeutic target.

Although several chemical inhibitors of EF2K (i.e., NH125, TX1918, A484954, and DFTD) have been identified, none are as specific, potent, and effective as the EF2K inhibitor demonstrated by Dr. Ozpolat et al. [139]. Therefore, other EF2 kinase inhibitors are not suitable for clinical applications. Recently, Ozpolat et al. have designed and synthesized a novel highly potent EF2K inhibitor compounds that have significant anti-proliferative activity at nanomolar concentrations and inhibit eEF2K in TNC and HER 2+ cancer cells and in vivo animal models. However, it has been observed that some EF2 kinase inhibitors have limited solubility, which can impede their therapeutic efficacy and clinical development.

To address the solubility limitation of EF2 kinase inhibitors and improve their therapeutic effectiveness, we used PEG-based CCMs that we reported as CCM2. We incorporated other drugs, such as EF2 kinase inhibitors, into our PEG-based CCMs to evaluate their loading capacity and assess the efficacy of the drug delivery system. This approach allowed us to investigate the versatility and efficacy of CCMs for delivering various therapeutic agents, demonstrating their potential as a promising delivery system for enhancing the solubility and bioavailability of a range of small molecules.

Lastly, since the aim of this part of the thesis is to develop a breast cancer-targeted nanoparticle system utilizing the EF2 kinase inhibitor loaded CCMs, we evaluated the efficacy of the developed drug delivery system in vitro testing on HER+ (HCC1954, BT474) and HER- (MCF7) cell lines, triple-negative breast cancer (TNBC)(MDA-MB-231) cell lines. Through this approach, we aimed to demonstrate the potential of the targeted nanoparticle system for delivering therapeutic agents to breast cancer cells, potentially paving the way for more effective and targeted treatments for this disease.

3.2 Methods

3.2.1 Synthesis of POEGMA

Firstly, the synthesis of poly(OEGMA) macroCTA was carried out following the protocol outlined in section 2.2.2.1 Synthesis of CCMs. Subsequently, ^{1}H-NMR analysis was conducted to verify the chemical structure.

3.2.2 Synthesis of Acetal-Based Crosslinker Synthesis

The acid-sensitive crosslinker (CL, 2,2-dimethacroyloxy-1-ethoxypropane) was synthesized according to the literature mentioned in "2.2.2.1 Synthesis of CCMs" [115]. Briefly, a mixture of HEMA (13.0 mg, 0.1 mmol), 2,2- dimethoxy propane (5.2 mg, 0.05 mmol), and p-TSA (0.09 mg, $5x10^{-4}$ mmol) was stirred at room temperature for 5 hours. However, after 3 hours, we noticed that the samples started to gelate, and color change occurred. After this reaction, we tried to isolate the crosslinker from this solution; however, this gel structure did not allow us to isolate the pure component. After several trials of this reaction with different concentrations (because we thought that after the crosslinker formation, the crosslinker also crosslinked the HEMA monomer, causing gelation), we decided to switch methods to synthesize to crosslinker. To do that, we used toluene as a solvent and kept this reaction overnight at 95 ℃. Then, the mixture was purified by silica gel chromatography using a hexane-triethylamine mixture (85:14:1 hexane/ethyl acetate/TEA). Then, the fractions were analyzed by TLC to obtain the fractions containing pure substance, and the solvent of related fractions was removed by a rotary evaporator. CL was obtained as an oily yellow substance. For confirmation, ^{1}H-NMR and mass spectroscopies were used. The chemical shift values of the corresponding groups and mass analysis confirmed the successful synthesis of 2,2-dimethacryloxy-1-ethoxy propane compatible with the literature.

3.2.3. Synthesis of CCMs

To synthesize the micelle, macroCTA was dissolved in 5 ml of water. Then, 0.25 mmol of 4-VP and DEGMA (0.5 mmol) together with CL (5% mmol) were added to the solution, and the reaction was performed overnight at 60 °C using ACVA as the initiator. The formation of the CMs was confirmed by the turbidity formed in the solution. After an overnight reaction, the solution was dialyzed against water to remove

unreacted substances using a 3500 MWCO cut-off dialysis membrane. The chemical structures of purified copolymer micelles were characterized by ^{1}H-NMR spectroscopies, while the size and size distribution of the samples were determined by Nanosight Tracking analysis.

3.2.4 Preparation of EF2 Kinase Inhibitor Loaded CCMs

12 mg of CCMs and 0.6 mg of an EF2 kinase inhibitor were dissolved in 0.5 ml of DMSO and incubated overnight. The resulting mixture was added to a 1.5-milliliter aqueous solution and placed within a 2000 MWCO dialysis cassette. The cassette was dialyzed against 500 ml of water, with the water being changed three times over a duration of approximately 8 hours. After the dialysis process was complete, the resulting solution was freeze-dried, and drug-loaded CCMs were obtained.

To determine the percentage of entrapment (% Entrapment) and loading efficiency (%LE) of the EF2 kinase inhibitor within the drug-loaded CCMs, a series of experimental steps were followed. Firstly, the absorbance spectrum of the drug was scanned to determine its highest absorbance value, which was then used to draw a calibration curve using different concentrations of the drug. Next, the drug-loaded CCMs were dissolved in DMSO, and the %LE and % Entrapment values were calculated using the calibration curve. In order to eliminate any absorbance from the polymer, the free polymer was also dissolved in DMSO, and an absorbance spectrum scan was performed. Finally, the size and charge of both the free CCMs and the EF2 kinase-loaded CCMs were characterized using Nanosight and Zeta Sizer analysis, respectively.

3.2.5 Effect of the CCMs on Breast Cancer Cells

3.2.5.1 Cell Lines and Culture Conditions

Since our aim was determining the efficacy of CCMs on breast cancer cell lines, a cell culture experiment was performed with different breast cancer cell lines, including HCC1954 and BT474 (HER2 positive), as well as MCF7 (HER2 negative) and MDA-MB-231 (TNBC) cultured in DMEM/F12 (10% FBS, Penicillin/Streptomycin added) cultured at 5% CO2 and 37ºC. Cells were passaged every 2-3 days based on their proliferation rate and density of coating the flask surface.

3.2.5.2 Cell Viability Tests

Before starting the cell viability experiment, the cell number of different cell lines was optimized for the MTT experiment. To do that, different numbers of HCC1954,

BT474, MCF7, and MDA-MB-231 cell lines were seeded, and the proliferation of cells was analyzed (3-(4,5-Dimethylthiazol-2-yl)-2,5-Diphenyltetrazolium Bromide) by (MTT) assay. Cells were seeded at 500, 1000, 2000, 5000, and 10000 cells/well in 96-well plates and incubated 24h,48h, and 72h, and then MTT dye was added, and plates were analyzed at 520 nm with on a VMax kinetic ELISA microplate reader (Molecular Devices). Following this step, the cytotoxicities of free polymer, EF2 kinase inhibitor, and EF2 kinase-loaded CCMs were evaluated using HCC1954, BT474, MCF7, and MDA-MB-231 cell lines.

3.3 Results

3.3.1 Synthesis of POEGMA

To confirm the synthesis of macroCTA, ^{1}H-NMR analysis was used. The RAFT-ended group ring protons were seen at 7.84, 7.48, and 7.32 ppm, and the peaks of -CH_2 protons adjacent to the carboxyl group of the RAFT agent appeared approximately at 2.2 ppm (Figure 3.1), which confirmed the synthesis of macroCTA.

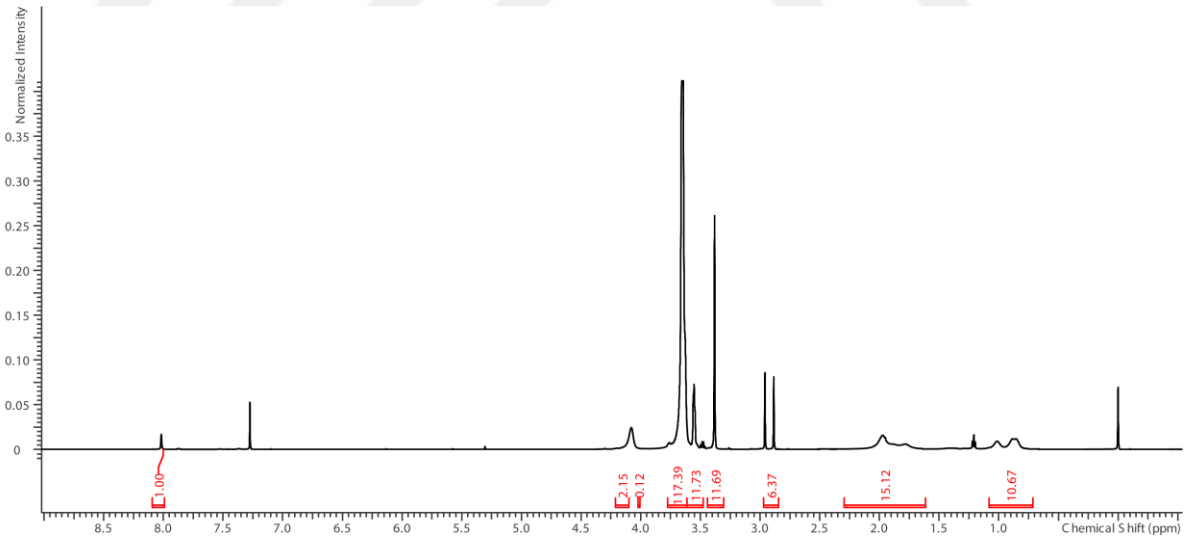

Figure 3.1 ^{1}H-NMR spectrum of MacroCTA in chloroform

3.3.2. Synthesis of Acetal-Based Crosslinker

The most challenging part was the synthesis and purification of the crosslinker. To do that, we changed the methodology and used different synthesis parameters. Following this, we synthesized and purified CL. The chemical shift values of the corresponding groups in the ^{1}H-NMR spectrum and mass spectroscopy peak confirmed the successful synthesis of 2,2-dimethacryloxy-1- ethoxy propane, which is consistent with the literature (Figure 3.2).

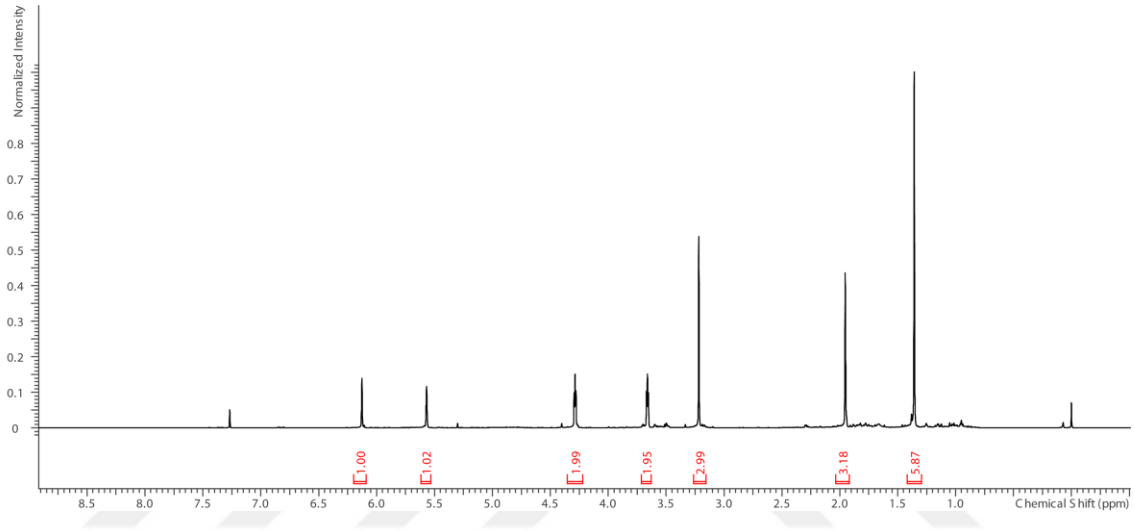

Figure 3.2 ^{1}H-NMR spectrum of crosslinker in DMSO-d$_6$

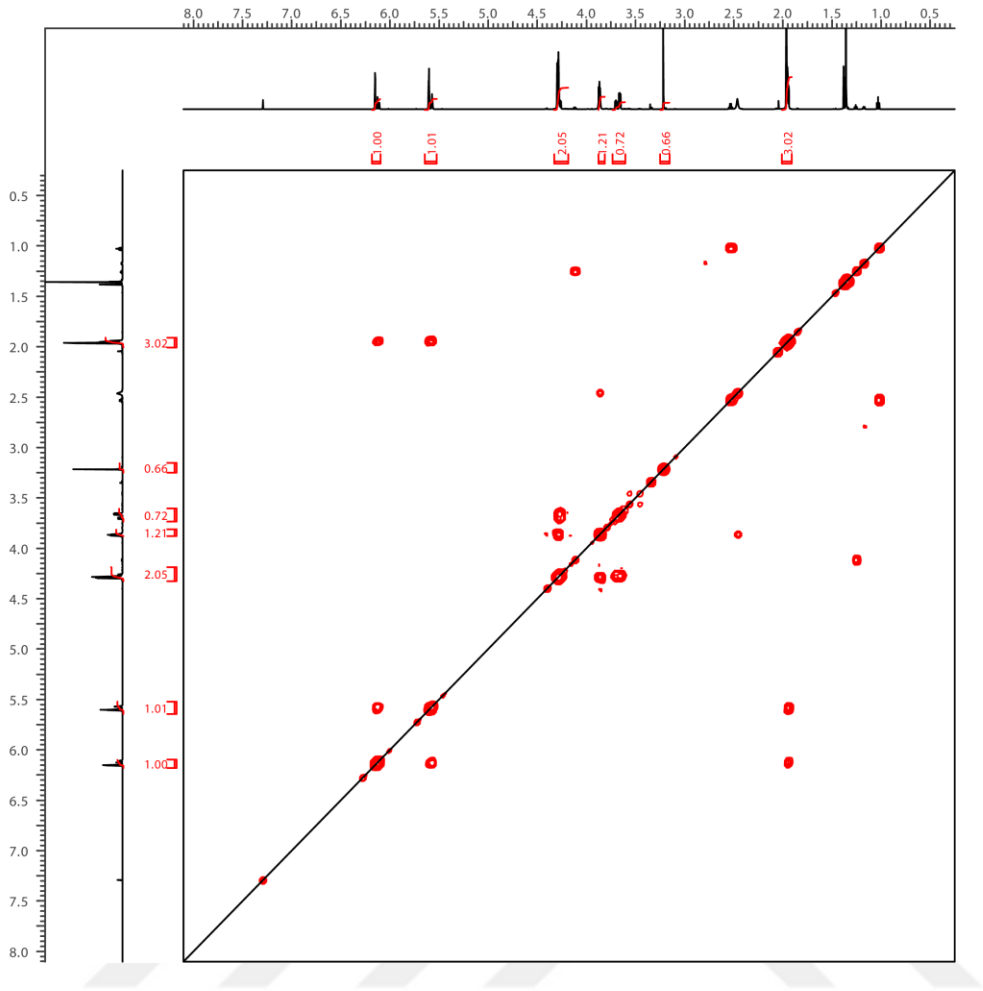

Figure 3.3 2D ^{1}H-NMR spectrum of crosslinker

3.3.3 Synthesis of CCMs

After macroCTA and crosslinker synthesis, we proceeded to CCMs synthesis. The formation of the CMs was confirmed by the turbidity formation of the solution. In addition, ^{1}H-NMR spectroscopy was used to confirm the chemical structure of the CCMs. Based on this analysis, DEGMA and crosslinker group signals were seen at 3-3.5 pm, and the 4VP group proton peak was at 7.0 and 8.5 ppm, which is in line with our previous studies (Figure 3.4).

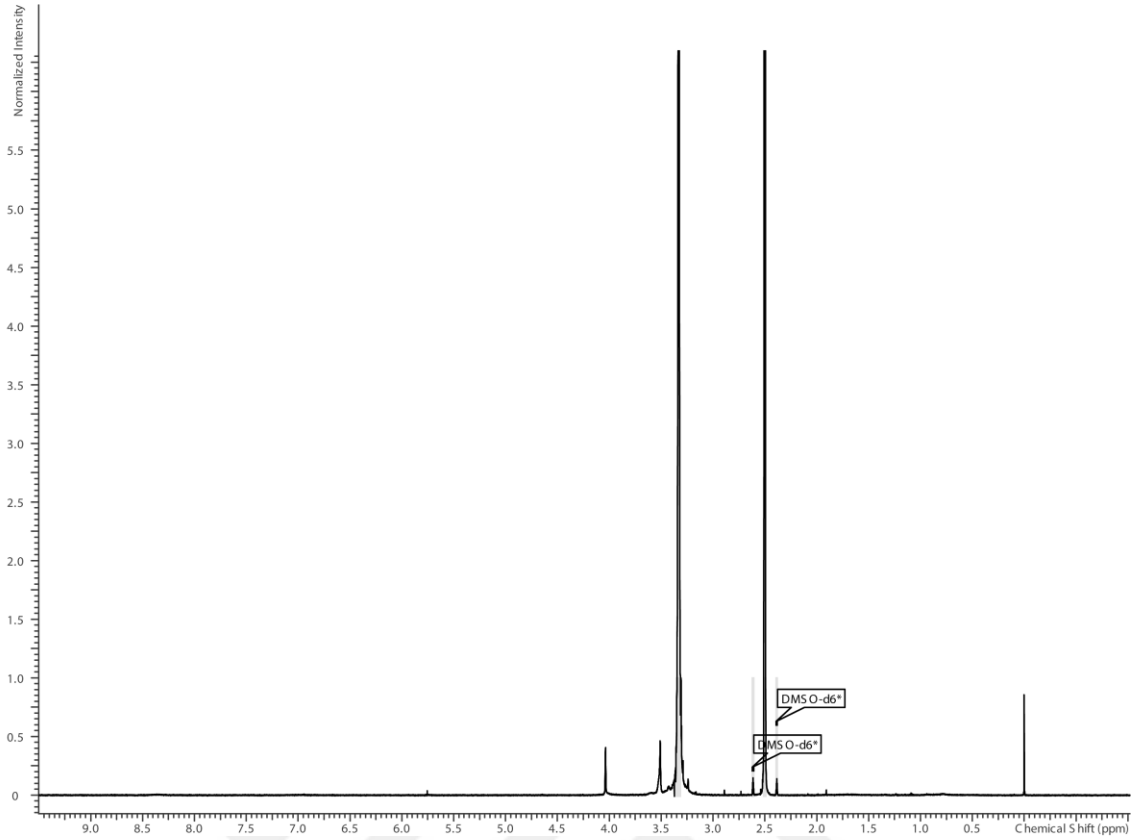

Figure 3.4 ^{1}H-NMR spectrum of CCMs in DMSO

Nanosight Tracking analysis was performed to determine the size and morphology analysis of the CCMs. Based on this analysis, CCMs were synthesized with 95 nm size and low polydispersity index (Figure 3.5E).

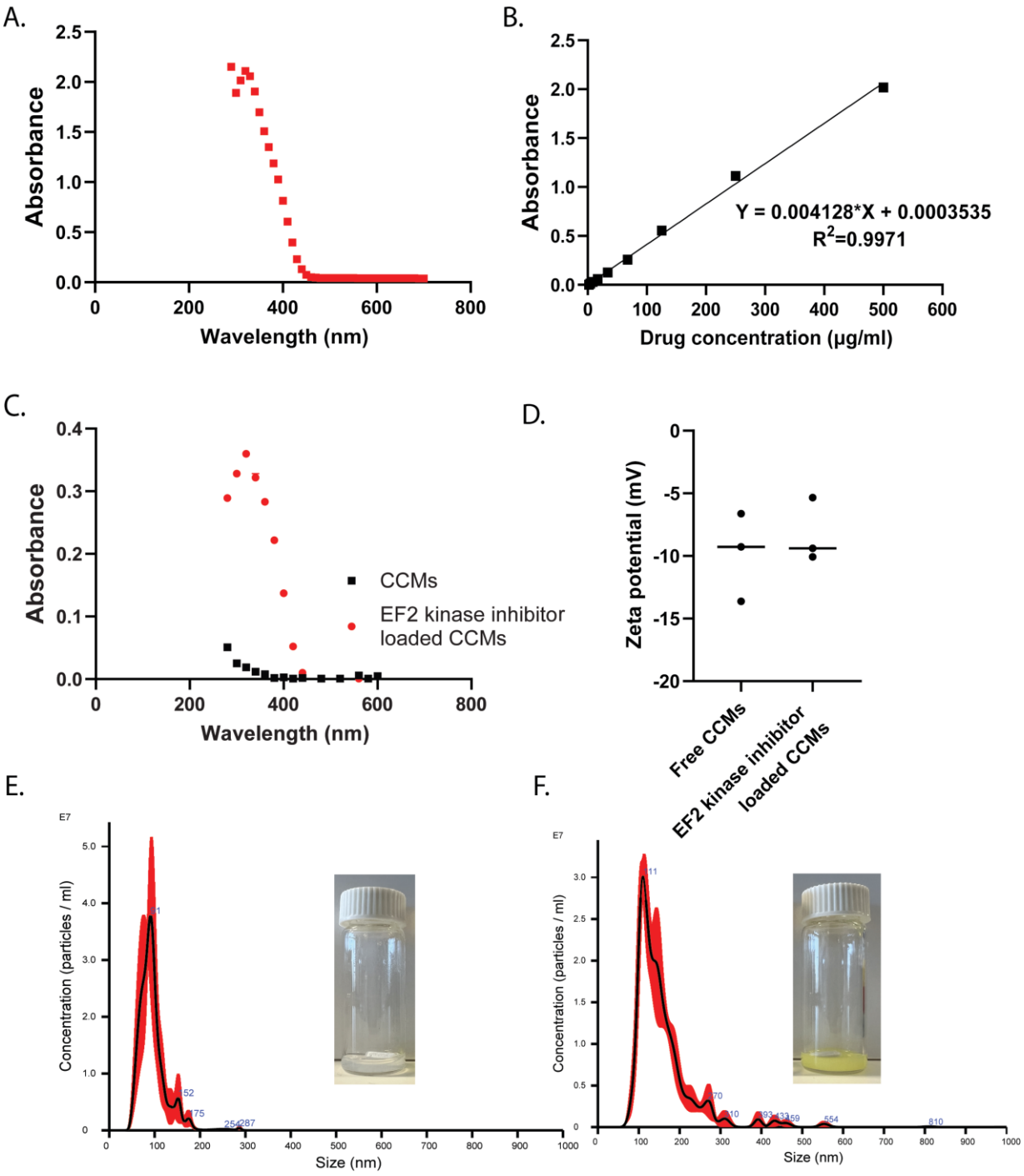

Figure 3.5 Absorbance scanning of EF2 kinase inhibitor (A), Calibration curve of EF2 kinase inhibitor (B), Free CCMs and EF2 kinase loaded CCMs absorbance spectrum (C) Zeta potential of free CCMs and EF2 kinase inhibitor loaded CCMs (D), Nanosight analysis of CCM(E) and EF2 kinase loaded CCMs

3.3.4 Preparation of EF2 Kinase Inhibitor Loaded CCMs

To determine the percentage of entrapment (% EE) and loading efficiency (%LE) of the EF2 kinase inhibitor within the drug-loaded CCMs, the absorbance spectrum of the drug was scanned to determine its highest absorbance value. Based on the analysis, it was determined that the highest absorbance value of the EF2 kinase inhibitor was 320 nm (Figure 3.5A). Therefore, a calibration curve was drawn using this value to assess the concentration of the drug in the drug-loaded CCMs. To draw the calibration curve for the EF2 kinase inhibitor, various concentrations of the drug were used, including 500, 250, 125, 62.5, 31.25, 15.62, 7.81, and 3.9 μg/ml, and absorbance of each concentration was measured at 320 nm, and the resulting data were plotted to generate the calibration curve given Figure 3.5B.

After drawing the calibration curve for the EF2 kinase inhibitor, the next step was to determine the loading efficiency (LE%) and entrapment efficiency (%EE) of the drug-loaded CCMs. To do this, the EF2 kinase-loaded CCMs and a sample of free polymer (used to eliminate any absorbance from the polymer) were dissolved in DMSO, and the absorbance was measured at 320 nm. The absorbance values were then used to calculate the concentration of the drug in the CCMs and to determine the LE% and EE %.

Based on the absorbance measurements at 320 nm, the absence of absorbance from the free polymer at 320 nm is a significant finding, as it suggests that there was no interference from the polymer in the absorbance measurements of the drug-loaded CCMs. This is important for ensuring the accuracy of drug concentration measurements and the subsequent calculation of LE% and %EE Figure (3.5C)

With these findings, the loading efficiency (LE%) and entrapment efficiency (EE%) of the EF2 kinase inhibitor in the CCMs were calculated to be 78% and 4.26%, respectively. The LE% represents the proportion of the drug that was successfully loaded into the CCMs, while the %EE reflects the amount of drug that was retained within the CCMs after the loading process. These values indicate that a significant proportion of the drug was successfully loaded into the CCMs, with a relatively low amount of drug remaining free in the solution.

3.3.5 Cell Viability Tests

The optimization of cell number is a critical step in evaluating the efficacy of drug-loaded CCMs. To determine the optimal cell number for our study, we seeded HER2 positive (BT474, HCC1954) and HER2 negative cell lines (MCF7, MDA-MB-231) with varying numbers of cells. Based on our analysis, we found that seeding 5000 or 10000 cells per well resulted in the highest absorbance values that did not exceed 1 at 72 hours, and there was a gradual increase in absorbance over time. These findings are illustrated in Figure 3.6, which shows the absorbance values for the different cell lines at varying cell numbers. The optimal cell number was determined based on a balance between achieving sufficient cell growth and avoiding saturation effects that can occur at higher cell densities.

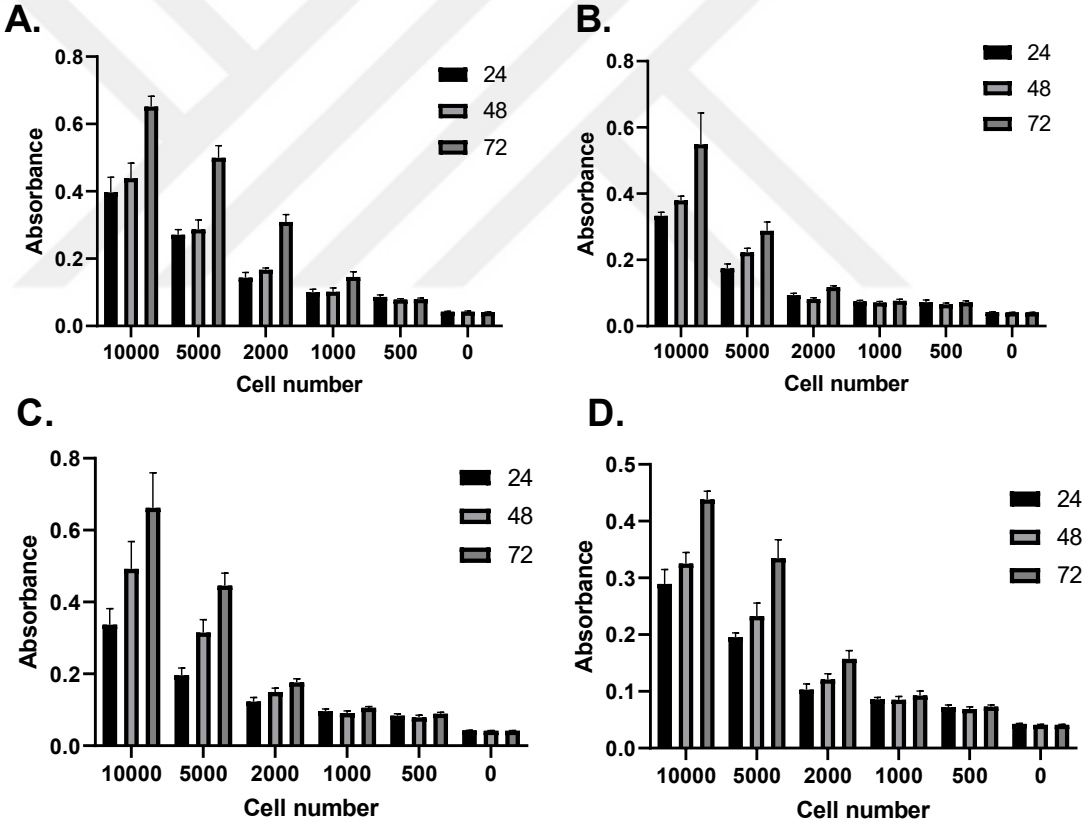

Figure 3.6 Cell number optimization of HER2 positive, HCC1954(A), BT474 (B) and HER2 negative MCF7(C), MDA-MB-231(D) cell lines

Once the optimal cell number was determined, we proceeded to evaluate the efficacy of the drug-loaded CCMs using a panel of breast cancer cell lines, including HCC1954, BT474, MCF7, and MDA-MB-231. The free polymer and EF2 kinase inhibitors were also evaluated alongside the EF2 kinase-loaded CCMs to assess their effects on cell growth and viability. This approach allowed us to compare the effectiveness of the drug-loaded CCMs with the unencapsulated drug and the polymer alone and to evaluate the potential impact of the CCMs on drug delivery and efficacy. After optimization, IC50 values of free EF2 kinase inhibitor were determined using 0.625-40 µM concentrations of EF2 kinase inhibitor on these cell lines at different time points. (Figure 3.7). IC50 values of EF2 kinase inhibitor were given in Table 3.1.

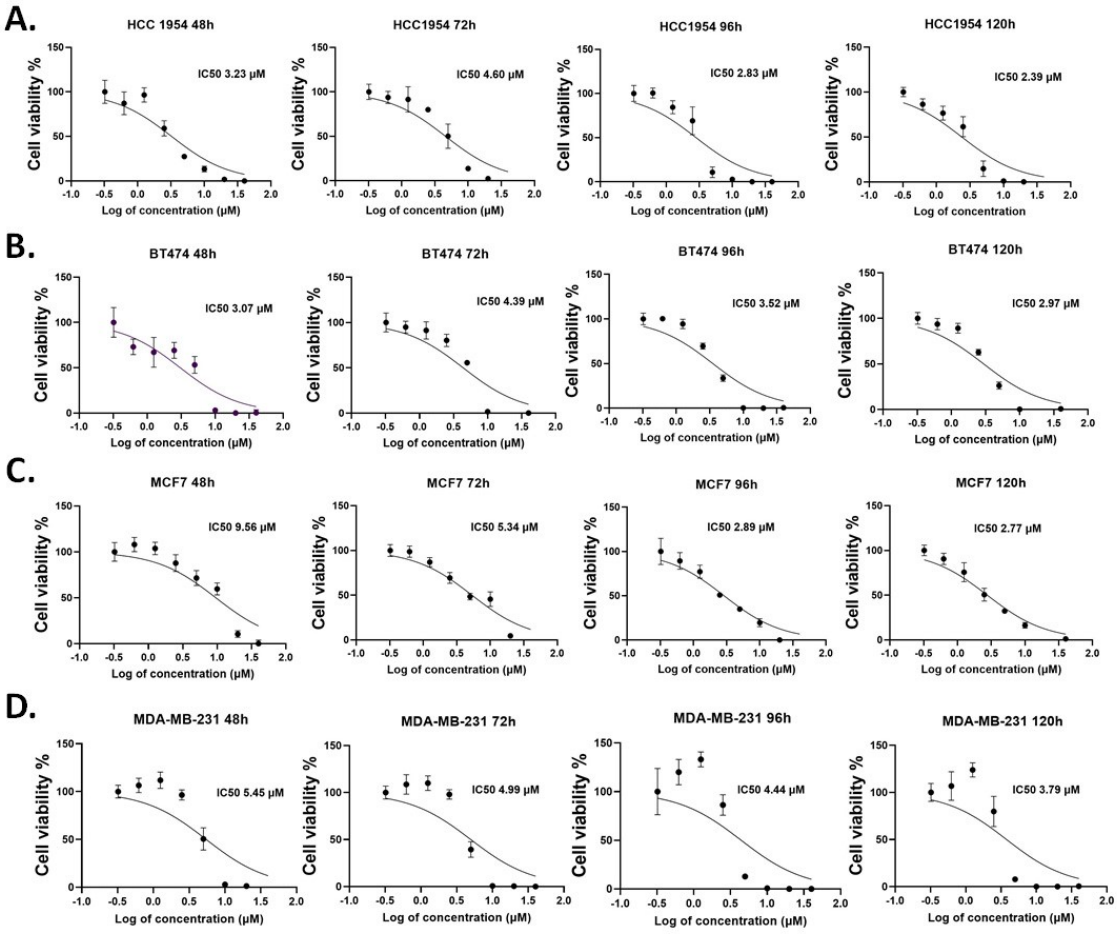

Figure 3.7 IC50 value of HER2 positive, HCC1954(A), BT474 (B), HER2 negative MCF7 (C) and MDA-MB-231 (D) cell lines 48h, 72h, 96h, and 120h

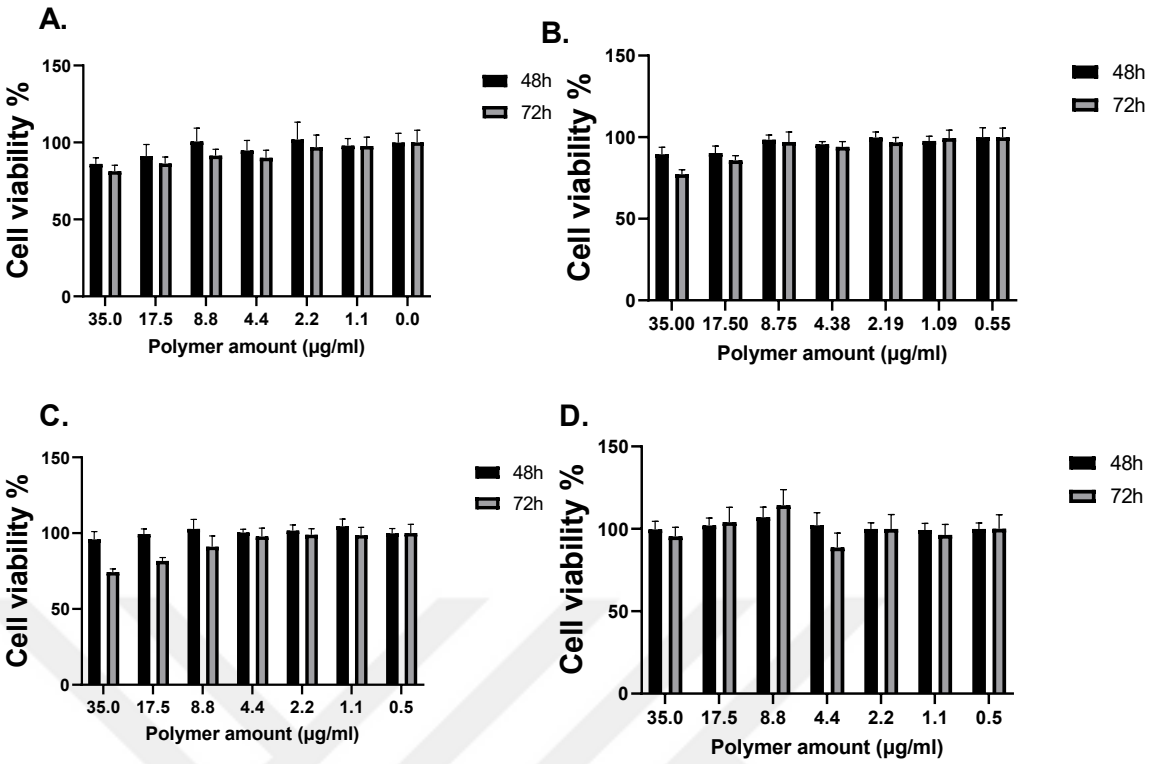

Figure 3.8 Cell viability of free polymer on HER2 positive, HCC1954 (A), BT474 (B), and HER2 negative MCF7 (C), MDA-MB-231 (D) cell lines

The cytotoxicity of free CCM on HCC1954, BT474, MCF7, and MDA-MB-231 was also evaluated by the MTT experiment. The results showed that the cell viability of HCC1954, BT474, MCF7, and MDA-MB-231 cells was slightly dependent on the CCMs amount. The polymer amount used ranged from 0.5 to 35 µg ml^{-1}, which are the polymer amounts that are used in EF2 kinase inhibitor-loaded CCMs. The viability of the cells was higher than 80% at the concentrations from 0.5 to 35 µg ml^{-1} for 48 and 72 h incubation which is given in Figure 3.8.

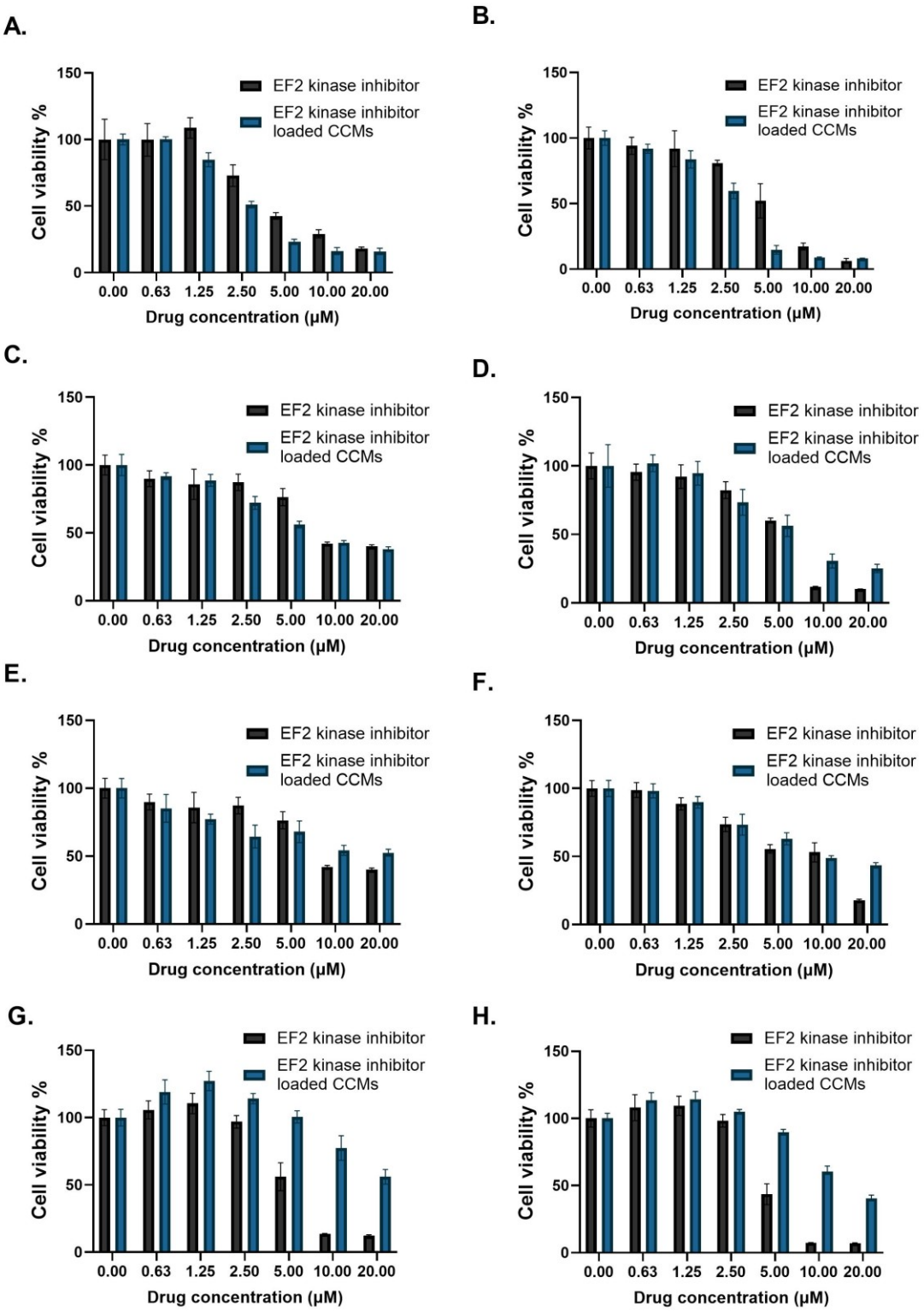

Figure 3. 9 Cell viability of EF2 kinase inhibitor (black) and EF2 kinase inhibitor loaded CCMs (blue) on HER2 positive HCC1954 (A), BT474 (C), HER2 negative MCF7 (E), MDA-MB- 231 (G) for 48 h and HER2 positive HCC1954 (B), BT474 (D), HER2 negative MCF7 (F), MDA-MB-231 (H) 72h

The cytotoxicity of EF2 kinase inhibitor-loaded CCMs on HCC1954, BT474, MCF7, and MDA-MB-231 was also evaluated by the MTT experiment. EF2 kinase inhibitor-loaded CCM showed higher toxicity on HCC1954, BT474, and MCF7 cell lines compared to the free EF2 kinase. However, free EF2 kinase inhibitor showed higher toxicity on MDA-MB-231 compared to the EF2 kinase inhibitor loaded CCMs (Figure 3.9). Also, IC50 values of EF2 kinase inhibitor and EF2 kinase inhibitor loaded CCMs were calculated and given in Table 3.1.

Table 3.1 IC50 values of EF2 kinase inhibitor and EF2 kinase inhibitor loaded CCMs

	EF2 kinase		**EF2 kinase-loaded CCMs**	
	48h	72h	48h	72h
HCC 1954	3.23 µM	4.60 µM	2.17 µM	2.33 µM
BT474	3.07 µM	4.39 µM	3.71 µM	3.75 µM
MCF7	9.56 µM	5.34 µM	1.74 µM	2.98 µM
MDA-MB-231	5.45 µM	4.99 µM	14.54 µM	9.09 µM

IC50 values of EF2 kinase inhibitor were calculated as 3.23 and 4.60 µM for HCC1954 cells, 3.07 and 4.39 µM for BT474 cells, 9.56 and 5.34 µM for MCF7 cells, 5.45 and 4.99 for MDA-MB-231 cells at 48- and 72h respectively. Furthermore, the IC50 values of EF2 kinase inhibitor loaded CCMs were calculated as 2.17 and 2.33 µM for HCC1954 cells, 3.71 and 3.75 µM for BT474 cells, 1.74 and 2.98 µM for MCF7 cells and 14.54 and 9.09 µM for MDA-MB-231 cells at 48h- and 72h. These results showed that EF2 kinase inhibitor-loaded CCMs enhanced the efficacy of EF2 kinase inhibitors on the HCC1954, BT474, and MCF7 cell lines. For the MDA-MB-231 cell line, EF2 kinase inhibitor-loaded CCMs showed toxicity and less efficacy compared to free EF2 kinase inhibitors. Since MDA-MB-231 is a triple-negative breast cancer cell line, ER-, PR- and HER2-, this result could be explained with the uptake of our nanoparticle system could be performed with the receptor-mediated mechanism, but further experiments are needed to confirm this explanation.

Chapter 4

Sulfobetaine-Based CCMs for Breast Cancer: HER2-Specific Peptide (LTVSPWY) and Antibody (Herceptin) Targeted Nanocarriers

4.1 Introduction

In recent years, nanocarriers have been used effectively in cancer treatment due to their remarkable properties, such as accumulation at the tumor site with the EPR (enhanced permeability and retention) effect, being stimulus-sensitive, and an ability to target the tumor site with a specific ligand. Numerous studies are still being carried out to increase the effect of nanoparticles by adding new properties to nanoparticles [140,141]. Polymeric micelles, one of the nanoparticle types, have been studied comprehensively due to their ability to increase solubility, reduce drug toxicity, and allow the targeting of tumor areas with specific ligands. Polymeric micelles are formed by self-assembling a diblock copolymer consisting of hydrophilic and hydrophobic blocks, giving the aforementioned properties. Numerous hydrophilic polymers have been studied as the shell of the micelles, and polyethylene glycol (PEG) is the most widely used due to its superior biocompatibility and stealth effect against proteins [142–144]. However, a recent study reported that PEG-carrying micelles showed an unexpected immunogenic response because of the accelerated blood clearance (ABC) phenomenon, resulting in the rapid removal of nanocarriers and reduced efficacy [145]. Although PEG is still frequently used in nanocarrier structures, potential

candidates with similar characteristics and non-immunogenicity have been searched. Recently, micelles containing zwitterions have received much interest due to their high biocompatibility and non-bioadhesive characteristics [146,147]. Betaine polymers consist of anion and cation groups in the same molecule that give these zwitterionic polymer properties. In addition, betaine polymers such as polysulfobetaine are characterized by a high biocompatibility rate due to their structure, similar to phosphatidylcholine (PC), which is, located in the cellular membrane [148]. Moreover, betaine polymers are sensitive to several stimuli, such as pH and temperature, as a type of upper critical solution temperature (UCST). Using zwitterionic polymers in the structure of carrier systems has been recently reported for cancer treatment purposes. Fuji et al. prepared betaine-based nanoparticle bearing zwitterionic polymers, and they found that these nanoparticles showed efficient tumor permeability compared to a nonionic POEGMA-based nanoparticle [149]. Studies have also shown that sulfobetaine methacrylate-functionalized nanoparticles improve cancer treatments due to their long circulation times and similarity to cell membranes that increase uptake by cancer cells [129,150–152]. Although micelles containing betaine groups have these superior properties, an early release may be encountered in self-assembly-formed micelles. To prevent early release and increase the stability of the micelles, there are several studies in which CCMs are synthesized. In the synthesis of CMs, acid-sensitive micelles can be obtained by using cross-linkers containing acid-sensitive acetal and ketal groups, thus preventing the early release and release of the drug in the tumor region, which is more acidic than the blood [63].

RAFT polymerization is the most demanded technique for synthesizing different macromolecular architectures, with a large range of monomer systems allowing uniformity in chain length and resulting in a well-defined polymer with a low PDI (polydispersity index). Besides that, self-assembled micelles can be easily cross-linked before, during, and after polymerization, with the micelles' living group by adding divinyl compounds to the solution [114,153–155]. It gives stability to the micellar structure, preventing premature drug release, with smart nanocarrier characteristics. Also, owing to the living radical group in the macromolecular structure, RAFT polymerization gives an opportunity to conjugate biomolecules like peptides and antibodies.

Since passive targeting of nanocarriers is insufficient to reach the desired location, more effective active targeting methods are needed. In this context, ligands recognizing target molecules expressed in large numbers on the surface of tumor cells are added to

the nanocarrier structure with appropriate methods to achieve results, such as directing the drug to the target and reducing the side effects of chemotherapy. Ligands bound to these carriers can be in peptide, antibody, or aptamer structures, which offer different targeting efficiencies [156–158]. Despite the absence of a naturally occurring ligand for the HER2 receptor, various artificial ligands such as antibodies, Fab fragments, single-chain variable fragments, affibodies, and peptides have been developed for targeted drug delivery. One of the most well-investigated strategies for targeted drug delivery to the HER2 receptor is the utilization of antibodies that can recognize the HER2 receptor and conjugate with them nanoscaled systems such as nanoparticles and immunoliposomes. Studies have shown that immunoliposomes conjugated with anti-HER2 antibodies have a prolonged circulation in the bloodstream and selectively deliver drugs, such as doxorubicin, to HER2-positive tumors [159–161]. Due to the loss of activity in antibody-based ligand studies, peptides specifically selected for the HER2 receptor region in SKBR3 cells by the phage display technique are also recommended as an alternative with more advantages [112,113,162,163]. The peptide LTVSPWY is another ligand that was discovered through a technique called biopanning, which uses a library of peptides to identify binding partners through affinity selection. This peptide has been used to target various receptors, including HER2. It has been used to deliver an antisense oligonucleotide specifically to HER2-positive tumor cells [7,164]. Additionally, it has been used to deliver a pro-apoptotic compound, called alpha-tocopheryl succinate (alpha-TOS), selectively to HER2-overexpressing cancer cells. Also, it has been conjugated into magnetic nanoparticles for imaging purposes [165,166]

Herein, we aimed to prepare CCMs, which targeted HER2-positive breast cancer cells with pH-sensitivity features, and compare targeting efficiencies of a HER2-specific peptide (LTVSPWY) and Herceptin antibody towards breast cancer cells. To synthesize the shell part of the micelles, firstly, a sulfobetaine block, as a macroCTA, was synthesized by RAFT polymerization. Following this step, macroCTA was copolymerized with di(ethylene glycol) methyl ether methacrylate (DEGMA) and aminoethyl methacrylamide (AEMA) and an acid-sensitive cross-linker to obtain CCMs. For comparison of the targeting efficiencies of peptide and antibody, a HER2-specific peptide (LTVSPWY) and a HER2-specific antibody (Herceptin) were conjugated to the micelles. Then, doxorubicin (DOX) was loaded into the micelles by the incubation method. In conclusion, these CCMs have a high potential as a drug delivery system for breast cancer, with improved stability, targeting, and pH sensitivity properties.

4.2 Material Methods

4.2.1 Materials

4-Cyano-4-(phenylcarbonothioylthio) pentanoic acid (CTA), 4,4′-Azobis(4-cyano valeric acid) (ACVA), diethylene glycol methyl ether methacrylate (DEGMA), 2,2-dimethoxy propane, 2-hydroxyethyl methacrylate (HEMA), p-toluenesulfonic acid monohydrate (p-TSA.H2O), triethylamine, N-(3-dimethyl aminopropyl)-N′-ethyl carbodiimide hydrochloride (EDAC.HCl), N, N-diisopropylethylamine (DIPEA), and 1-hydroxy benzotriazole hydrate (HOBT), were purchased from Sigma-Aldrich, Waltham, MA, USA. N-(3-Sulfopropyl)-N-methacroyloxyethyl-N,N-dimethylammonium betaine (sulfobetaine), 1,4 Dioxane, 2-Propanol, hexane, ethyl acetate, sodium nitrate, and acetonitrile for liquid chromatography, were purchased from Merck, Darmstadt, Germany. N-(2-Aminoethyl) methacrylamide hydrochloride (AEMA) was purchased from Polyscience, Evanston, Ilinois, USA, and sodium azide from SERVA, Heidelberg, Germany. A synthetic peptide (LTVSPWY) was purchased from CASLO Laboratory ApS, Lyngby, Denmark, with a purity of 95% and a molecular weight of 864.99 g/mol. Pierce™ BCA Protein Assay Kit and Pierce Quantitative Fluorometric Peptide Assay were purchased from Thermo Scientific, Waltham, MA, USA. All other chemicals used were of analytical grade.

4.2.2 Methods

4.2.2.1 Synthesis of Homopolymer and CCMs by RAFT Polymerization

Poly(SBMA) was synthesized with RAFT polymerization to obtain the macroCTA, according to our previous study [167]. Briefly, SBMA (sulfobetaine methacrylate), a chain transfer agent (CTA, 4-cyano-4-(thiobenzoylthio) pentatonic acid), and an initiator (ACVA) were dissolved in 0.5 M aqueous NaCl with pH 7–7.5, with the initial mo-lar ratios of monomer to the chain transfer agent to the initiator, [M]0/[CTA]0/[I]0 = 65/1/0.2, and the solution was sealed and purged with N2 for 30 min. Then, the solution was heated to 70 °C. To analyze the reaction mechanism, if it undergoes RAFT, aliquots were withdrawn with a syringe from the reaction medium at predetermined intervals during polymerization. All the samples were precipitated with cold diethyl ether three times and dried under a vacuum. The conversion of the monomer was calculated gravimetrically.

All the samples were analyzed with ^{1}H-NMR spectroscopy and GPC (Gel Permeation Chromatography). GPC analysis was performed by a TOSOH EcoSEC HLC-8320 GPC/SEC System with an RI Detector, Wyatt miniDAWN Treos-II MALS (Multi-Angle Light Scattering) detector equipped with PSS SUPREMA analytical 100 Å column (8 × 300 mm, 10 um, PSS Polymer Standards Service Inc, MA, USA) at room temperature. As a mobile phase, 80% aqueous 0.1 M ammonium sulfate−20% acetonitrile with 0.0125% sodium azide was used, with a flow rate of 2.0 ml/min. The injection volume of the filtered (by 0.2 µm PTFE filter) poly(SBMA) solutions was adjusted to 50 ml. For RAFT-functionality estimation, macroCTA's conversion was kept at a low degree (for 2 h), and the resulting pure polymer was analyzed by ^{1}H-NMR spectroscopy.
To synthesize the CCMs, we first synthesized an acid-sensitive cross-linker (CL, 2,2-dimethacroyloxy-1-ethoxypropane), according to the literature [115]. Following cross-linker synthesis, we proceeded to synthesize macroCTA, followed by the syn-thesis of CCMs by RAFT polymerization (Figure 4.1), as reported in our previous study. To synthesize the micelle, macroCTA (0.0033 mmol), AEMA (0.26 mmol), DEGMA (0.75 mmol), and CL (5% mmol) were dissolved in water, and the reaction was kept overnight at 70 °C, using ACVA as the initiator. The chemical structures of the purified copolymer micelles were characterized by FTIR and ^{1}H-NMR spectroscopies. The sample size and size distribution analyses were determined by dynamic light scattering spectroscopy [167].

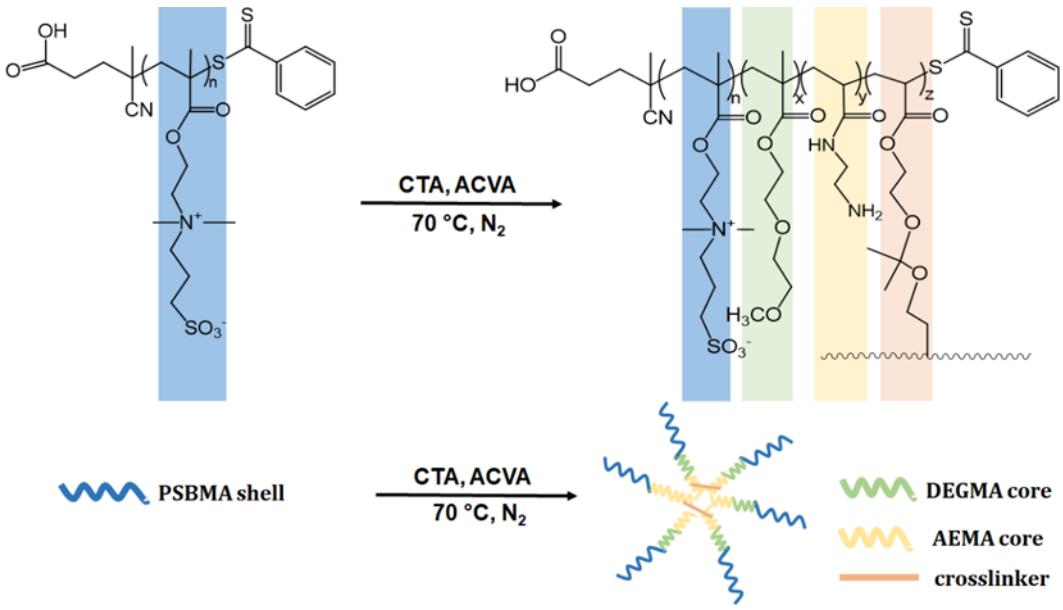

Figure 4.1 Synthesis of CCMs by RAFT polymerization

4.2.2.2 Preparation of Targeted CCMs

Due to the hydrophobic nature of the peptide, the peptide conjugation reaction was carried out in an organic solvent. For the peptide conjugation to the CCMs' COOH groups, which come from the RAFT polymerization, 100 mg of CCMs was first dis-solved in 3 ml of DMSO/DMF (3:1) mixture. Then, this solution was stirred at 60 °C overnight and cooled to 25 °C. Following this step, EDC (3.07 mg), HOBT (2.23 mg), DIPEA (4.18 μL), and varying amounts of peptide (13.84, 1.38, 0.55, 0.27, 0.14 mg, LTVSPWY) were added to the solution and stirred at 35 °C for two days. In order to remove unbounded peptide, the solution was dialyzed against water for about 24 h and then freeze-dried. (Fisherbrand Regenerated Cellulose Dialysis Tubing, MWCO 3500) [168–170].

For antibody conjugation to the CCMs' COOH groups, 100 mg of CCMs was dis-solved in 4 ml of PBS containing 0.9% NaCl, stirred at 60 °C overnight, and cooled to room temperature. EDC (3.07 mg), sulfo-NHS (4.4 mg), and varying amounts of Herceptin (60, 30, 15, 5, and 1 mg) were added to this solution and stirred at room temperature for two days. The solution was dialyzed against water (Fisherbrand Regenerated Cellulose Dialysis Tubing, MWCO 3500) for about 24 h. Then, the sample was centrifuged in the tubes with a 300,000 MWCO membrane to remove unconjugated Herceptin (Vivaspin, 300,000 MWCO), and the product was lyophilized [171,172]. The products were analyzed by FTIR and ^{1}H-NMR spectroscopies to confirm peptide and anti-body coupling. A BCA protein assay kit (Pierce BCA Protein Assay, Thermo Scientific, Waltham, MA, USA) was used for the antibody coupling quantification. We estimated the peptide content on the nanocarrier using a fluorescence spectrophotometer at Ex/Em 280/350 nm. Size and charge analyses of the micelles were performed by a Malvern Zetasizer (Malvern). The morphology of the peptide and antibody-coupled CCMs were examined by SEM (scanning electron microscope; Carl Zeiss EVO LS10, NTS, Germany).

4.2.2.3 Drug Loading Study

The CCMs, peptide-conjugated CCMs, and antibody-conjugated CCMs were dis-solved in DMSO. Then, doxorubicin.HCl and TEA (3×DOX.HCl) were added to the solution and stirred overnight, with protection from light. In order to remove unbounded DOX from micelles, these solutions were dialyzed against water (Fisherbrand Regenerated Cellulose Dialysis Tubing, MWCO 3500), and the water solution was changed three times and lyophilized [173,174]. To calculate the amount of doxorubicin,

1 mg of micelles was dissolved in 1 ml of DMSO, and the absorbance of the micelles was measured using UV-Vis spectrophotometry at 496 nm, and EE% and LE% were calculated based on the formula given below [154];

Loading efficiency (%) (LE%) = (Amount of DOX in micelles (mg)/Amount of the micelles (mg)) × 100
Encapsulation efficiency (%) (EE%) = (Amount of DOX in micelles (mg)/Initial amount of DOX (mg)) × 100

(4.1)

The method used for the DOX quantification was validated according to the ICH Guidelines [175].

4.2.2.4 Drug Release

Doxorubicin-loaded micelle solution (2 ml), with a concentration of 1 mg/ml, was placed in a dialysis membrane (Fisherbrand Regenerated Cellulose Dialysis Tubing, 12,000 MWCO). The dialysis membrane was placed into 0.05% SDS, containing acetate buffer (10 mM, 150 mM NaCl, pH 5) or PBS (10 mM, pH 7.4) buffer, and shaken (100 rpm) at 37 °C. At predetermined time intervals, 1 ml of buffer solution was withdrawn and replaced with fresh buffer. DOX release was determined by measuring the absorption (at 496 nm) of the DOX molecule in withdrawn buffers, and the cumulative release plots were obtained using the formula below.

$$CR\ (\%) = [(100 \times ((V_m \times CDOX_{(n)}) + (1\ ml \times \Sigma\ CDOX_{(n-1)}))]/W_0 \quad (4.2)$$

According to this, V_m: emission media volume; W_0 (mg): the amount of drug loaded; $CDOX_{(n)}$: the amount of DOX (mg/ml) in the sample taken from the release medium; $CDOX_{(n-1)}$: (n − 1). the amount of DOX in the sample taken from the media.

4.3 Results

4.3.1 Synthesis and Characterization of Homopolymers, CCMs, and Targeted CCMs

4.3.1.1 Characterization of Homopolymers and CCMs

In the first step, sulfobetaine homopolymer, as a macroCTA, was synthesized by RAFT polymerization. As explained in the methods section, molecular weight, and conversion analyses were performed to show whether the reaction was carried out by the

RAFT mechanism. The molecular weight and conversion analyses were carried out by GPC and ^{1}H-NMR spectroscopy, respectively. Figure 4.2A shows the GPC chromatograms of the homopolymers' molecular weights, analyzed at certain time intervals by taking samples from the reaction medium. A clear shift in the molecular weight of the samples is shown by GPC, as the overlapping molecular weight distributions are shown [176]. Also, Figure 4.2B shows the ^{1}H-NMR spectrum of the homopolymers taken from the reaction medium while the reaction is in progress. A decrease in monomer peaks (vinyl protons) shown at 5.8 and 6.2 was seen as the polymerization time in-creased. Figure 4.2C, D shows the conversion-time and molecular weight-conversion relationships drawn with the obtained data, and the relative amount of monomer/CTA/initiator that increased linearly was determined as 65/1/0.2.

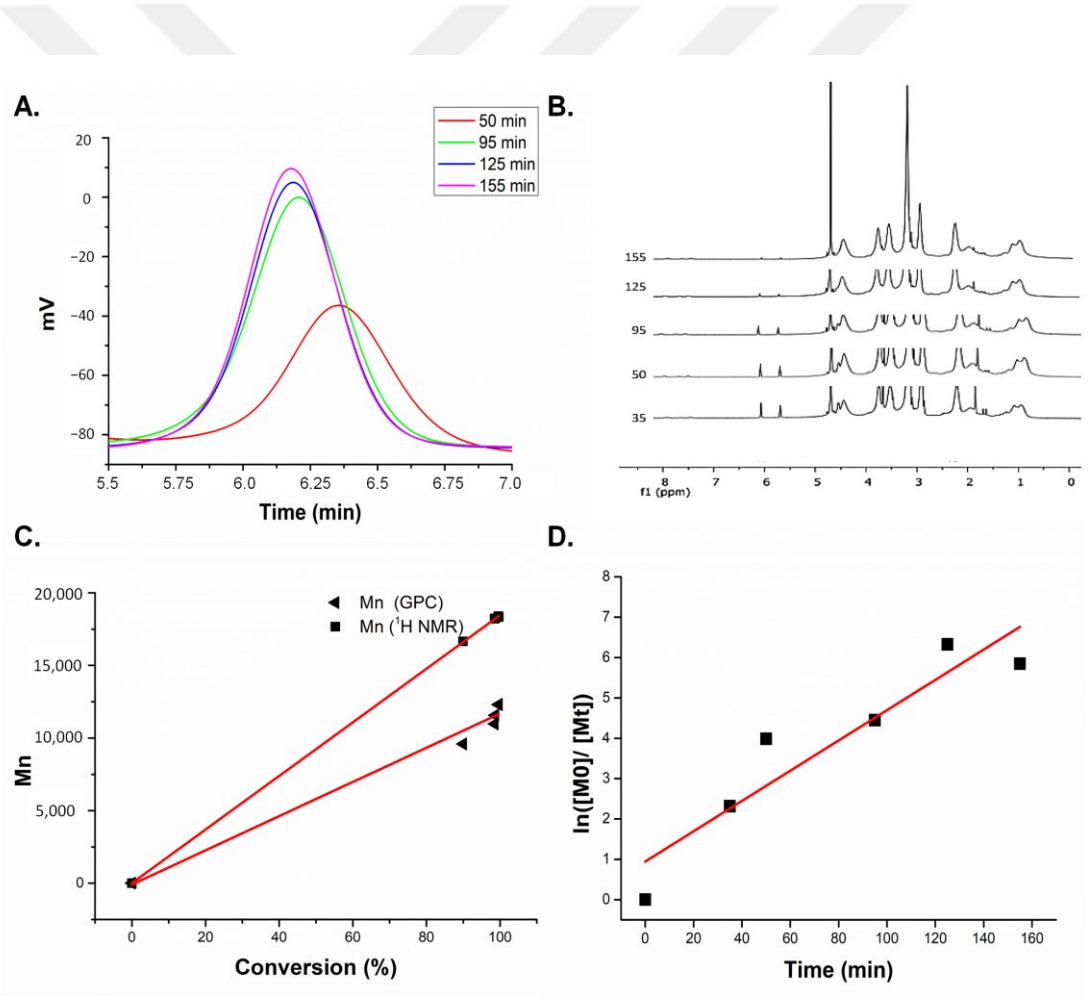

Figure 4.2 Evolution of GPC chromatograms of sulfobetaine at different times of RAFT polymerization acquired from LS detector (A) ^{1}H-NMR spectrum of sulfobetaine at different times. (B) Relationship between molecular weight and monomer conversion of sulfobetaine polymerizations. (C) Kinetics of RAFT polymerization of sulfobetaine (D)

Following this step, we characterized the polymers and micelles by ^{1}H-NMR spectra. Although homopolymer and CCM structural characterizations by ^{1}H-NMR spectra were performed in our previous study [177], we used these data for comparison and to under-stand the efficiency of peptide- and antibody-binding to the CCMs. Due to this reason, we obtained ^{1}H-NMR spectra of the homopolymer and CCM again and have reported it here. As discussed thoroughly in our previous study, Figure 4.2A shows the homopolymer's (macroCTA's) ^{1}H-NMR spectrum, in which the polymer backbone and $CH_2CH_2SO_3^-$of SBMA's side chain signals are seen at 0.8–2.5 ppm. SBMA's side chain signals are also seen at 2.96–3.13, 3.22–3.38, 3.80–4.00, and 4.46–4.65 ppm, respectively. The RAFT-ended group signal is seen at 7.49–8.20 ppm. For the CCMs' ^{1}H-NMR spectrum, which is shown in Figure 4.2B, signals of the polymer backbone and -$CH_2CH_2SO_3^-$ of SBMA's side chain were observed at 0.8–2.5 ppm [178]. The signal of CTA end groups was not seen in the ^{1}H-NMR spectrum of CCMs, because of the higher molecular weight of CCMs, and the RAFT end group remaining in the internal structure of the micelle, as also discussed in our previous study [177]. As mentioned above, ^{1}H-NMR analysis of the homopolymer and micelle was utilized for the characterization of targeted NCs (as given in Figure 4.2A, B).

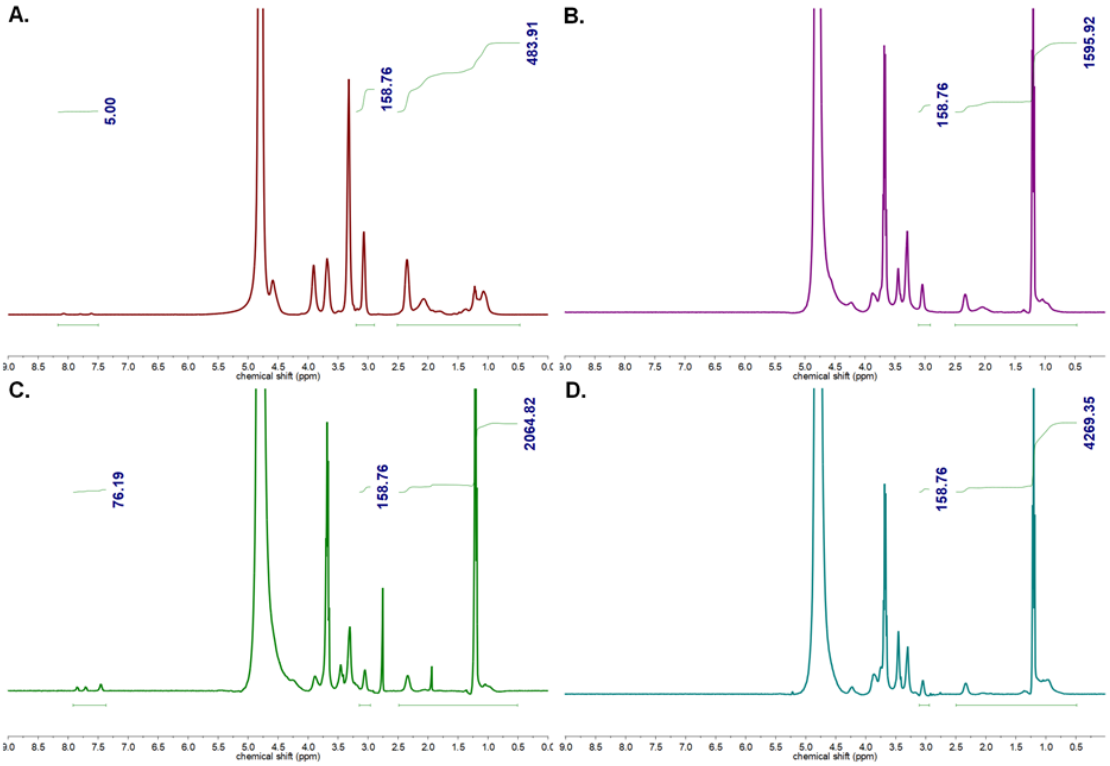

Figure 4. 3 ^{1}H-NMR spectrum of macroCTA (A), CCMs (B), peptide conjugated CCMs (C), and Herceptin conjugated CCMs (D) in D_2O

4.3.2 Characterization of Peptide and Antibody Conjugated CCMs

In this study, a HER2-specific peptide and antibody (Herceptin) were conjugated to the CCMs, to obtain targeted nanocarriers, with the aim of comparing the peptide and antibody targeting. In order to do that, the LTVSPWY peptide was attached to the CCMs structure due to its reported HER2-binding ability with weak immunogenic properties, and Herceptin was attached to the CCMs to obtain an antibody-based targeting molecule. Conjugation of the hydrophobic peptide to the nanoparticles might cause solubility problems due to its amino acid content. PEG-coupling to the LTVSPWY peptide has been applied to overcome this problem, resulting in better aqueous solubility characteristics [166,179,180]. In our case, instead of using PEG-coupling to LTVSPWY, we directly conjugated LTVSPWY peptides towards the carboxylic group into the polysufobetaine shell part of the micelles. However, this drove us to use varying amounts of peptides to find the peptide-conjugated micelle with optimum size and solubility properties.

It is also well known that the conjugation of HER2 antibodies causes an increase in nanocarrier size. Additionally, due to the high molecular weight of Herceptin, the nanoparticles may cause precipitation due to the increased nanoparticle molecular weight upon Herceptin binding. Therefore, we decided to use different amounts of antibodies to find antibody-conjugated micelles with good properties in terms of size and solubility. According to the literature, various amounts of Herceptin have been used to obtain Herceptin conjugated nanoparticles. Peng et al. used a molar ratio of the aldehyde group of polymers to amino groups of 5:1 due to one Herceptin molecule containing 66 free primary amino groups; Fiandra et al. incubated nanoparticles (1 mg) at room temperature for 2 h in the presence of Herceptin (0.3 mg) [156,181].

Here, we obtained a series of peptide- (PC1-PC5) and antibody-conjugated (AC1–AC5) CCMs by changing their mass ratios, as seen in Table 1. ^{1}H-NMR, FTIR, and fluorescence spectroscopies were used for the characterization of these targeted micelles, and the results are given in Table 1. ^{1}H-NMR spectra of a series of peptide- (PC1–PC5) and antibody-conjugated (AC1–AC5) CCMs are given in Figures 4.4. and 4.5.

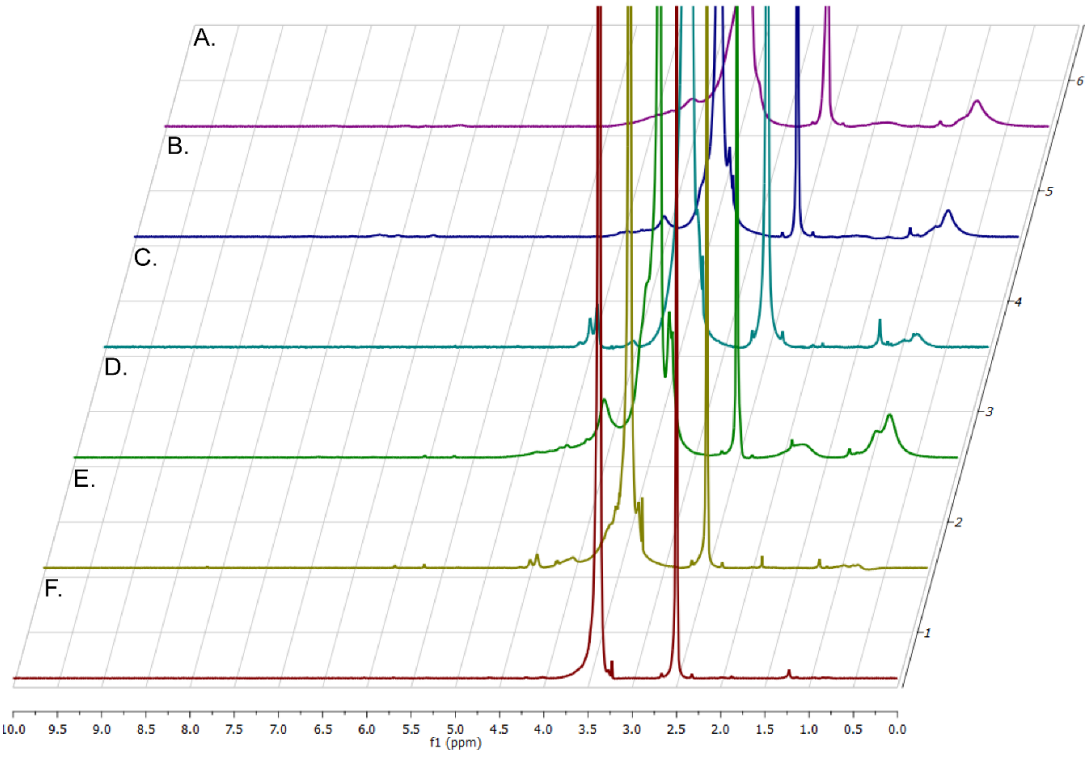

Figure 4.4 ^{1}H-NMR of AC1 (A), AC2 (B), AC3 (C), AC4 (D), AC5 (E), and CCMs (F) in DMSO

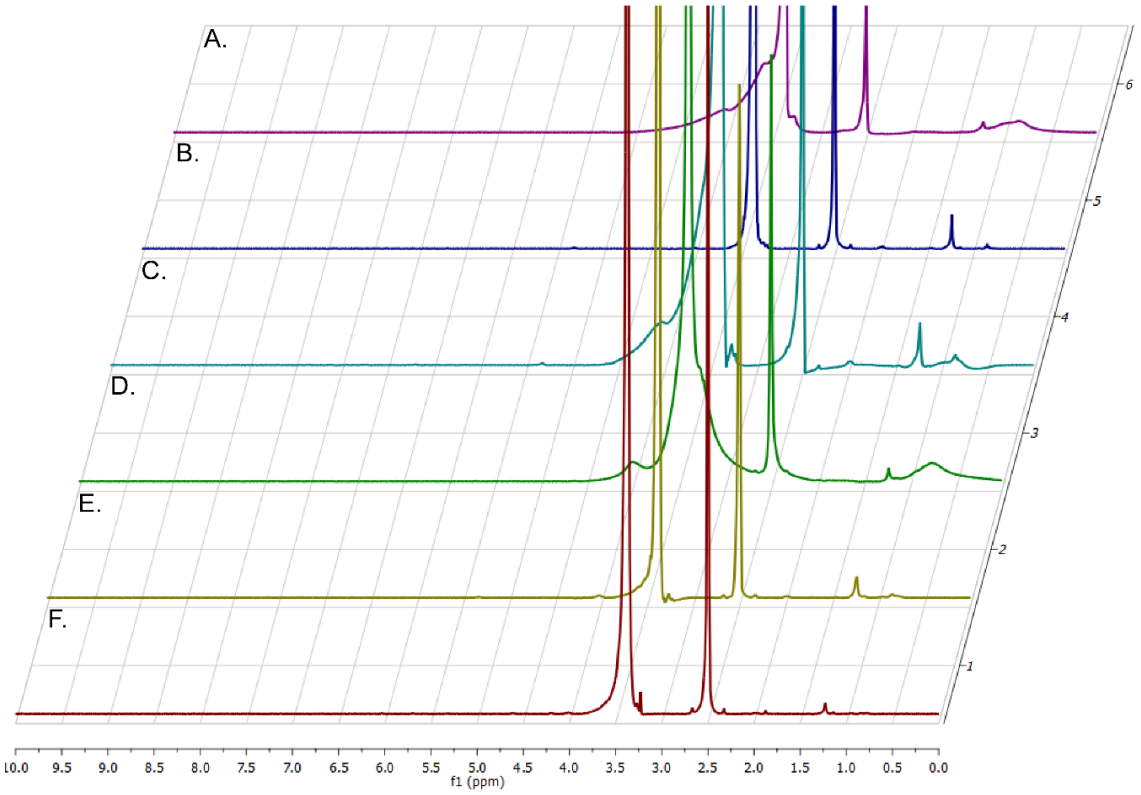

Figure 4.5 ^{1}H-NMR of PC1 (A), PC2 (B), PC3 (C), PC4 (D), PC5 (E), and CCMs (F) in DMSO

Table 4.1 Hydrodynamic diameter, size distribution, zeta potential, peptide, and antibody amount of CCMs

	Hydrodynamic Diameter (nm)	**PDI**	**Zeta Potential (mV)**	**Peptide Amount (µg/ml)**
CCMs	65.5 ± 6.2	0.269	14.5 ± 0.7	-
PC1	235 ± 127	0.345	9.15 ± 3.3	15.47 ± 0.49
PC2	141 ± 60	0.318	13.4 ± 3.8	3.19 ± 0.37
PC3	141 ± 33	0.415	13.8 ± 3.8	0.66 ± 0.09
PC4	118 + 43	0.482	14.7 ± 3.6	0.60 ± 0.27
PC5	113 ± 17	0.486	14.5 ± 3.7	0.34 ± 0.04
	Hydrodynamic Diameter (nm)	**PDI**	**Zeta Potential (mV)**	**Antibody amount (µg/ml)**
CCMs	65.5 ± 6.2	0.269	14.5 ± 0.7	-
AC1	428 ± 113	0.466	13.3 ± 5.4	580.4 ± 21
AC2	316 ± 119	0.499	16.2 ± 3.8	407.6 ± 10.2
AC3	90 ± 40	0.344	10.2 ± 4.3	279 ± 9.5
AC4	79 ± 45	0.287	11.4 ± 4.1	113.7 ± 3.0
AC5	78 ± 38	0.280	15.0 ± 4.7	52.33 ± 2.7

In the peptide conjugated CCMs' (PC2) ^{1}H-NMR spectrum, shown in Figure 4.3C, besides the peaks belonging to the structure of the CCMs, new peaks were obtained at 1.46, 7.46, 7.71, and 7.85 ppm. While the signals of CTA end groups were not seen in the ^{1}H-NMR spectrum of CCMs, due to its high molecular weight, these aromatic signals were seen at 7.46, 7.71, and 7.85 ppm in the spectrum of peptide-bound CCMs originating from the tryptophan, tyrosine, and proline amino acids of the peptide. Similarly, Jie et al. synthesized LTVSPWY peptide-modified magnetic nanoparticles and showed benzene protons in the tryptophan and tyrosine units at 8.32 ppm [166]. In the ^{1}H-NMR spectrum of antibody-conjugated CCMs shown in Figure 4.3D, amine-related peaks were not observed clearly. However, we noticed that signals of -$CH_2CH_2SO_3^-$ of the SBMA side chain were overlayed at 2.96–3.13 ppm in the ^{1}H-NMR spectra of macroCTA, CCMs, peptide conjugated CCMs, and antibody-conjugated CCMs, which are shown in Figure 2A–D. When the integration of -$CH_2CH_2SO_3^-$ of SBMA side chain is calculated using RAFT end group signal set to be 5, which is shown at 7.49–8.20 ppm from macroCTA's ^{1}H-NMR spectrum, the integration peak corresponding to the SBMA signal was calculated to be 158.76 (equivalent to 2H from the group). Then we set the 2.96–3.13 signal as 158.76 for CCMs, antibody-conjugated CCMs, and pep-tide-conjugated CCMs; the integration of polymer backbone peaks, which was shown at 0.5–2.5 ppm in CCMs, peptide conjugated CCMs, and antibody-conjugated CCMs (AC3) were 1595.92, 2064.82, 4269.35, respectively. This shows that this increase in integration in the polymer backbone is due to the binding of the peptide and antibody to the carboxyl group at the end group of the micelle, which also confirmed the conjugation of peptide and antibody to the micelles. AC1–AC5 and PC1–PC5 series' ^{1}H-NMR spectra are given in Figures 4.4 and 4.5, respectively.

After confirming the structure with the ^{1}H-NMR spectrum, we continued with FTIR spectroscopy. In the FTIR spectra of CCMs, peptide, and antibody-conjugated CCMs, which are shown in Figure 4.6A, C, the peak intensities at 3450 cm^{-1}, assigned to O–H bending, and at 1600 cm^{-1}, assigned to N–H bending, increased due to the addition of peptide and Herceptin to the micelles compared to the CCMs. Moreover, the intensity of the peaks increased as the proportion of peptide, and Herceptin conjugated to the micelles in-creased. This might be explained by an increase in the N–H bonds arising from the peptide and antibody.

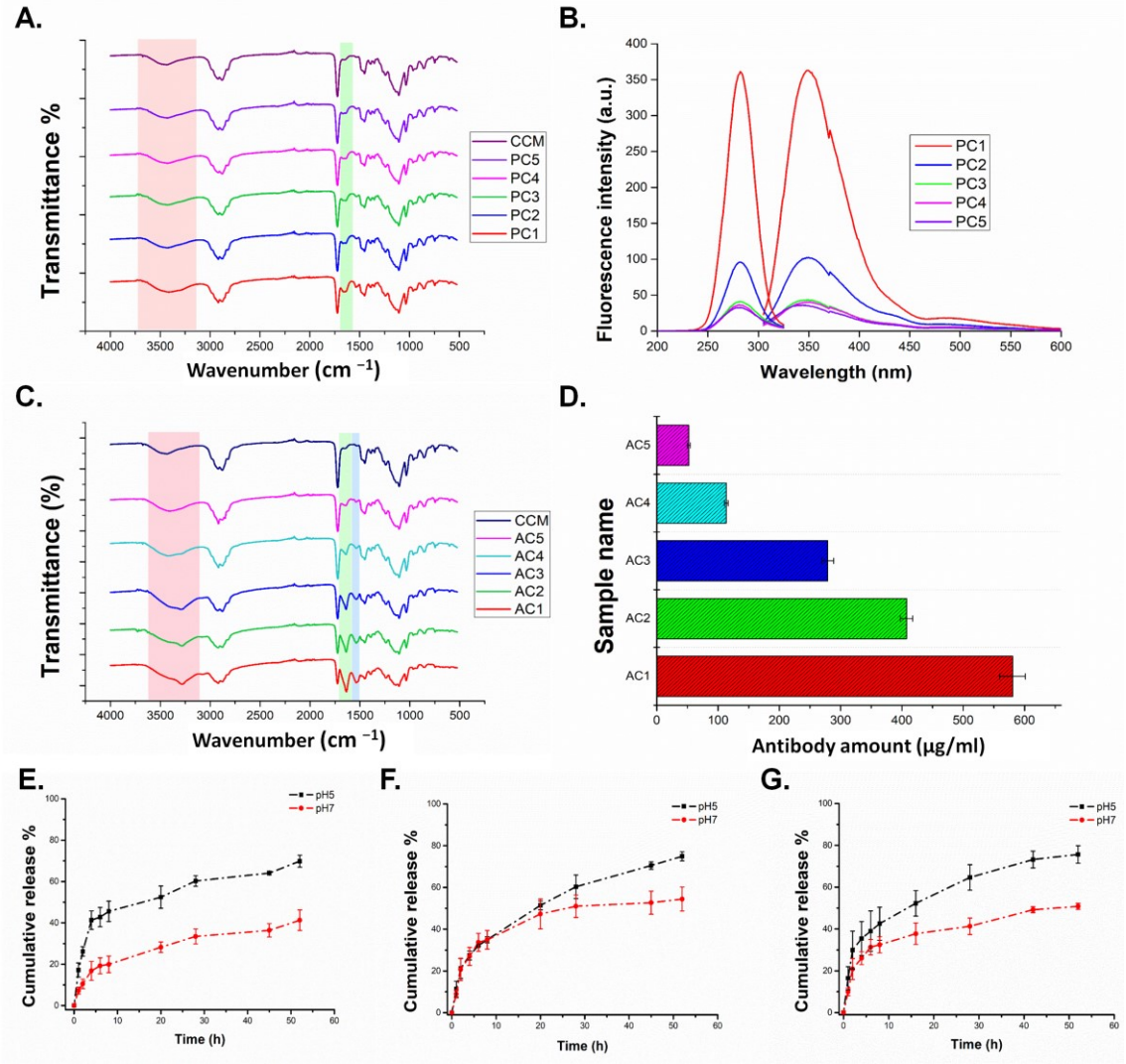

Figure 4.6 FTIR spectra of PC1-5 and CCMs (A), excitation and emission spectrum of peptide conjugated PCs (B), FTIR spectrum of AC1-5 and CCMs (C) antibody amount of ACs (D) release graph of CCMs (E) peptide-conjugated CCMs (F), antibody-conjugated CCMs (G)

After confirming the structure with ^{1}H-NMR spectrum and FTIR spectroscopies, we proceeded with fluorescence spectroscopy to determine the peptide and antibody amounts of the PC and AC series. Since our peptide sequence has amino acids (tryptophan and tyrosine) as a fluorescent feature, fluorescence scanning of the peptide (LTVSPWY) was performed to find the excitation and emission values with a 1 mg/ml concentration of peptide solution in DMSO. Here, the value where the peptide gave the highest absorbance was determined as 280 nm, which has also been shown to be the absorption value of tryptophan and tyrosine amino acids [182]. Then, we used this value as an

excitation value of the peptide and performed emission scanning, following this step, based on the highest emission value obtained from this scanning. Thus, the necessary Ex/Em values to measure the concentration of our peptide-bound micelle were determined as 280/350 nm. Afterward, a 1–100µg/ml concentration of the peptide solutions in DMSO was prepared, and a calibration graph was obtained (Figure 4.7).

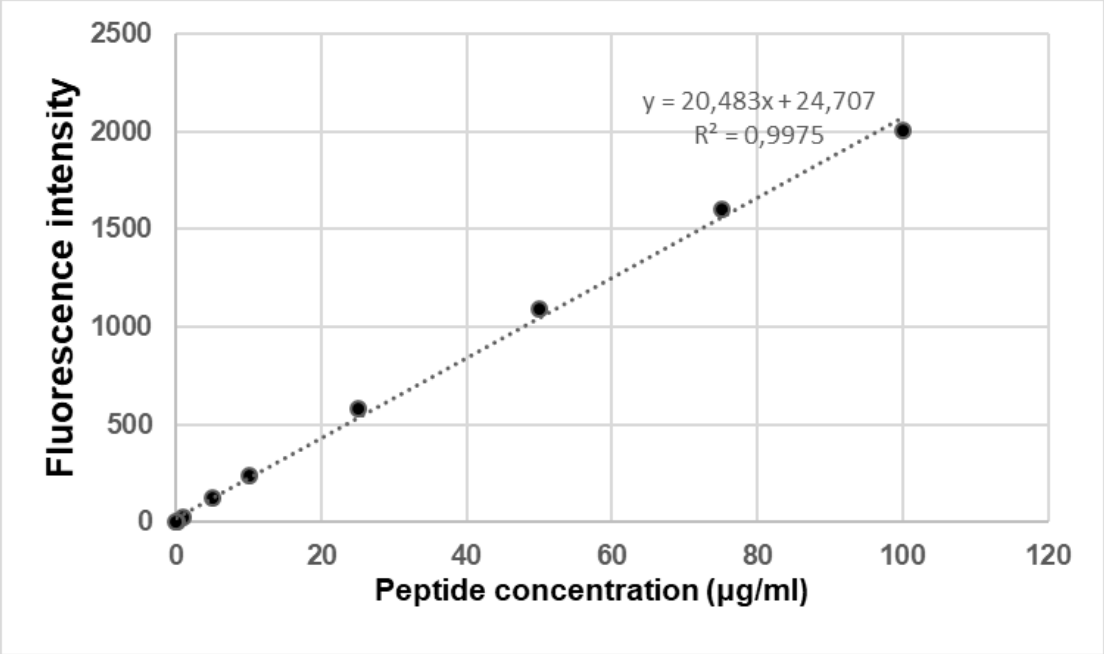

Figure 4.7 Calibration curve of peptide

PC1–PC5 and CCMs, as control group solutions, were prepared, and the peptide amount of these micelles was determined using this calibration graph. According to the fluorescence screening, which is shown in Figure 4.6B, the PC1 sample with the highest peptide ratio gave the highest fluorescence values, while a decrease in fluorescence values occurred when going toward PC5, and the fluorescence values of the PC4 and PC5 samples were close to the values of the CCMs. After this scanning process, the peptide amounts of the peptide-bound micelles were calculated as µg/ml using the fluorescence values obtained at Ex/Em 280/350 nm and are given in Table 4. In order to determine the Herceptin amount in the micelles, a BCA assay was per-formed. Figure 4.6D shows the amount of AC1–5 and CCMs with a 1 mg/ml concentration. According to these results, the AC1 sample had the highest amount of Herceptin, with 600 µg/ml, which is approximately 50% (w/w) of the micelles, and the amount of Herceptin decreased in the AC5 sample.

Following this chemical characterization, we determined the size and charge of the antibody and peptide micelles. Table 4. shows the size and zeta potential of the AC1–5 samples. The AC1–2 samples had the largest size at 400 and 300 nm, respectively, and their PDI (polydispersity index) values are very high. Since the increase in the Herceptin ratio caused the molecular weights of the AC1 and AC2 samples to increase, a tendency to precipitate was observed in the solutions of these samples (Figure 4.8).

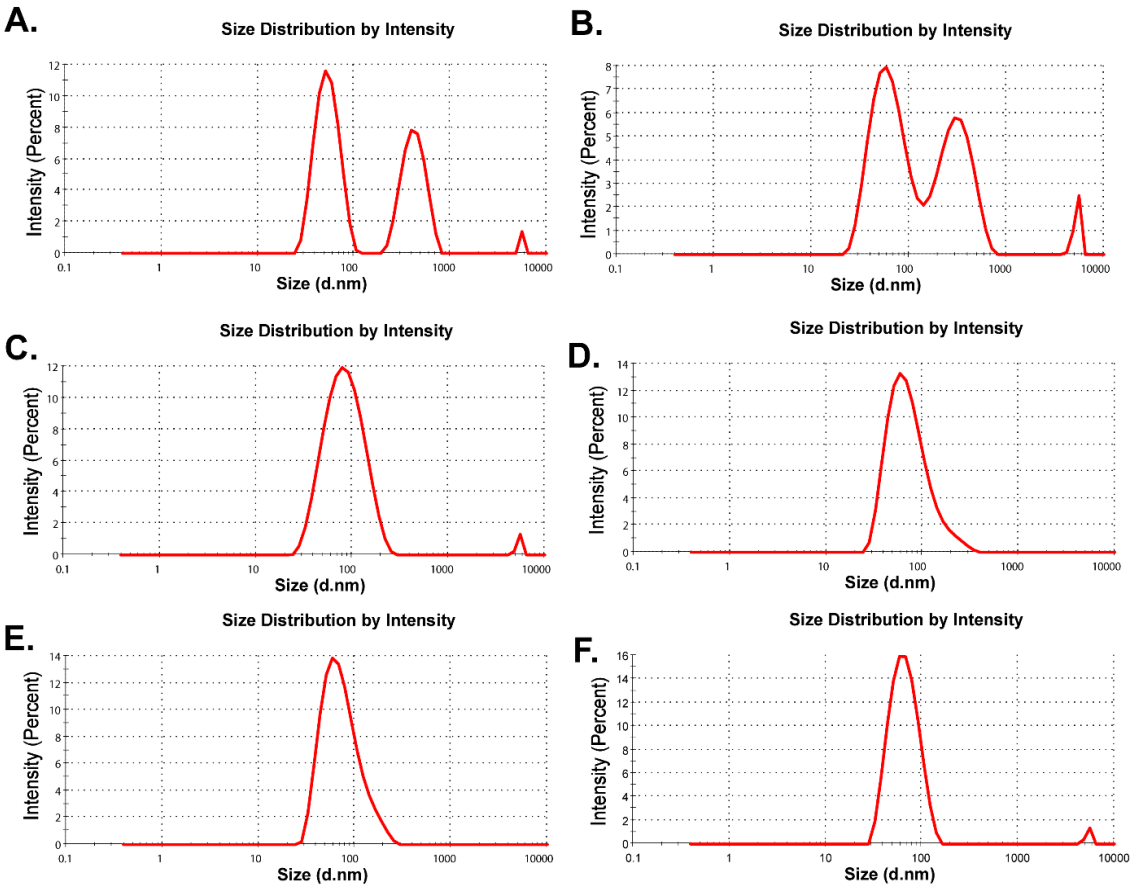

Figure 4.8 Size distributions of AC1 (A), AC2 (B), AC3 (C), AC4 (D), AC5 (E) CCMs (F)

However, it was observed that the AC3–5 samples exhibited superior characteristics in terms of size and solubility properties when compared to the AC1 and AC2 samples. Zhao et al. and Bolu et al. showed that Herceptin increased micelles' size and PDI values with conjugation [183,184]. Furthermore, it was observed that the zeta potential of Herceptin-conjugated micelles decreased as the ratio of Herceptin conjugation increased. Peng et al. also showed this type of phenomenon in their study. It might be explained by the increased number of –COOH groups on the micelles' surfaces, which reduces the micelles' charges [156]. Since this study aimed to show the importance of targeting, we

conducted our study with the AC3 samples, with high antibody content, good solubility, size, and charge properties (90 ± 40 nm, 10.2 ± 4.3 mV, 279 ± 9.5 µg/ml antibody).
For peptide-conjugated micelles, the PC1 samples had a larger size, and the micelle size decreased as the amount of peptide decreased (Figure 4.9).

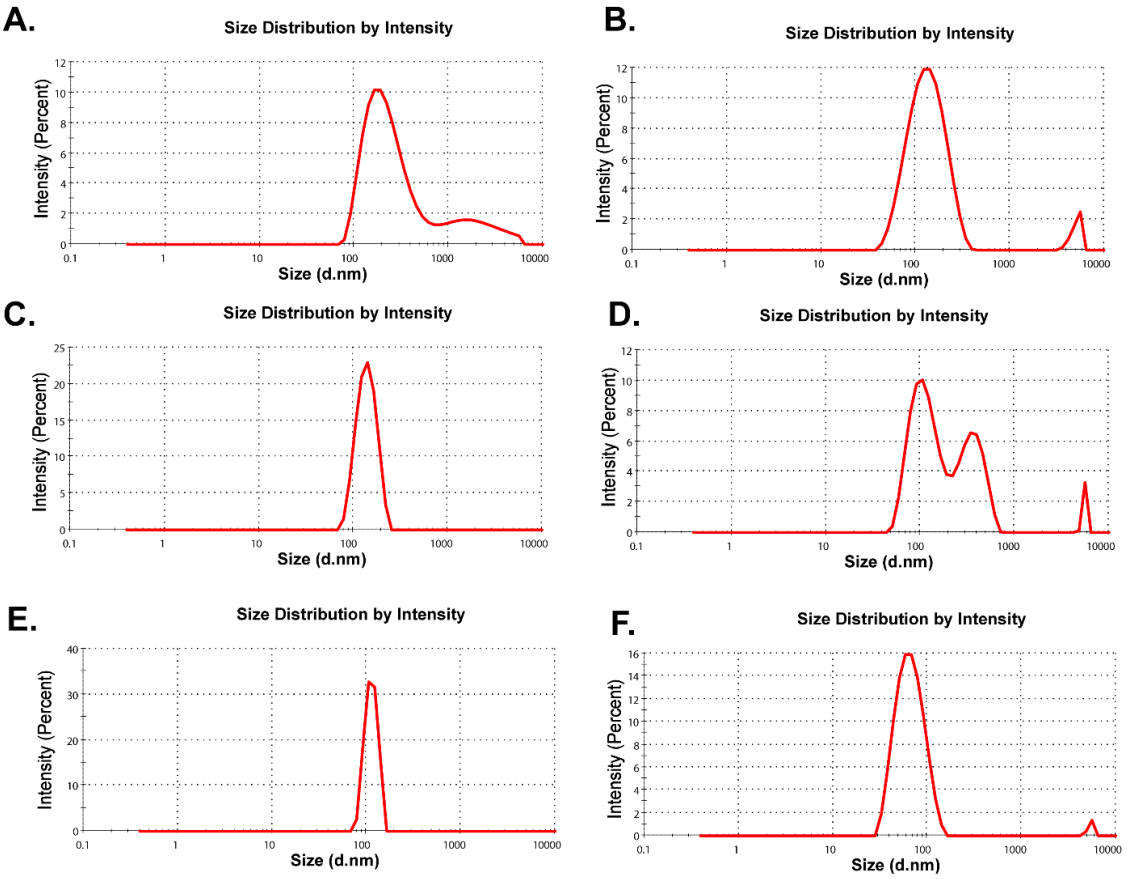

Figure 4.9 Size distributions of PC1 (A), PC2 (B), PC3 (C), PC4 (D), PC5 (E) CCMs (F)

However, the larger size of PC1, and higher hydrophobic peptide content of these micelles, caused a solubility problem. Also, the zeta potential of peptide-conjugated micelles decreased with an increased peptide ratio. It also has the same trend with antibody-conjugated micelles. Compared with PC1, the PC2–5 samples had good size, PDI, and solubility features. According to these data, we decided to continue with PC2, the most suitable sample, with high peptide content, good solubility, size, and charge properties. In summary, peptide and antibody conjugation increased micelle size, as CCMs have a size of 65.5 ± 6.2 nm, which is shown in Figure 4.8. and 4.9. Besides, SEM

images of AC1, AC3, and PC2 are shown in Figure 4.10 CCMs' sizes, determined by SEM and DLS spectrometry, have concurred with each other.

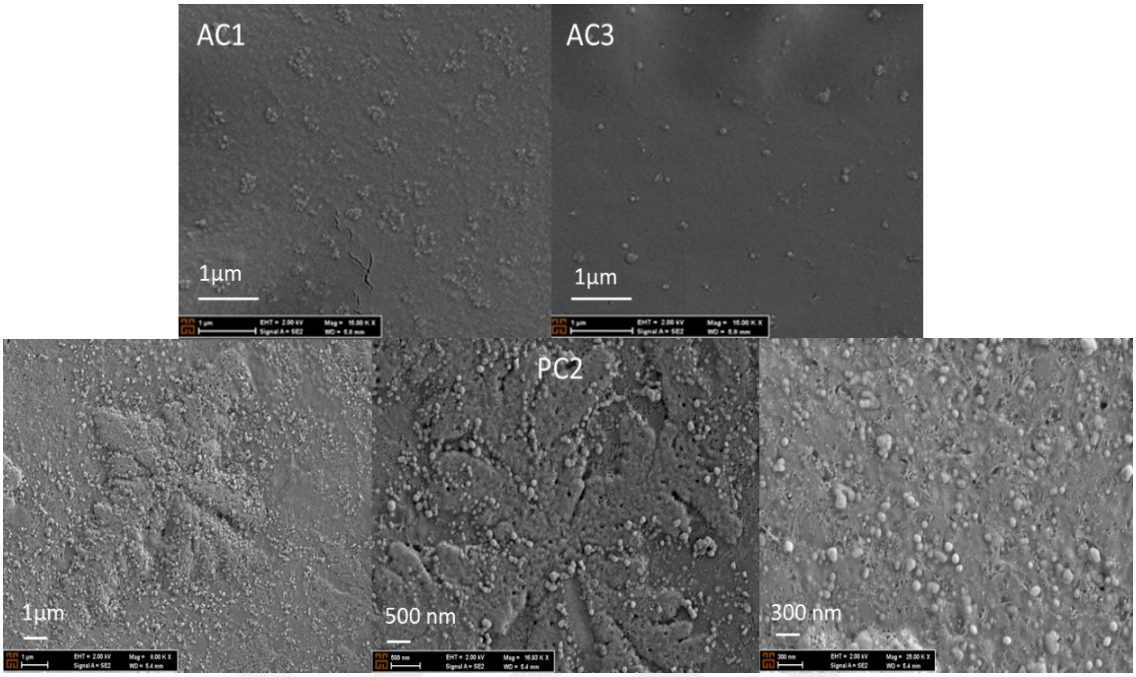

Figure 4.10 SEM images of selected samples (AC1, AC3, and PC2) of peptide and antibody-conjugated micelles

After the selection of AC3 and PC2 as the targeted CCMs, we proceeded to the drug-loading study. In this study, we used dialysis as a standard loading method. Based on this method, the drug amount can be calculated as either supernatant or pellet to calculate drug loading and entrapment efficiencies. Once we calculated both methods, we noticed that the supernatant method's loading and entrapment efficiencies were higher than the pellet ones. The difference between the two methods could be due to the adhesion of free DOX to the dialysis membrane, affecting its penetration to the supernatant. Therefore, we decided to proceed by pellet, which is more accurate than the supernatant procedure, and calculated the loading and entrapment efficiency with this method. The drug loading efficiencies of CCMs, PC2, and AC3 were 26, 50, and 56%, respectively, and the entrapment efficiencies of CCMs, PC2, and AC3 were 1.7, 2, and 3.1, respectively. Conjugation of the peptide and antibody increased their drug loading efficiency and entrapment efficiency. This might be explained by the hydrophobic peptides interacting with more of the hydrophobic doxorubicin and the higher molecular

weight of antibodies providing more interaction sites for doxorubicin, resulting in an increase in the loading and entrapment efficiencies.

4.3.3 Drug Release

Since we designed acid-sensitive CCMs, we performed a re-lease study in acidic and neutral environments (Figure 4.6E–G). According to the release graphs of the peptide and antibody-linked formulations, a varying release regime was observed at acidic and neutral pH. Peptide/antibody conjugation caused some changes in the release profiles. This proves the contribution of polymeric components to the non-targeted nanocarrier's release behavior. In the peptide-conjugated CCMs, a delayed drug release was obtained. In all three cases, drug release in acidic media is associated with cleavage of acetal bonds and with the zwitterionic character of sulfobetaine and its interaction with both DOX and the environment due to this feature. It can be expected that sulfobetaine, since it is negatively charged, has a lower preference for interacting with an acidic medium at pH 4.5, interacting with DOX (pKa > 7), and delaying the release in an acidic medium. In addition, it is a possibility that negatively charged sulfobetaine chains prefer to interact with the medium at neutral pH, and the release increases at this pH. It was seen that the release of DOX molecules is slightly higher at pH 7 with the addition of additional molecules, such as peptides or antibodies, to the structure. This may be because DOX also interacts with the peptide or anti-body on the carrier during loading, which was also released during release. In addition, the presence of molecules such as peptides/antibodies on the nanocarrier may cause a slight delay in the release by slowing down the solution entry into the structure, as reported in previous studies [161]. In summary, it can be said that, although a higher release is observed in the acidic medium due to peptide and antibody binding, the presence of peptides and antibodies causes lower than expected release. However, acid-induced release was observed in all three types of carriers.

Chapter 5

Conclusions and Future Prospects

5.1 Conclusion

In the scope of this thesis, two potential drug delivery systems, POEGMA, and sulfobetaine-based breast cancer-targeted CCMs, were prepared to target breast cancer.

In the first chapter, POEGMA-based CCMs polymeric micelles were prepared with double-moiety pH-sensitivity in which the drug is conjugated to the polymer with pH-degradable hydrazone bonds, and the micelle is core cross-linked with pH-degradable acetal bonds. To do that, MacroCTA was synthesized with functionality between about 60-70%, and then, the monomer/CTA/initiator ratio was determined as 100/1/0.2, and copolymer synthesis was conducted at this ratio. The MacroCTA functionality was maintained at 60-70%, allowing the RAFT-ended group required for conjugation with MALDOX to remain a living chain. Following this step, CCMs were synthesized successfully, and micelles with low PDIs were obtained. The increase in comonomer ratios (DEGMA and 4-VP, 0.25-0.75 mmol and 0.25-1 mmol, respectively) resulted in a noticeable increase in micelle size. In addition, increasing the amount of crosslinker (1, 5, 10%) cause an increase in size as expected due to core cross-linking. Since our aim was to use nanoparticles below 100 nm, we continued our experiment with CCM2. Following this selection, PDS modification was performed, and peaks of the ring proton shifted to around 7.3-7.6-8.4, which confirmed PDS modification. Doxorubicin maleimide was synthesized and confirmed with ^{1}H-NMR and MALDI-TOF analysis, and the expected maleimide peak and hydrazine peak appeared at 5 ppm and 6 ppm, respectively. Doxorubicin maleimide ($C_{37}H_{42}N_4O_{13}$) was analyzed by high-resolution MALDI-TOF mass spectrometer, and the molecular ion signal was observed as 809.24 m/z. MALDOX was conjugated to micelles, and it was confirmed by ^{1}H-NMR and UV-Vis spectrophotometer. In the ^{1}H-NMR spectrum, the hydrazine group signal was clearly observed on the spectrum of DOX-polymer conjugate at 9.64 ppm. The spectra of the micelle and drug-micelle conjugate were compared, and absorbance at 502 nm of the drug was observed, indicating that the drug was bound to the micelle. Also, peptide

(VSSTQDFP) binding to the micelles was confirmed by ^{1}H-NMR and size measurement. The size of the purified peptide-bound micelles increased from 70 nm to 90 nm, which was a demonstration of the peptide binding to the micelle structure. The peptide amount was also determined by Pierce Quantitative Fluorometric Peptide Assay, and the peptide amount of 1 mg/ml micelles was determined as 7.30±1.56 μg/ml. Following this step, release studies were performed in acidic and neutral pH environments to prove the acid-triggered degradation of micelles, and 78% of DOX was released from the micelle at pH 4.5 while only 31% of DOX was released at pH 7.4 in 24 h, which showed that CCMs exhibit a pH-dependent drug release profile.

Furthermore, the stability of micelles was checked during the six months in PBS, albumin-containing blood stimulation solution, and albumin-free blood stimulation solution with size measurement. Based on stability studies, the micelles remained stable in the PBS solution for up to 24 weeks. There is no change in the size of the CCMs observed in albumin-containing blood-stimulating solution at 37°C, even after one week, which confirms that in the case of i.v. Administration, these CCMs will maintain their stability in the presence of albumin for up to 1 week after the injection. Because these CCMs can be kept in PBS in a refrigerator (4°C), we investigated their stability in terms of size in these conditions and obtained that the size of the CCMs was almost the same at 4°C up to 24 weeks. These results confirmed that the CCMs are stable in shelf conditions and can be kept for six months in PBS without any change. Following this step, degradation studies were performed, and the degradation of micelles in acidic conditions was analyzed with GPC, ^{1}H-NMR, and size measurements. Due to acid-degradable bonds in the core cross-links of the micelles, they are expected to degrade at acidic conditions. In order to prove this, micelles were incubated at pH 4.5 and 37°C for 24 hours. Samples were withdrawn from the medium (between 0-24 hours) and analyzed by DLS, FTIR, ^{1}H-NMR spectroscopies, and GPC. According to the size analysis, the diameters of the particles decreased with degradation time. This was also proved by GPC, in which the retention volume of the particles shifted to larger values meaning that the size of particles was smaller and eluting from the column later. We also confirmed the degradation with FTIR analysis. All findings showed that CCMs could be degraded into tiny particles that can facilitate drug release by the effect of pH. Finally, this drug delivery system was tested in in vitro studies on breast cancer cells in the scope of TUBITAK 116R057 and the collaboration with Prof. Dr. Yusuf Baran (İYTE Molecular Biology and Genetics Department). Since cell culture studies were reported as a master thesis in Gizem Tuğçe

Ulu's thesis number 573239 at YÖK Thesis Center, we did not report these results within the scope of this thesis. However, we would like to discuss these results in the conclusion section to show the efficacy of our nanoparticle system on breast cancer. According to these results, the cytotoxicity of free CCMs and HER2 peptide conjugated CCMs were tested on SKBR-3 and MCF-10A cell lines, and it was found to be slightly dependent on the CCMs amount with high viabilities. Following this step, the cytotoxicity of DOX containing formulations were tested on SKBR3 (HER2 positive) and MCF10A (HER2 negative) cell lines. According to these results, DOX-HER-2-CCMs were 2-fold more effective on SKBR-3 cells as compared to DOX-CCMs which shows the targeting effect of the HER2-specific peptide on breast cancer cells. Note that the addition of targeting peptide to CCMs did not reveal any difference in terms of selectivity for MCF-10A cells which demonstrates no preferential uptake of targeted CCMs by healthy cells according to the IC50 values. The effects of DOX-HER-2-CCMs were higher on HER-2 overexpressed SKBR-3 cells. Also, DOX-conjugated HER-2 micelles increased the effect of DOX as compared to both only DOX and DOX-CCMs. Moreover, less toxicity was observed towards MCF-10A cells, and it means that using CCMs with or without peptide revealed a kind of masking effect on the toxicity by DOX. The concentration of IC50 values of CCMs for SKBR-3 cells was applied, and it was shown that the fluorescence intensity density value of DOX-CCMs-HER-2 is higher as compared to DOX-CCMs despite a low concentration application of DOX-CCMs-HER-2. The conjugated HER-2 peptide on CCMs provided a high uptake rate by SKBR-3 cells. This result revealed that the DOX-CCMs-HER-2 was more effective than DOX-CCMs on SKBR-3 HER-2 positive cells.

The second section of the thesis was carried out at MD Anderson Cancer Center, supported by the TUBITAK in the scope of the 2214 A project. According to these results, POEGMA-based CCMs (CCM2, in the first chapter) were used, and EF2 kinase inhibitor was loaded to these CCMs by dialysis methods. CCMs were synthesized successfully, and micelles with low PDIs were obtained as determined with Nanosight Tracking analysis. For drug loading studies, absorbance scanning of EF2 kinase inhibitor was performed, and 320 nm was used to determine drug loading and entrapment efficiency. Drug loading was performed with dialysis methods, and %LE and % EE were calculated as 78% and 4.13%. Since our aim was to determine the efficiency of CCMs on breast cancer cell lines, we used four different cell lines, including HER2, ER, PR positive cell lines such as BT474, HCC1954, and HER2 negative, ER and PR positive cell lines such

as MCF7, and triple-negative breast cancer cell line such as MDA-MB-23. These cell lines' cell numbers are optimized for the MTT experiment. Following this step, the IC50 value of free EF2 kinase inhibitor was calculated on BT474, HCC1954, MCF7, and MDA-MB-231 cell lines. Free CCMs also treated on cells and tested with an MTT experiment, and CCMs did not show toxicity on these cell lines. To compare the efficacy of free EF2 kinase inhibitor and EF2 kinase loaded CCMs were treated on BT474, HCC1954, MCF7, and MDA-MB-231, and IC50 values were calculated. IC50 values of EF2 kinase inhibitor were calculated as 3.23 and 4.60 μM for HCC1954 cells, 3.07 and 4.39 μM for BT474 cells, 9.56 and 5.34 μM for MCF7 cells, 5.45 and 4.99 for MDA-MB-231 cells at 48- and 72h respectively. Furthermore, the IC50 values of EF2 kinase inhibitor loaded CCMs were calculated as 2.17 and 2.33 μM for HCC1954 cells, 3.71 and 3.75 μM for BT474 cells, 1.74 and 2.98 μM for MCF7 cells and 14.54 and 9.09 μM for MDA-MB-231 cells at 48h- and 72h. These results showed that EF2 kinase inhibitor-loaded CCMs enhanced the efficacy of EF2 kinase inhibitors on the HCC1954, BT474, and MCF7 cell lines. For the MDA-MB-231 cell line, EF2 kinase inhibitor-loaded CCMs showed toxicity and less efficacy compared to free EF2 kinase inhibitors. Since MDA-MB-231 is a triple-negative breast cancer cell line, ER-, PR-, and HER2-, this result could be explained by that the uptake of our nanoparticle system could be performed with the receptor-mediated mechanism, but further experiments are needed to confirm this explanation. Also, in our delivery system, CCMs designed for enhancing in vivo efficacy of water-insoluble EF2 kinase inhibitors, we need to test their efficacy in the in vivo breast cancer tumor model. In light of these findings, our nanoparticle system enhanced the efficacy not only with Doxorubicin but also with EF2 kinase inhibitors. This provides the opportunity to be a broad-scale drug delivery system by being tested with different drugs in the future.

In the third chapter, poly sulfobetaine-based, breast cancer-targeted, and acid-cleavable CCMs were prepared. First, macroCTA (poly(SBMA)) was synthesized, and the monomer/CTA/Initiator ratio was determined as 65/1 /0.2, and copolymer synthesis was conducted at this ratio. CCMs were synthesized successfully by RAFT polymerization, and low PDI-micelles with 65.5 ± 6.2 nm in size and 14.5 ± 0.7 mV in charge were obtained. Since the hydrophobic nature of the peptide and the high molecular weight of the antibody caused the solubility problem, peptide (LTVSPWY) and antibody (Herceptin) were conjugated to CCMs with different amounts to optimize the structures' physicochemical properties. In this context, PC1-5 formulations containing different

ratios of peptide and AC1-5 formulations containing different ratios of antibody were synthesized, and ^{1}H-NMR, FTIR, size and charge measurement and fluorescent intensity techniques were used for confirmation of peptide and antibody conjugation. As a result, the size of the peptide and antibody conjugated micelle increased with the increase in the amount of peptide and antibody. Also, the conjugation of peptides and antibodies leads to a slight decrease in the charge of the CCMs. Following these characterization methods, we selected PC2 and AC3 formulations. Doxorubicin was loaded into CCM, PC2, and AC3 with the incubation method, and drug loading efficiencies of CCMs, PC2, and AC3 were calculated as 26, 50, and 56%, respectively. Following this step, release studies were performed in acidic and neutral pH environments, and pH-dependent release was achieved for CCMs, PC2, and AC3 formulations. We noticed that the PC3 formulation released the drug later, and we explained this by the fact that the hydrophobic peptide chains formed by the degradation of the conjugation interact with the hydrophobic drug, causing a delay in the release of the drug. However, all formulations showed greater release in the acidic environment, confirming the desired pH sensitivity of our nanoparticle systems. Finally, the drug delivery system was tested in vitro on breast cancer cells in the scope of TUBITAK, 216S639, 216S991 projects and the collaboration with Prof. Dr. Yusuf Baran (İYTE Molecular Biology and Genetics Department). Since cell culture studies were reported as a master thesis in Nusaibah Abdulsalam Abdulhad Abdulhadi's thesis with the number 684216 at YÖK Thesis Center, we did not report these results within the scope of this thesis. However, we would like to discuss these results in the conclusion section to show the efficacy of our nanoparticle system on breast cancer. According to these results, the efficacy of the HER2 peptide (LTVSPWY) and HER2 antibody (Herceptin®) conjugated micelles was investigated by cytotoxic, apoptotic, cytostatic, and genotoxic assays. The cytotoxicity of the targeted CCMs was determined on SKBR3 cells with control of MCF-10A. The DOX-HER2 peptide-CCMs were 2-fold more effective on SKBR-3 cells compared to DOX-HER2 antibody-CCMs. Also, no difference in selectivity for healthy cells was observed. The effects of DOX-HER2-peptide and DOX-HER2-antibody conjugated CCMs were higher on HER2 overexpressed SKBR-3 cells compared to DOX-CCMs. According to the fluorescence analysis, the uptake of DOX-HER2 peptide-CCMs and DOX-HER2 antibody-CCMs were higher compared to DOX-CCMs for SKBR-3 cells. Additionally, peptide-based formulations showed better uptake than the others. However, no difference was observed in the uptake of the all formulations for MCF-10A cells. This suggests that DOX-HER2

peptide-CCMs were more effective than the other two on SKBR-3 cells. Moreover, the results emphasize the selective targeting ability of the HER2-specific peptide and antibody-conjugated CCMs, which has the potential to enhance the therapeutic efficacy of the drugs while reducing the side effects. Furthermore, the study found that peptide targeting had more advantages over antibody targeting. This phenomenon implies that peptide conjugation could be a better option for HER2-positive cancer cell targeting. This nanocarrier formulation was also tested in vivo within the scope of 216S990 by Assoc.Prof. Hüsamettin Ekici and his group (Kırıkkale University), but the results was not published yet.

With all these findings, our studies show that the designed systems for HER2-targeted breast cancer therapy with multifunctional nanocarriers, which have higher stability, pH sensitivity, and selectivity, can be efficient for targeted anticancer drug delivery. They can also be used in different drug-targeting strategies by changing targeting agents and drugs. Although in vitro efficacy of these CCMs has been shown, it should be noted that these structures should be investigated based on their pharmacokinetic properties. Thus, further investigations are necessary to achieve in vivo efficacy. This thesis has great potential as a multifunctional drug-conjugated carrier system with enhanced stability and pH sensitivity for targeted breast cancer therapy. This study is most likely to have an impact as a putative treatment method for breast cancer, which shows a very high incidence in women. Besides, future in vivo studies can be designed for potential national and international projects based on the results of in vitro studies performed during this project.

5.2 Societal Impact and Contribution to Global Sustainability

The potential drug delivery systems developed in this thesis have a significant societal impact and contribution to global sustainability. Breast cancer is one of the most prevalent forms of cancer among women, and effective drug delivery systems are crucial for the successful treatment of this disease. The POEGMA and sulfobetaine-based breast cancer-targeted CCMs developed in this thesis offer a promising approach to the targeted and efficient delivery of breast cancer drugs. The use of targeted drug delivery systems, such as the ones developed in this thesis, can significantly reduce the side effects of cancer treatment, improve treatment outcomes, and enhance the quality of life for cancer

patients. By delivering drugs directly to cancer cells, these systems minimize damage to healthy cells and reduce the risk of systemic toxicity. This approach can also reduce the need for multiple doses of chemotherapy, which can further minimize the side effects of treatment and improve patient compliance. Overall, the potential drug delivery systems developed in this thesis have a significant societal impact and can contribute to global sustainability by improving the efficacy and safety of breast cancer treatment while minimizing the existing drugs' side effects. These systems offer a promising approach as a targeted and efficient delivery of breast cancer drugs and have the potential to significantly improve patient outcomes and quality of life.

5.3 Future Prospects

In the future, it is envisaged that the efficacy of targeted and non-targeted drug delivery systems will be further evaluated in vivo by assessing the toxicities of drug-loaded and unloaded targeted delivery systems. Moreover, these systems can be tested for their potential to serve as model delivery systems by loading them with diverse drug types. The ultimate goal is to obtain successful results that could pave the way for planning clinical studies in the future.

BIBLIOGRAPHY

[1] M. Arnold et al., *Current and Future Burden of Breast Cancer: Global Statistics for 2020 and 2040*, The Breast **66**, 15 (2022).

[2] S. V. S. Deo, J. Sharma, and S. Kumar, *GLOBOCAN 2020 Report on Global Cancer Burden: Challenges and Opportunities for Surgical Oncologists*, Ann. Surg. Oncol. **29**, 6497 (2022).

[3] G. N. Sharma, R. Dave, J. Sanadya, P. Sharma, and K. Sharma, *Various Types and Management of Breast Cancer: An Overview*, J. Adv. Pharm. Technol. Res. **1**, 109 (2010).

[4] B. Weigelt, F. C. Geyer, and J. S. Reis-Filho, *Histological Types of Breast Cancer: How Special Are They?*, Mol. Oncol. **4**, 192 (2010).

[5] G. Viale, *The Current State of Breast Cancer Classification*, Ann. Oncol. **23**, x207 (2012).

[6] M. Colombo, F. Corsi, D. Foschi, E. Mazzantini, S. Mazzucchelli, C. Morasso, E. Occhipinti, L. Polito, D. Prosperi, and S. Ronchi, *HER2 Targeting as a Two-Sided Strategy for Breast Cancer Diagnosis and Treatment: Outlook and Recent Implications in Nanomedical Approaches*, Pharmacol. Res. **62**, 150 (2010).

[7] W. Tai, R. Mahato, and K. Cheng, *The Role of HER2 in Cancer Therapy and Targeted Drug Delivery*, J. Control. Release **146**, 264 (2010).

[8] L. Rossi, C. Mazzara, and O. Pagani, *Diagnosis and Treatment of Breast Cancer in Young Women*, Curr. Treat. Options Oncol. **20**, 86 (2019).

[9] T. Shien and H. Iwata, *Adjuvant and Neoadjuvant Therapy for Breast Cancer*, Jpn. J. Clin. Oncol. **50**, 225 (2020).

[10] D.-Y. Oh and Y.-J. Bang, *HER2-Targeted Therapies — a Role beyond Breast Cancer*, Nat. Rev. Clin. Oncol. **17**, 33 (2020).

[11] L. A. Korde, M. R. Somerfield, L. A. Carey, J. R. Crews, N. Denduluri, E. S. Hwang, S. A. Khan, S. Loibl, E. A. Morris, and A. Perez, *Neoadjuvant Chemotherapy, Endocrine Therapy, and Targeted Therapy for Breast Cancer: ASCO Guideline*, J. Clin. Oncol. **39**, 1485 (2021).

[12] J. Wang and B. Xu, *Targeted Therapeutic Options and Future Perspectives for HER2-Positive Breast Cancer*, Signal Transduct. Target. Ther. **4**, 34 (2019).

[13] D. Gajria and S. Chandarlapaty, *HER2-Amplified Breast Cancer: Mechanisms of Trastuzumab Resistance and Novel Targeted Therapies.*, Expert Rev. Anticancer Ther. **11**, 263 (2011).

[14] Y. Yao, Y. Zhou, L. Liu, Y. Xu, Q. Chen, Y. Wang, S. Wu, Y. Deng, J. Zhang, and A. Shao, *Nanoparticle-Based Drug Delivery in Cancer Therapy and Its Role in Overcoming Drug Resistance.*, Front. Mol. Biosci. **7**, 193 (2020).

[15] Z. Cheng, M. Li, R. Dey, and Y. Chen, *Nanomaterials for Cancer Therapy: Current Progress and Perspectives*, J. Hematol. Oncol. **14**, 85 (2021).

[16] M. J. Mitchell, M. M. Billingsley, R. M. Haley, M. E. Wechsler, N. A. Peppas, and R. Langer, *Engineering Precision Nanoparticles for Drug Delivery*, Nat. Rev. Drug Discov. **20**, 101 (2021).

[17] I. Ekladious, Y. L. Colson, and M. W. Grinstaff, *Polymer–Drug Conjugate Therapeutics: Advances, Insights and Prospects*, Nat. Rev. Drug Discov. **18**, 273 (2019).

[18] J. Li, F. Yu, Y. Chen, and D. Oupický, *Polymeric Drugs: Advances in the Development of Pharmacologically Active Polymers.*, J. Control. Release Off. J. Control. Release Soc. **219**, 369 (2015).

[19] G. Pasut, *Polymers for Protein Conjugation*, Polymers (Basel). **6**, 160 (2014).

[20] E. M. Pelegri-O'Day, E.-W. Lin, and H. D. Maynard, *Therapeutic Protein–Polymer Conjugates: Advancing beyond PEGylation*, J. Am. Chem. Soc. **136**, 14323 (2014).

[21] J. S. Suk, Q. Xu, N. Kim, J. Hanes, and L. M. Ensign, *PEGylation as a Strategy for Improving Nanoparticle-Based Drug and Gene Delivery.*, Adv. Drug Deliv. Rev. **99**, 28 (2016).

[22] E. Sanchez Armengol, A. Unterweger, and F. Laffleur, *PEGylated Drug Delivery Systems in the Pharmaceutical Field: Past, Present and Future Perspective*, Drug Dev. Ind. Pharm. **48**, 129 (2022).

[23] K. Knop, R. Hoogenboom, D. Fischer, and U. S. Schubert, *Poly (Ethylene Glycol) in Drug Delivery: Pros and Cons as Well as Potential Alternatives*, Angew. Chemie Int. Ed. **49**, 6288 (2010).

[24] T. T. Hoang Thi, E. H. Pilkington, D. H. Nguyen, J. S. Lee, K. D. Park, and N. P. Truong, *The Importance of Poly (Ethylene Glycol) Alternatives for Overcoming PEG Immunogenicity in Drug Delivery and Bioconjugation*, Polymers (Basel). **12**, 298 (2020).

[25] M. D. McSweeney et al., *Overcoming Anti-PEG Antibody Mediated Accelerated Blood Clearance of PEGylated Liposomes by Pre-Infusion with High Molecular Weight Free PEG.*, J. Control. Release Off. J. Control. Release Soc. **311**–**312**, 138 (2019).

[26] S. Abbina and A. Parambath, *PEGylation and Its Alternatives: A Summary*, in *Engineering of Biomaterials for Drug Delivery Systems* (Elsevier, 2018), pp. 363–376.

[27] N. Hadjesfandiari and A. Parambath, *Stealth Coatings for Nanoparticles: Polyethylene Glycol Alternatives*, in *Engineering of Biomaterials for Drug Delivery Systems* (Elsevier, 2018), pp. 345–361.

[28] M. Khuphe and P. D. Thornton, *Poly (Amino Acids)*, in *Engineering of Biomaterials for Drug Delivery Systems* (Elsevier, 2018), pp. 199–228.

[29] X. Yao, C. Qi, C. Sun, F. Huo, and X. Jiang, *Poly (Ethylene Glycol) Alternatives in Biomedical Applications*, Nano Today **48**, 101738 (2023).

[30] N. Larson and H. Ghandehari, *Polymeric Conjugates for Drug Delivery.*, Chem. Mater. **24**, 840 (2012).

[31] S. Wadhwa and R. J. Mumper, *Polymer-Drug Conjugates for Anticancer Drug Delivery.*, Crit. Rev. Ther. Drug Carrier Syst. **32**, 215 (2015).

[32] K. S. Soppimath, T. M. Aminabhavi, A. R. Kulkarni, and W. E. Rudzinski, *Biodegradable Polymeric Nanoparticles as Drug Delivery Devices*, J. Control. Release **70**, 1 (2001).

[33] C. Vauthier and K. Bouchemal, *Methods for the Preparation and Manufacture of Polymeric Nanoparticles*, Pharm. Res. **26**, 1025 (2009).

[34] B. V. N. Nagavarma, H. K. S. Yadav, A. Ayaz, L. S. Vasudha, and H. G. Shivakumar, *Different Techniques for Preparation of Polymeric Nanoparticles-a Review*, Asian J. Pharm. Clin. Res **5**, 16 (2012).

[35] J. K. Patra et al., *Nano Based Drug Delivery Systems: Recent Developments and Future Prospects*, J. Nanobiotechnology **16**, 71 (2018).

[36] R. Panday, A. J. Poudel, X. Li, M. Adhikari, M. W. Ullah, and G. Yang, *Amphiphilic Core-Shell Nanoparticles: Synthesis, Biophysical Properties, and Applications*, Colloids Surfaces B Biointerfaces **172**, 68 (2018).

[37] M. Elsabahy and K. L. Wooley, *Design of Polymeric Nanoparticles for Biomedical Delivery Applications.*, Chem. Soc. Rev. **41**, 2545 (2012).

[38] S. Bhatia and S. Bhatia, *Natural Polymers vs Synthetic Polymer*, Nat. Polym. Drug

Deliv. Syst. Nanoparticles, Plants, Algae 95 (2016).

[39] A. Zielińska et al., *Polymeric Nanoparticles: Production, Characterization, Toxicology and Ecotoxicology.*, Molecules **25**, (2020).

[40] D. Chenthamara, S. Subramaniam, S. G. Ramakrishnan, S. Krishnaswamy, M. M. Essa, F.-H. Lin, and M. W. Qoronfleh, *Therapeutic Efficacy of Nanoparticles and Routes of Administration*, Biomater. Res. **23**, 20 (2019).

[41] S. S. Chakravarthi, D. H. Robinson, and S. De, *Nanoparticles Prepared Using Natural and Synthetic Polymers*, Nanoparticulate Drug Deliv. Syst. 51 (2007).

[42] Z. Tang, C. He, H. Tian, J. Ding, B. S. Hsiao, B. Chu, and X. Chen, *Polymeric Nanostructured Materials for Biomedical Applications*, Prog. Polym. Sci. **60**, 86 (2016).

[43] C. Pathak, F. U. Vaidya, and S. M. Pandey, *Mechanism for Development of Nanobased Drug Delivery System*, Appl. Target. Nano Drugs Deliv. Syst. 35 (2019).

[44] C. E. Mora-Huertas, H. Fessi, and A. Elaissari, *Polymer-Based Nanocapsules for Drug Delivery*, Int. J. Pharm. **385**, 113 (2010).

[45] S. D. Allen, S. Bobbala, N. B. Karabin, and E. A. Scott, *On the Advancement of Polymeric Bicontinuous Nanospheres toward Biomedical Applications*, Nanoscale Horizons **4**, 258 (2019).

[46] A. A. Chis, C. Dobrea, C. Morgovan, A. M. Arseniu, L. L. Rus, A. Butuca, A. M. Juncan, M. Totan, A. L. Vonica-Tincu, and G. Cormos, *Applications and Limitations of Dendrimers in Biomedicine*, Molecules **25**, 3982 (2020).

[47] F. Sabir, M. I. Asad, M. Qindeel, I. Afzal, M. J. Dar, K. U. Shah, A. Zeb, G. M. Khan, N. Ahmed, and F. Din, *Polymeric Nanogels as Versatile Nanoplatforms for Biomedical Applications*, J. Nanomater. **2019**, (2019).

[48] B. Ghosh and S. Biswas, *Polymeric Micelles in Cancer Therapy: State of the Art*, J. Control. Release **332**, 127 (2021).

[49] M. C. I. M. Amin, A. M. Butt, M. W. Amjad, and P. Kesharwani, *Polymeric Micelles for Drug Targeting and Delivery*, in *Nanotechnology-Based Approaches for Targeting and Delivery of Drugs and Genes* (Elsevier, 2017), pp. 167–202.

[50] K. Kuperkar, D. Patel, L. I. Atanase, and P. Bahadur, *Amphiphilic Block Copolymers: Their Structures, and Self-Assembly to Polymeric Micelles and Polymersomes as Drug Delivery Vehicles*, Polymers (Basel). **14**, 4702 (2022).

[51] Y. H. A. Hussein and M. Youssry, *Polymeric Micelles of Biodegradable Diblock*

Copolymers: Enhanced Encapsulation of Hydrophobic Drugs, Materials (Basel). **11**, 688 (2018).

[52] W. Xu, P. Ling, and T. Zhang, *Polymeric Micelles, a Promising Drug Delivery System to Enhance Bioavailability of Poorly Water-Soluble Drugs.*, J. Drug Deliv. **2013**, 340315 (2013).

[53] S. R. Croy and G. S. Kwon, *Polymeric Micelles for Drug Delivery*, Curr. Pharm. Des. **12**, 4669 (2006).

[54] G. S. Kwon and T. Okano, *Polymeric Micelles as New Drug Carriers*, Adv. Drug Deliv. Rev. **21**, 107 (1996).

[55] H. M. Aliabadi and A. Lavasanifar, *Polymeric Micelles for Drug Delivery*, Expert Opin. Drug Deliv. **3**, 139 (2006).

[56] Q. Zhou, L. Zhang, T. Yang, and H. Wu, *Stimuli-Responsive Polymeric Micelles for Drug Delivery and Cancer Therapy.*, Int. J. Nanomedicine **13**, 2921 (2018).

[57] X. L. Wu, J. H. Kim, H. Koo, S. M. Bae, H. Shin, M. S. Kim, B.-H. Lee, R.-W. Park, I.-S. Kim, and K. Choi, *Tumor-Targeting Peptide Conjugated PH-Responsive Micelles as a Potential Drug Carrier for Cancer Therapy*, Bioconjug. Chem. **21**, 208 (2010).

[58] J. Akimoto, M. Nakayama, and T. Okano, *Temperature-Responsive Polymeric Micelles for Optimizing Drug Targeting to Solid Tumors*, J. Control. Release **193**, 2 (2014).

[59] R. L. McCarley, *Redox-Responsive Delivery Systems*, Annu. Rev. Anal. Chem. **5**, 391 (2012).

[60] Y. Zhao, *Light-Responsive Block Copolymer Micelles*, Macromolecules **45**, 3647 (2012).

[61] J. Hu, G. Zhang, and S. Liu, *Enzyme-Responsive Polymeric Assemblies, Nanoparticles and Hydrogels*, Chem. Soc. Rev. **41**, 5933 (2012).

[62] S. C. Owen, D. P. Y. Chan, and M. S. Shoichet, *Polymeric Micelle Stability*, Nano Today **7**, 53 (2012).

[63] I. Alper Isoglu, Y. Ozsoy, and S. Dincer Isoglu, *Advances in Micelle-Based Drug Delivery: Cross-Linked Systems*, Curr. Top. Med. Chem. **17**, 1469 (2017).

[64] Y. Zheng, S. Li, Z. Weng, and C. Gao, *Hyperbranched Polymers: Advances from Synthesis to Applications*, Chem. Soc. Rev. **44**, 4091 (2015).

[65] W. Fan, L. Zhang, Y. Li, and H. Wu, *Recent Progress of Crosslinking Strategies for Polymeric Micelles with Enhanced Drug Delivery in Cancer Therapy.*, Curr.

Med. Chem. **26**, 2356 (2019).

[66] J. S. Kim and J. H. Youk, *Preparation of Core Cross-Linked Micelles Using a Photo-Cross-Linking Agent*, Polymer (Guildf). **50**, 2204 (2009).

[67] Y. Li, K. Xiao, W. Zhu, W. Deng, and K. S. Lam, *Stimuli-Responsive Cross-Linked Micelles for on-Demand Drug Delivery against Cancers*, Adv. Drug Deliv. Rev. **66**, 58 (2014).

[68] D. Xiong, N. Yao, H. Gu, J. Wang, and L. Zhang, *Stimuli-Responsive Shell Cross-Linked Micelles from Amphiphilic Four-Arm Star Copolymers as Potential Nanocarriers for "PH/Redox-Triggered" Anticancer Drug Release*, Polymer (Guildf). **114**, 161 (2017).

[69] J. Qu, Q. Wang, K. Chen, J. Luo, Q. Zhou, and J. Lin, *Reduction/Temperature/PH Multi-Stimuli Responsive Core Cross-Linked Polypeptide Hybrid Micelles for Triggered and Intracellular Drug Release*, Colloids Surfaces B Biointerfaces **170**, 373 (2018).

[70] E. S. Read and S. P. Armes, *Recent Advances in Shell Cross-Linked Micelles*, Chem. Commun. 3021 (2007).

[71] Y. Chan, T. Wong, F. Byrne, M. Kavallaris, and V. Bulmus, *Acid-Labile Core Cross-Linked Micelles for PH-Triggered Release of Antitumor Drugs*, Biomacromolecules **9**, 1826 (2008).

[72] M. Talelli, M. Barz, C. J. F. Rijcken, F. Kiessling, W. E. Hennink, and T. Lammers, *Core-Crosslinked Polymeric Micelles: Principles, Preparation, Biomedical Applications and Clinical Translation*, Nano Today.

[73] C. F. van Nostrum, *Covalently Cross-Linked Amphiphilic Block Copolymer Micelles*, Soft Matter **7**, 3246 (2011).

[74] J. Park, N. Y. Ahn, and M. Seo, *Cross-Linking Polymerization-Induced Self-Assembly to Produce Branched Core Cross-Linked Star Block Polymer Micelles*, Polym. Chem. **11**, 4335 (2020).

[75] S. Li, G. Han, and W. Zhang, *Cross-Linking Approaches for Block Copolymer Nano-Assemblies via RAFT-Mediated Polymerization-Induced Self-Assembly*, Polym. Chem. **11**, 4681 (2020).

[76] C. Huang, C. Hong, and C. Pan, *Formation of Flower-like Aggregates from Self-Assembling of Micelles with PEO Shells and Cross-Linked Polyacrylamide Cores*, Chinese J. Polym. Sci. **26**, 341 (2008).

[77] L. Nuhn, M. Hirsch, B. Krieg, K. Koynov, K. Fischer, M. Schmidt, M. Helm, and

R. Zentel, *Cationic Nanohydrogel Particles as Potential SiRNA Carriers for Cellular Delivery*, ACS Nano **6**, 2198 (2012).

[78] S. Hajebi, N. Rabiee, M. Bagherzadeh, S. Ahmadi, M. Rabiee, H. Roghani-Mamaqani, M. Tahriri, L. Tayebi, and M. R. Hamblin, *Stimulus-Responsive Polymeric Nanogels as Smart Drug Delivery Systems*, Acta Biomater. **92**, 1 (2019).

[79] F. Meng, W. E. Hennink, and Z. Zhong, *Reduction-Sensitive Polymers and Bioconjugates for Biomedical Applications*, Biomaterials **30**, 2180 (2009).

[80] A. Blencowe, J. F. Tan, T. K. Goh, and G. G. Qiao, *Core Cross-Linked Star Polymers via Controlled Radical Polymerisation*, Polymer (Guildf). **50**, 5 (2009).

[81] C. Boyer, V. Bulmus, T. P. Davis, V. Ladmiral, J. Liu, and S. Perrier, *Bioapplications of RAFT Polymerization*, Chem. Rev. **109**, 5402 (2009).

[82] M. H. Stenzel, *RAFT Polymerization: An Avenue to Functional Polymeric Micelles for Drug Delivery*, Chem. Commun. 3486 (2008).

[83] S. Perrier, *50th Anniversary Perspective: RAFT Polymerization A User Guide*, Macromolecules **50**, 7433 (2017).

[84] G. Moad, E. Rizzardo, and S. H. Thang, *End-functional Polymers, Thiocarbonylthio Group Removal/Transformation and Reversible Addition–Fragmentation–Chain Transfer (RAFT) Polymerization*, Polym. Int. **60**, 9 (2011).

[85] L. Zhang, J. Bernard, T. P. Davis, C. Barner-Kowollik, and M. H. Stenzel, *Acid-degradable Core-crosslinked Micelles Prepared from Thermosensitive Glycopolymers Synthesized via RAFT Polymerization*, Macromol. Rapid Commun. **29**, 123 (2008).

[86] L. Zhang, W. Liu, L. Lin, D. Chen, and M. H. Stenzel, *Degradable Disulfide Core-Cross-Linked Micelles as a Drug Delivery System Prepared from Vinyl Functionalized Nucleosides via the RAFT Process*, Biomacromolecules **9**, 3321 (2008).

[87] S. Chu, X. Shi, Y. Tian, and F. Gao, *PH-Responsive Polymer Nanomaterials for Tumor Therapy.*, Front. Oncol. **12**, 855019 (2022).

[88] R. Cheng, S. Wang, and H. A. Santos, *Acid-Labile Chemical Bonds-Based Nanoparticles for Endosome Escape and Intracellular Delivery*, Biomed. Technol. **3**, 52 (2023).

[89] S. Gavas, S. Quazi, and T. M. Karpiński, *Nanoparticles for Cancer Therapy: Current Progress and Challenges.*, Nanoscale Res. Lett. **16**, 173 (2021).

[90] T. D. Clemons, R. Singh, A. Sorolla, N. Chaudhari, A. Hubbard, and K. S. Iyer,

Distinction Between Active and Passive Targeting of Nanoparticles Dictate Their Overall Therapeutic Efficacy, Langmuir **34**, 15343 (2018).

[91] M. F. Attia, N. Anton, J. Wallyn, Z. Omran, and T. F. Vandamme, *An Overview of Active and Passive Targeting Strategies to Improve the Nanocarriers Efficiency to Tumour Sites*, J. Pharm. Pharmacol. **71**, 1185 (2019).

[92] J. D. Byrne, T. Betancourt, and L. Brannon-Peppas, *Active Targeting Schemes for Nanoparticle Systems in Cancer Therapeutics*, Adv. Drug Deliv. Rev. **60**, 1615 (2008).

[93] R. Bazak, M. Houri, S. El Achy, S. Kamel, and T. Refaat, *Cancer Active Targeting by Nanoparticles: A Comprehensive Review of Literature*, J. Cancer Res. Clin. Oncol. **141**, 769 (2015).

[94] J. Yoo, C. Park, G. Yi, D. Lee, and H. Koo, *Active Targeting Strategies Using Biological Ligands for Nanoparticle Drug Delivery Systems*, Cancers (Basel). **11**, 640 (2019).

[95] N. Muhamad, T. Plengsuriyakarn, and K. Na-Bangchang, *Application of Active Targeting Nanoparticle Delivery System for Chemotherapeutic Drugs and Traditional/Herbal Medicines in Cancer Therapy: A Systematic Review*, Int. J. Nanomedicine **13**, 3921 (2018).

[96] Z. R. Goddard, M. J. Marín, D. A. Russell, and M. Searcey, *Active Targeting of Gold Nanoparticles as Cancer Therapeutics*, Chem. Soc. Rev. **49**, 8774 (2020).

[97] J. Sudimack and R. J. Lee, *Targeted Drug Delivery via the Folate Receptor*, Adv. Drug Deliv. Rev. **41**, 147 (2000).

[98] F. Esmaeili, M. H. Ghahremani, S. N. Ostad, F. Atyabi, M. Seyedabadi, M. R. Malekshahi, M. Amini, and R. Dinarvand, *Folate-Receptor-Targeted Delivery of Docetaxel Nanoparticles Prepared by PLGA–PEG–Folate Conjugate*, J. Drug Target. **16**, 415 (2008).

[99] E. Pérez-Herrero and A. Fernández-Medarde, *Advanced Targeted Therapies in Cancer: Drug Nanocarriers, the Future of Chemotherapy.*, Eur. J. Pharm. Biopharm. **93**, 52 (2015).

[100] Y. Shi, R. Van der Meel, X. Chen, and T. Lammers, *The EPR Effect and beyond: Strategies to Improve Tumor Targeting and Cancer Nanomedicine Treatment Efficacy*, Theranostics **10**, 7921 (2020).

[101] M. Talelli, M. Barz, C. J. F. Rijcken, F. Kiessling, W. E. Hennink, and T. Lammers, *Core-Crosslinked Polymeric Micelles: Principles, Preparation, Biomedical*

Applications and Clinical Translation, Nano Today **10**, 93 (2015).

[102] I. Biancacci, Q. Sun, D. Möckel, F. Gremse, S. Rosenhain, F. Kiessling, M. Bartneck, Q. Hu, M. Thewissen, and G. Storm, *Optical Imaging of the Whole-Body to Cellular Biodistribution of Clinical-Stage PEG-b-PHPMA-Based Core-Crosslinked Polymeric Micelles*, J. Control. Release **328**, 805 (2020).

[103] B. J. Crielaard, C. J. F. Rijcken, L. Quan, S. Van Der Wal, I. Altintas, M. Van Der Pot, J. A. W. Kruijtzer, R. M. J. Liskamp, R. M. Schiffelers, and C. F. Van Nostrum, *Glucocorticoid-loaded Core-cross-linked Polymeric Micelles with Tailorable Release Kinetics for Targeted Therapy of Rheumatoid Arthritis*, Angew. Chemie Int. Ed. **51**, 7254 (2012).

[104] X. T. Cao, C. M. Q. Le, H. H. P. Thi, G. D. Kim, Y. S. Gal, and K. T. Lim, *Redox-Responsive Core Cross-Linked Prodrug Micelles Prepared by Click Chemistry for PH-Triggered Doxorubicin Delivery*, Express Polym. Lett. **11**, 832 (2017).

[105] Z. Jia, L. Wong, T. P. Davis, and V. Bulmus, *One-Pot Conversion of RAFT-Generated Multifunctional Block Copolymers of HPMA to Doxorubicin Conjugated Acid-and Reductant-Sensitive Crosslinked Micelles*, Biomacromolecules **9**, 3106 (2008).

[106] T. Ramasamy, H. B. Ruttala, B. Gupta, B. K. Poudel, H.-G. Choi, C. S. Yong, and J. O. Kim, *Smart Chemistry-Based Nanosized Drug Delivery Systems for Systemic Applications: A Comprehensive Review.*, J. Control. Release Off. J. Control. Release Soc. **258**, 226 (2017).

[107] S. Binauld and M. H. Stenzel, *Acid-Degradable Polymers for Drug Delivery: A Decade of Innovation*, Chem. Commun. **49**, 2082 (2013).

[108] H. Wei, R.-X. Zhuo, and X.-Z. Zhang, *Design and Development of Polymeric Micelles with Cleavable Links for Intracellular Drug Delivery*, Prog. Polym. Sci. **38**, 503 (2013).

[109] A. D. Friedman, S. E. Claypool, and R. Liu, *The Smart Targeting of Nanoparticles.*, Curr. Pharm. Des. **19**, 6315 (2013).

[110] G. T. Hermanson, *Bioconjugate Techniques* (Academic press, 2013).

[111] F. Masood, *Polymeric Nanoparticles for Targeted Drug Delivery System for Cancer Therapy*, Mater. Sci. Eng. C **60**, 569 (2016).

[112] G. Abbineni, S. Modali, B. Safiejko-Mroczka, V. A. Petrenko, and C. Mao, *Evolutionary Selection of New Breast Cancer Cell-Targeting Peptides and Phages with the Cell-Targeting Peptides Fully Displayed on the Major Coat and Their*

Effects on Actin Dynamics during Cell Internalization, Mol. Pharm. **7**, 1629 (2010).

[113] N. Gandra, G. Abbineni, X. Qu, Y. Huai, L. Wang, and C. Mao, *Bacteriophage Bionanowire as a Carrier for Both Cancer-targeting Peptides and Photosensitizers and Its Use in Selective Cancer Cell Killing by Photodynamic Therapy*, Small **9**, 215 (2013).

[114] M. Topuzogullari, V. Bulmus, E. Dalgakiran, and S. Dincer, *PH-and Temperature-Responsive Amphiphilic Diblock Copolymers of 4-Vinylpyridine and Oligoethyleneglycol Methacrylate Synthesized by RAFT Polymerization*, Polymer (Guildf). **55**, 525 (2014).

[115] N. Bhuchar, R. Sunasee, K. Ishihara, T. Thundat, and R. Narain, *Degradable Thermoresponsive Nanogels for Protein Encapsulation and Controlled Release*, Bioconjug. Chem. **23**, 75 (2012).

[116] C. Boyer, V. Bulmus, and T. P. Davis, *Efficient Usage of Thiocarbonates for Both the Production and the Biofunctionalization of Polymers*, Macromol. Rapid Commun. **30**, 493 (2009).

[117] M. B. Thomas, K. Radhakrishnan, D. P. Gnanadhas, D. Chakravortty, and A. M. Raichur, *Intracellular Delivery of Doxorubicin Encapsulated in Novel PH-Responsive Chitosan/Heparin Nanocapsules*, Int. J. Nanomedicine 267 (2013).

[118] Y. Zhou, Z. Guo, Y. Zhang, W. Huang, Y. Zhou, and D. Yan, *Hyperbranched Polyamidoamines Containing β-Cyclodextrin for Controlled Release of Chlorambucil*, Macromol. Biosci. **9**, 1090 (2009).

[119] D. J. Keddie, *A Guide to the Synthesis of Block Copolymers Using Reversible-Addition Fragmentation Chain Transfer (RAFT) Polymerization*, Chem. Soc. Rev. **43**, 496 (2014).

[120] D. Willner, P. A. Trail, S. J. Hofstead, H. D. King, S. J. Lasch, G. R. Braslawsky, R. S. Greenfield, T. Kaneko, and R. A. Firestone, *(6-Maleimidocaproyl) Hydrazone of Doxorubicin. A New Derivative for the Preparation of Immunoconjugates of Doxorubicin*, Bioconjug. Chem. **4**, 521 (1993).

[121] F. Kratz, U. Beyer, P. Collery, F. LECHENAULT, A. CAZABAT, P. SCHUMACHER, U. FALKEN, and C. UNGER, *Preparation, Characterization and in Vitro Efficacy of Albumin Conjugates of Doxorubicin*, Biol. Pharm. Bull. **21**, 56 (1998).

[122] M. Hrubý, Č. Koňák, and K. Ulbrich, *Polymeric Micellar PH-Sensitive Drug*

Delivery System for Doxorubicin, J. Control. Release **103**, 137 (2005).

[123] A. Mahmud, X.-B. Xiong, and A. Lavasanifar, *Development of Novel Polymeric Micellar Drug Conjugates and Nano-Containers with Hydrolyzable Core Structure for Doxorubicin Delivery*, Eur. J. Pharm. Biopharm. **69**, 923 (2008).

[124] F.-Q. Hu, L.-N. Liu, Y.-Z. Du, and H. Yuan, *Synthesis and Antitumor Activity of Doxorubicin Conjugated Stearic Acid-g-Chitosan Oligosaccharide Polymeric Micelles*, Biomaterials **30**, 6955 (2009).

[125] H. S. Yoo and T. G. Park, *Biodegradable Polymeric Micelles Composed of Doxorubicin Conjugated PLGA-PEG Block Copolymer.*, J. Control. Release Off. J. Control. Release Soc. **70**, 63 (2001).

[126] H.-H. Chen, W.-C. Huang, W.-H. Chiang, T.-I. Liu, M.-Y. Shen, Y.-H. Hsu, S.-C. Lin, and H.-C. Chiu, *PH-Responsive Therapeutic Solid Lipid Nanoparticles for Reducing P-Glycoprotein-Mediated Drug Efflux of Multidrug Resistant Cancer Cells*, Int. J. Nanomedicine **10**, 5035 (2015).

[127] A. Suo, J. Qian, Y. Yao, and W. Zhang, *Galactosylated Poly (Ethylene Glycol)-b-Poly (L-Lactide-Co-β-Malic Acid) Block Copolymer Micelles for Targeted Drug Delivery: Preparation and in Vitro Characterization*, Int. J. Nanomedicine 1029 (2010).

[128] X. Wang, G. Wu, C. Lu, W. Zhao, Y. Wang, Y. Fan, H. Gao, and J. Ma, *A Novel Delivery System of Doxorubicin with High Load and PH-Responsive Release from the Nanoparticles of Poly (α,β-Aspartic Acid) Derivative.*, Eur. J. Pharm. Sci. Off. J. Eur. Fed. Pharm. Sci. **47**, 256 (2012).

[129] Y. Men, S. Peng, P. Yang, Q. Jiang, Y. Zhang, B. Shen, P. Dong, Z. Pang, and W. Yang, *Biodegradable Zwitterionic Nanogels with Long Circulation for Antitumor Drug Delivery*, ACS Appl. Mater. Interfaces **10**, 23509 (2018).

[130] Y. Lee, S. Y. Park, H. Mok, and T. G. Park, *Synthesis, Characterization, Antitumor Activity of Pluronic Mimicking Copolymer Micelles Conjugated with Doxorubicin via Acid-Cleavable Linkage*, Bioconjug. Chem. **19**, 525 (2008).

[131] W. Chen, F. Meng, F. Li, S.-J. Ji, and Z. Zhong, *PH-Responsive Biodegradable Micelles Based on Acid-Labile Polycarbonate Hydrophobe: Synthesis and Triggered Drug Release*, Biomacromolecules **10**, 1727 (2009).

[132] Y. Wang, J. Zheng, Y. Tian, and W. Yang, *Acid Degradable Poly (Vinylcaprolactam)-Based Nanogels with Ketal Linkages for Drug Delivery*, J. Mater. Chem. B **3**, 5824 (2015).

[133] A. G. Waks and E. P. Winer, *Breast Cancer Treatment: A Review*, Jama **321**, 288 (2019).

[134] I. Tekedereli, S. N. Alpay, C. D. J. Tavares, Z. E. Cobanoglu, T. S. Kaoud, I. Sahin, A. K. Sood, G. Lopez-Berestein, K. N. Dalby, and B. Ozpolat, *Targeted Silencing of Elongation Factor 2 Kinase Suppresses Growth and Sensitizes Tumors to Doxorubicin in an Orthotopic Model of Breast Cancer*, PLoS One **7**, e41171 (2012).

[135] R. Bayraktar, C. Ivan, E. Bayraktar, P. Kanlikilicer, N. N. Kabil, N. Kahraman, H. A. Mokhlis, D. Karakas, C. Rodriguez-Aguayo, and A. Arslan, *Dual Suppressive Effect of MiR-34a on the FOXM1/EEF2-Kinase Axis Regulates Triple-Negative Breast Cancer Growth and InvasionmiR-34a Regulates TNBC Development Through FOXM1/EEF2K Axis*, Clin. Cancer Res. **24**, 4225 (2018).

[136] R. Bayraktar, M. Pichler, P. Kanlikilicer, C. Ivan, E. Bayraktar, N. Kahraman, B. Aslan, S. Oguztuzun, M. Ulasli, and A. Arslan, *MicroRNA 603 Acts as a Tumor Suppressor and Inhibits Triple-Negative Breast Cancer Tumorigenesis by Targeting Elongation Factor 2 Kinase*, Oncotarget **8**, 11641 (2017).

[137] Z. Hamurcu, N. Delibaşı, U. Nalbantoglu, E. F. Sener, N. Nurdinov, B. Tascı, S. Taheri, Y. Özkul, H. Donmez-Altuntas, and H. Canatan, *FOXM1 Plays a Role in Autophagy by Transcriptionally Regulating Beclin-1 and LC3 Genes in Human Triple-Negative Breast Cancer Cells*, J. Mol. Med. **97**, 491 (2019).

[138] E. Asik, Y. Akpinar, A. Caner, N. Kahraman, T. Guray, M. Volkan, C. Albarracin, A. Pataer, B. Arun, and B. Ozpolat, *EF2-Kinase Targeted Cobalt-Ferrite SiRNA-Nanotherapy Suppresses BRCA1-Mutated Breast Cancer*, Nanomedicine **14**, 2315 (2019).

[139] A. K. Devkota, C. D. J. Tavares, M. Warthaka, O. Abramczyk, K. D. Marshall, T. S. Kaoud, K. Gorgulu, B. Ozpolat, and K. N. Dalby, *Investigating the Kinetic Mechanism of Inhibition of Elongation Factor 2 Kinase by NH125: Evidence of a Common in Vitro Artifact*, Biochemistry **51**, 2100 (2012).

[140] Y. Haggag, B. Abu Ras, Y. El-Tanani, M. M. Tambuwala, P. McCarron, M. Isreb, and M. El-Tanani, *Co-Delivery of a RanGTP Inhibitory Peptide and Doxorubicin Using Dual-Loaded Liposomal Carriers to Combat Chemotherapeutic Resistance in Breast Cancer Cells*, Expert Opin. Drug Deliv. **17**, 1655 (2020).

[141] Y. A. Haggag, M. Yasser, M. M. Tambuwala, S. S. El Tokhy, M. Isreb, and A. A. Donia, *Repurposing of Guanabenz Acetate by Encapsulation into Long-*

Circulating Nanopolymersomes for Treatment of Triple-Negative Breast Cancer, Int. J. Pharm. **600**, 120532 (2021).

[142] S. Schöttler, G. Becker, S. Winzen, T. Steinbach, K. Mohr, K. Landfester, V. Mailänder, and F. R. Wurm, *Protein Adsorption Is Required for Stealth Effect of Poly(Ethylene Glycol)- and Poly(Phosphoester)-Coated Nanocarriers*, Nat. Nanotechnol. **11**, 372 (2016).

[143] A. Lu, Z. Wu, X. Luo, and S. Li, *Protein Adsorption and Macrophage Uptake of Zwitterionic Sulfobetaine Containing Micelles*, Colloids Surf. B Biointerfaces **167**, 252 (2018).

[144] Y. D. Taghipour, A. Zarebkohan, R. Salehi, F. Rahimi, V. P. Torchilin, M. R. Hamblin, and A. Seifalian, *An Update on Dual Targeting Strategy for Cancer Treatment*, J. Control. Release **349**, 67 (2022).

[145] Q. T. Phan, M. P. Patil, T. T. K. Tu, G.-D. Kim, and K. T. Lim, *Synthesis of Zwitterionic Redox-Responsive Nanogels by One-Pot Amine-Thiol-Ene Reaction for Anticancer Drug Release Application*, React. Funct. Polym. **147**, 104463 (2020).

[146] K. P. García, K. Zarschler, L. Barbaro, J. A. Barreto, W. O'Malley, L. Spiccia, H. Stephan, and B. Graham, *Zwitterionic-Coated "Stealth" Nanoparticles for Biomedical Applications: Recent Advances in Countering Biomolecular Corona Formation and Uptake by the Mononuclear Phagocyte System*, Small **10**, 2516 (2014).

[147] Q. Jin, Y. Chen, Y. Wang, and J. Ji, *Zwitterionic Drug Nanocarriers: A Biomimetic Strategy for Drug Delivery*, Colloids Surf. B Biointerfaces **124**, 80 (2014).

[148] D. Kim, H. Matsuoka, and Y. Saruwatari, *Formation of Sulfobetaine-Containing Entirely Ionic PIC (Polyion Complex) Micelles and Their Temperature Responsivity*, Langmuir **36**, 10130 (2020).

[149] S. Fujii, S. Takano, K. Nakazawa, and K. Sakurai, *Impact of Zwitterionic Polymers on the Tumor Permeability of Molecular Bottlebrush-Based Nanoparticles*, Biomacromolecules **23**, 2846 (2022).

[150] C. G. Alves, D. de Melo-Diogo, R. Lima-Sousa, and I. J. Correia, *IR780 Loaded Sulfobetaine Methacrylate-Functionalized Albumin Nanoparticles Aimed for Enhanced Breast Cancer Phototherapy*, Int. J. Pharm. **582**, 119346 (2020).

[151] M. M. Leitao, C. G. Alves, D. de Melo-Diogo, R. Lima-Sousa, A. F. Moreira, and I. J. Correia, *Sulfobetaine Methacrylate-Functionalized Graphene Oxide-IR780*

Nanohybrids Aimed at Improving Breast Cancer Phototherapy, RSC Adv. **10**, 38621 (2020).

[152] S. Peng, B. Ouyang, Y. Men, Y. Du, Y. Cao, R. Xie, Z. Pang, S. Shen, and W. Yang, *Corrigendum to "Biodegradable Zwitterionic Polymer Membrane Coating Endowing Nanoparticles with Ultra-Long Circulation and Enhanced Tumor Photothermal Therapy"[Biomaterials 231 (2020) 119680]*, Biomaterials **275**, 120920 (2021).

[153] Z. Özdemir, M. Topuzoğulları, İ. A. İşoğlu, and S. Dinçer, *RAFT-Mediated Synthesis of Poly(N-(2-Hydroxypropyl)Methacrylamide-b-4-Vinylpyridine) by Conventional and Microwave Heating*, Polym. Bull. (Berl.) **70**, 2857 (2013).

[154] N. N. Bayram, M. Topuzoğulları, İ. A. İşoğlu, and S. Dinçer İşoğlu, *RAFT-Synthesized POEGMA-b-P4VP Block Copolymers: Preparation of Nanosized Micelles for Anticancer Drug Release*, Polym. Bull. (Berl.) **79**, 9575 (2022).

[155] N. N. Bayram, G. T. Ulu, M. Topuzoğulları, Y. Baran, and S. Dinçer İşoğlu, *HER2-targeted, Degradable Core Cross-linked Micelles for Specific and Dual PH-sensitive DOX Release*, Macromol. Biosci. **22**, 2100375 (2022).

[156] J. Peng, J. Chen, F. Xie, W. Bao, H. Xu, H. Wang, Y. Xu, and Z. Du, *Herceptin-Conjugated Paclitaxel Loaded PCL-PEG Worm-like Nanocrystal Micelles for the Combinatorial Treatment of HER2-Positive Breast Cancer*, Biomaterials **222**, 119420 (2019).

[157] O. Furman, A. Zaporozhets, D. Tobi, A. Bazylevich, M. A. Firer, L. Patsenker, G. Gellerman, and B. C. R. Lubin, *Novel Cyclic Peptides for Targeting EGFR and EGRvIII Mutation for Drug Delivery*, Pharmaceutics **14**, 1505 (2022).

[158] A. Yogi et al., *Brain Delivery of IGF1R5, a Single-Domain Antibody Targeting Insulin-like Growth Factor-1 Receptor*, Pharmaceutics **14**, 1452 (2022).

[159] J. W. Park et al., *Anti-HER2 Immunoliposomes: Enhanced Efficacy Attributable to Targeted Delivery*, Clin. Cancer Res. **8**, 1172 (2002).

[160] D. R. Siwak, A. M. Tari, and G. Lopez-Berestein, *The Potential of Drug-Carrying Immunoliposomes as Anticancer Agents - Commentary Re*, Clin. Cancer Res **8**, 955 (2002).

[161] D. Goldstein, O. Gofrit, A. Nyska, and S. Benita, *Anti-HER2 Cationic Immunoemulsion as a Potential Targeted Drug Delivery System for the Treatment of Prostate Cancer*, Cancer Res. **67**, 269 (2007).

[162] M. Shadidi and M. Sioud, *Identification of Novel Carrier Peptides for the Specific*

Delivery of Therapeutics into Cancer Cells, FASEB J. **17**, 256 (2003).

[163] K. Meschenmoser, Y. Kim, S. Franken, M. Nowak, G. Feldmann, G. Bendas, M. Wolfgarten, D. Messmer, and I. G. H. Schmidt-Wolf, *Targeting Cancer with a Bi-Functional Peptide: In Vitro and in Vivo Results*, In Vivo (Brooklyn). **27**, 431 (2013).

[164] J. Newton and S. L. Deutscher, *Phage Peptide Display*, in *Molecular Imaging II* (Springer Berlin Heidelberg, Berlin, Heidelberg, 2008), pp. 145–163.

[165] X.-F. Wang et al., *A Peptide Conjugate of Vitamin E Succinate Targets Breast Cancer Cells with High ErbB2 Expression*, Cancer Res. **67**, 3337 (2007).

[166] Y.-Z. Du, Jie, Cai, Wang, Ying, Yu, and M. Zhang, *Actively-Targeted LTVSPWY Peptide-Modified Magnetic Nanoparticles for Tumor Imaging*, Int. J. Nanomedicine 3981 (2012).

[167] S. Gürdap, N. N. Bayram, İ. A. İşoğlu, and S. Dinçer İşoğlu, *Sulfobetaine-Based Homo- and Copolymers by RAFT: Cross-Linked Micelles and Aqueous Solution Properties*, ACS Appl. Polym. Mater. **4**, 6303 (2022).

[168] A. J. van der Vlies, C. P. O'Neil, U. Hasegawa, N. Hammond, and J. A. Hubbell, *Synthesis of Pyridyl Disulfide-Functionalized Nanoparticles for Conjugating Thiol-Containing Small Molecules, Peptides, and Proteins*, Bioconjug. Chem. **21**, 653 (2010).

[169] H. Kulhari, D. Pooja, S. Shrivastava, Naidu, and R. Sistla, *Peptide Conjugated Polymeric Nanoparticles as a Carrier for Targeted Delivery of Docetaxel*, Colloids Surf. B Biointerfaces **117**, 166 (2014).

[170] D. Hu, O. Mezghrani, L. Zhang, Y. Chen, X. Ke, and T. Ci, *GE11 Peptide Modified and Reduction-Responsive Hyaluronic Acid-Based Nanoparticles Induced Higher Efficacy of Doxorubicin for Breast Carcinoma Therapy*, Int. J. Nanomedicine **11**, 5125 (2016).

[171] S. Son, S. Shin, N. V. Rao, W. Um, J. Jeon, H. Ko, V. G. Deepagan, S. Kwon, J. Y. Lee, and J. H. Park, *Anti-Trop2 Antibody-Conjugated Bioreducible Nanoparticles for Targeted Triple Negative Breast Cancer Therapy*, Int. J. Biol. Macromol. **110**, 406 (2018).

[172] A. C. Marques, P. J. Costa, S. Velho, and M. H. Amaral, *Functionalizing Nanoparticles with Cancer-Targeting Antibodies: A Comparison of Strategies*, J. Control. Release **320**, 180 (2020).

[173] Z.-S. Liao, S.-Y. Huang, J.-J. Huang, J.-K. Chen, A.-W. Lee, J.-Y. Lai, D.-J. Lee,

and C.-C. Cheng, *Self-Assembled PH-Responsive Polymeric Micelles for Highly Efficient, Noncytotoxic Delivery of Doxorubicin Chemotherapy to Inhibit Macrophage Activation: In Vitro Investigation*, Biomacromolecules **19**, 2772 (2018).

[174] Q. Lu, M. Yi, M. Zhang, Z. Shi, and S. Zhang, *Folate-Conjugated Cell Membrane Mimetic Polymer Micelles for Tumor-Cell-Targeted Delivery of Doxorubicin*, Langmuir **35**, 504 (2018).

[175] P. S. Jain, A. J. Chaudhari, S. A. Patel, Z. N. Patel, and D. T. Patel, *Development and Validation of the UV-Spectrophotometric Method for Determination of Terbinafine Hydrochloride in Bulk and in Formulation*, Pharm. Methods **2**, 198 (2011).

[176] M. S. Donovan, B. S. Sumerlin, A. B. Lowe, and C. L. McCormick, *Controlled/"Living" Polymerization of Sulfobetaine Monomers Directly in Aqueous Media via RAFT*, Macromolecules **35**, 8663 (2002).

[177] S. Gurdap, N. N. Bayram, I. A. İşoğlu, and S. Dinçer İşoğlu, *Sulfobetaine-Based Homo-and Copolymers by RAFT: Cross-Linked Micelles and Aqueous Solution Properties*, ACS Appl. Polym. Mater. **4**, 6303 (2022).

[178] K. E. B. Doncom, H. Willcock, and R. K. O'Reilly, *The Direct Synthesis of Sulfobetaine-Containing Amphiphilic Block Copolymers and Their Self-Assembly Behavior*, Eur. Polym. J. **87**, 497 (2017).

[179] J.-P. Nam, K.-J. Lee, J.-W. Choi, C.-O. Yun, and J.-W. Nah, *Targeting Delivery of Tocopherol and Doxorubicin Grafted-Chitosan Polymeric Micelles for Cancer Therapy: In Vitro and in Vivo Evaluation*, Colloids Surfaces B Biointerfaces **133**, 254 (2015).

[180] Y.-J. Kim, J.-H. Ha, and Y.-J. Kim, *Self-Assembled Polymeric Micelles for Targeted Photodynamic Therapy of Human Epidermal Growth Factor Receptor 2 Overexpressing Breast Cancer*, Nanotechnology **32**, 275101 (2021).

[181] L. Fiandra, S. Mazzucchelli, C. De Palma, M. Colombo, R. Allevi, S. Sommaruga, E. Clementi, M. Bellini, D. Prosperi, and F. Corsi, *Assessing the in Vivo Targeting Efficiency of Multifunctional Nanoconstructs Bearing Antibody-Derived Ligands*, ACS Nano **7**, 6092 (2013).

[182] A. B. T. Ghisaidoobe and S. J. Chung, *Intrinsic Tryptophan Fluorescence in the Detection and Analysis of Proteins: A Focus on Förster Resonance Energy Transfer Techniques*, Int. J. Mol. Sci. **15**, 22518 (2014).

[183] J. Zhao, Y. Mi, and S.-S. Feng, *Targeted Co-Delivery of Docetaxel and SiPlk1 by Herceptin-Conjugated Vitamin E TPGS Based Immunomicelles*, Biomaterials **34**, 3411 (2013).

[184] B. S. Bolu, B. Golba, A. Sanyal, and R. Sanyal, *Trastuzumab Targeted Micellar Delivery of Docetaxel Using Dendron–Polymer Conjugates*, Biomater. Sci. **8**, 2600 (2020).

CURRICULUM VITAE

2011 – 2016	B.Sc., Pharmacy Faculty, Erciyes University, Kayseri, TURKEY
2017 – 2023	Ph.D. Bioengineering, Abdullah Gül University, Kayseri, TURKEY

SELECTED PUBLICATIONS AND PRESENTATIONS

J1) N.N. Bayram, G.T. Ulu, S. Gürdap, N.A. Abdulhadi, İ. A. İşoğlu, Y. Baran, S. Dinçer İşoğlu* "HER2-Specific Peptide (LTVSPWY) and Antibody (Herceptin) Targeted Core Cross-Linked Micelles for Breast Cancer: A Comparative Study" Pharmaceutics, 2023, 15(3), 733.

J2) S. Gurdap, **N.N. Bayram**, İ.A. İşoğlu, S. Dinçer İşoğlu* " Sulfobetaine-Based Homo- and Copolymers by RAFT: Cross-Linked Micelles and Aqueous Solution Properties". ACS Applied Polymer Materials, 2022, 4(9), 6303-6311.

J3) N.N. Bayram, G.T. Ulu, M. Topuzoğulları, İ. A. İşoğlu, Y. Baran, S. Dinçer İşoğlu* " HER2-Targeted, Degradable Core Cross-Linked Micelles for Specific and Dual pH-Sensitive DOX Release" Macromolecular Bioscience, 2022, 22(1), 2100375.

J4) N.N. Bayram, M. Topuzoğulları, İ. A. İşoğlu, S. Dinçer İşoğlu* "RAFT-synthesized POEGMA-b-P4VP block copolymers: preparation of nanosized micelles for anticancer drug release" Polymer Bulletin, 2022 1-14.

J5) N.N. Bayram, S. Gurdap, S. Dinçer İşoğlu, İ. A. İşoğlu * Preparation of antibacterial electrospun poly (D, L-lactide-co-glycolide)/gelatin blend membranes containing Hypericum capitatum var. capitatum. International Journal of Polymeric Materials and Polymeric Biomaterials, 2021, 70(11), 797-809.

C1) N.N. Bayram, G.T. Ulu, S. Gürdap, İ. A. İşoğlu, Y. Baran, S. Dinçer İşoğlu* "Peptide Targeted Core Cross-linked Micelles For Dox Delivery To HER2 Expressing Cancer Cells" in Tissue Engineering and Regenerative Medicine International Society (TERMIS2021), 15-19 November 2021, Maastricht/ Netherlands.

C2) S. Gurdap, **N.N. Bayram**, İ.A. İşoğlu, S. Dinçer İşoğlu* "Polysulfobetaine-based Core Cross-linked Micelles: Synthesis by RAFT Polymerization and Solution Properties" in IUPAC-MACRO2020+, The 48th World Polymer Congress, 16-21 May 2021, Jeju, South Korea.

C3) N. N. Akşit, G. T. Ulu, Y. Baran, S. Dinçer İşoğlu* "Drug Conjugated Smart Cross-Linked Micelles for Breast Cancer Delivery" in 30th Annual Conference of the European Society for Biomaterials, 9-13 September 2019, Dresden/Germany.

C4) N. N. Akşit, S. Dinçer İşoğlu* "Cross-linked micelles by RAFT polymerization" in European Polymer Congress, 9-14 June 2019, Heraklion/ Crete / Greece.

C5) N. N. Akşit, S.Gürdap, İ.A. İşoğlu, S. Dinçer İşoğlu* **"**Preparation of Antibacterial Electrospun Poly (D, L-lactide-co-glycolide)/Gelatin Blend Membranes Containing Hypericum capitatum var. Capitatum" in 16th Nanoscience and Nanotechnology Conference (NANOTR-16), 03-06 November 2019 Antalya/Turkey.

C6) N. N. Akşit, M.Topuzoğulları, İ.A. İşoğlu, M.Elkahtib, S. Dinçer İşoğlu* **"**PCL-b-mPEG Block Copolymer Nanocarriers for Anticancer Agent Release" in 15th Nanoscience and Nanotechnology Conference (NANOTR-14), 22-25 September 2018, Çeşme/Turkey.

C7) N. N. Akşit, M.Topuzoğulları, İ.A. İşoğlu, M.Elkahtib, S. Dinçer İşoğlu* "Poly(OEGMA)-b-Poly(4VP) Block Copolymer Nanocarriers For Anticancer Agent Release" in 43rd FEBS Congress, 7-12 July 2018, Praque/ Czech Republic.